

Scientific Report No. 49-2012

Evaluation of Global Climate Models as Regional Climate Model Drivers

Martin Wolfgang Jury

September 2012

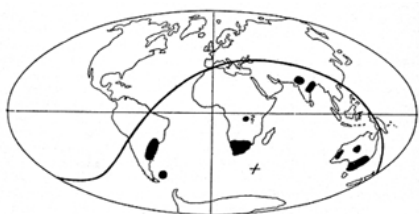


Wegener Center
www.wegcenter.at



The **Wegener Center for Climate and Global Change** combines as an interdisciplinary, internationally oriented research center the competences of the University of Graz in the research area „Climate, Environmental and Global Change“. It brings together, in a dedicated building close to the University central campus, research teams and scientists from fields such as geo- and climate physics, meteorology, economics, geography, and regional sciences. At the same time close links exist and are further developed with many cooperation partners, both nationally and internationally. The research interests extend from monitoring, analysis, modeling and prediction of climate and environmental change via climate impact research to the analysis of the human dimensions of these changes, i.e, the role of humans in causing and being effected by climate and environmental change as well as in adaptation and mitigation. (more informationen at www.wegcenter.at)

The present report is the result of a Master thesis work completed in July 2012.



Alfred Wegener (1880-1930), after whom the Wegener Center is named, was founding holder of the University of Graz Geophysics Chair (1924-1930) and was in his work in the fields of geophysics, meteorology, and climatology a brilliant, interdisciplinary thinking and acting scientist and scholar, far ahead of his time with this style. The way of his ground-breaking research on continental drift is a shining role model — his sketch on the relationship of the continents based on traces of an ice age about 300 million years ago (left) as basis for the Wegener Center Logo is thus a continuous encouragement to explore equally innovative scientific ways: *Jæ@ emerge in that we , æ\ them* (Motto of the Wegener Center).

Wegener Center Verlag • Graz, Austria

© 20FG All Rights Reserved.

Selected use of individual figures, tables or parts of text is permitted for non-commercial purposes, provided this report is correctly and clearly cited as the source. Publisher contact for any interests beyond such use: wegcenter@uni-graz.at.

ISBN 978-3-9503112-6-6

September 2012

Contact: *Martin Jury, M.Sc., B.A.*
martin.jury@uni-graz.at

Wegener Center for Climate and Global Change
University of Graz
Brandhofgasse 5
A-8010 Graz, Austria
www.wegcenter.at

Evaluation of Global Climate Models as Regional Climate Model Drivers

Master Thesis

to obtain the degree of a Master of Natural Sciences
at the Department of Natural Sciences
Karl-Franzens-University of Graz

Author

Bakk.rer.nat. Bakk.rer.soc.oec. Martin Wolfgang Jury
Wegener Center for Climate and Global Change
Matr. Nr.: 0330379

First Reviewer

Dr.rer.nat. Andreas Gobiet
Wegener Center for Climate and Global Change
Institute for Geophysics Astrophysics and Meteorology
Karl-Franzens-University of Graz

Graz, 12th July, 2012

Acknowledgments

I am grateful to my supervisor Mag. Dr.rer.nat. Andreas Gobiet who gave me the opportunity to be a member of the Regional and Local Climate Modeling and Analysis Research Group at the Wegener Center in Graz. I want to thank him, my co-supervisor Mag. Dr.rer.nat. Heimo Truhetz and my buddy Mag.rer.nat. Andreas Prein for his guidance, his invaluable support, his revisions and his useful suggestions during my research work.

Furthermore, I thank my colleagues and especially my roommates at the Wegener Center for the warm reception in their group, their mental and physical support and for the many constructive discussions. My thankfulness also goes to the PCMDI (Program for Climate Model Diagnosis and Intercomparison), the E-OBS dataset from the EU-FP6 project ENSEMBLES (<http://ensembles-eu.metoffice.com>) and the data providers in the ECA&D project (<http://eca.knmi.nl>), as well as the ECMWF (European Center for Medium-Range Weather Forecasts) for the provision of necessary data.

Immeasurable gratitude must be expressed to my mother Mrs. Gabriele Jury and to my father Mr. Wolfgang Jury, as well as to my sister Mrs. Ulrike Jury, who supported me in every imaginable way during my whole studies. This thesis would have been impossible without them. Finally I'd like to thank the University of Graz as the Wegener Center for the scholarship during the work on my diploma thesis.

Contents

Acronyms and Abbreviations	vii
Abstract	xi
Zusammenfassung	xii
1 Introduction	1
1.1 The Climate	2
1.2 Climate Models	3
1.2.1 Globale Climate Models (GCMs)	3
1.2.2 Regional Climate Models (RCMs)	4
1.3 Evaluation of GCMs in the Context of Regional Climate Modelling	9
1.3.1 Evaluations Based on Reanalysis Data	9
1.3.2 Evaluations of the Lateral Boundary Conditions	10
1.3.3 Coordinated Regional Downscaling	12
1.3.4 Model Performance Metrics	13
2 Research Domains, Variables, Data Sets, and Methods	17
2.1 Research Domain	17
2.2 Variables	18
2.2.1 Air Temperature (ta)	19
2.2.2 Precipitation Rate (pr)	20
2.2.3 Sea-Level Pressure (psl)	21
2.2.4 Specific Humidity (hus)	21
2.2.5 Horizontal Wind Components	21
2.3 Global Climate Models (GCMs)	22
2.4 Observational Data Sets	26
2.4.1 European High-Resolution Gridded Data Set (E-OBS) . .	26
2.4.2 ECMWF 40 years re-analysis data set (ERA-40)	26
2.5 Regridding and Data Processing	27
2.6 Methods	28
2.6.1 Map Plots	28
2.6.2 Seasonal Cycle	30
2.6.3 Quantile-Quantile (QQ) Plots	30
2.6.4 Trends and Interannual Variability	30
2.6.5 Model Performance Index (MPI)	33

3	Results	37
3.1	Evaluation of Surface Parameters over Europe	37
3.1.1	Surface Air Temperature (tas)	38
3.1.2	Precipitation Rate (pr)	38
3.1.3	Sea-Level Pressure (psl)	44
3.1.4	Combined treatment of the ground parameters	49
3.2	Evaluation of Parameters over the Lateral Boundary	50
3.2.1	Air Temperature (ta)	50
3.2.2	Specific Humidity (hus)	58
3.2.3	Eastward Wind (ua)	65
3.2.4	Northward Wind (va)	72
3.2.5	Combined Assessment	79
4	Discussion	81
4.1	The Quality of ERA-40 Reference Data	82
4.2	Integrated Considerations	84
5	Conclusion	89
	References	91
	List of Figures	99
	List of Tables	103

Acronyms and Abbreviations

Below follows a list of *acronyms* and *abbreviations* used in the present document.

Symbols

E-OBS European high-resolution gridded data set.

ERA-40 European re-analysis data set.

A

AR4 Fourth Assessment Report.

AR5 Fifth Assessment Report.

C

CMIP Coupled Model Intercomparison Project.

CORDEX Coordinated Regional Climate Downscaling Experiment.

D

DJF December, January and February.

E

ECMWF European Centre for Medium-Range Weather Forecasts.

ESG Earth System Grid.

F

FAR First Assessment Report.

G

GCM Global Climate Model.

GCMs Global Climate Models.

H

hus specific humidity.

I

ICSU International Council for Science.

IOC Intergovernmental Oceanographic Commission.

IPCC Intergovernmental Panel on Climate Change.

J

JJA June, July and August.

M

MAM March, April and May.

MMM Multimodel Mean.

MPI Model Performance Index.

N

NEU Northern Europe.

NH Northern Hemisphere.

P

PCMDI Program for Climate Model Diagnosis and Intercomparison.

pr precipitation rate.

psl sea-level pressure.

Q

QQ Quantile-Quantile.

R

RCD Regional Climate Downscaling.

RCM Regional Climate Model.

RCMs Regional Climate Models.

S

SAR Second Assessment Report.

SEU Southern Europe.

SH Southern Hemisphere.

SON September, October and November.

T

ta air temperature.

TAR Third Assessment Report.

tas surface air temperature.

TFRC Task Force on Regional Climate Downscaling.

U

ua eastward wind.

V

va northward wind.

W

WCRP World Climate Research Programme.

WGCM Working Group on Coupled Modelling.

WMO World Meteorological Organization.

Abstract

In 2013 the Fifth assessment report of the Intergovernmental Panel on Climate Change (IPCC) will be published. Therein contained data from global climate models (GCMs) is collected by the fifth Coupled Model Intercomparison Project (CMIP5) since February 2011. To obtain regional information from the GCMs with their rather coarse resolution ($\approx 150 \text{ km} \times 150 \text{ km}$), the Coordinated Regional Climate Downscaling Experiment (CORDEX) – in the case of Europe EURO-CORDEX – regionalises data of several GCMs via regional climate models (RCMs).

This thesis evaluates the different CMIP5 GCMs in terms of their ability to reproduce the climate between 1961 and 2000 and to provide correct data necessary to drive RCMs. For this purpose near surface (2m) air temperature, precipitation and sea-level pressure over the land area of Europe, as well as as the upper air parameters air temperature, specific humidity and horizontal wind components in the form of how they are taken over from a RCM – three dimensional on different pressure levels over an area enveloping Europe (lateral boundary) – have been analysed. In doing so, applied evaluation methods include spatial distributions, seasonal cycles and respective deviations of it, quantile-quantile plots, trends and interannual variability, and also a model performance index. As a reference for the near surface parameters serves the European high-resolution gridded data set (E-OBS) and for parameters on pressure levels the European re-analysis data set (ERA-40).

The analysis shows a good agreement between modeled ground fields and the reference, while parameters over the lateral boundary zone deviate stronger. Results moreover suggest, that a model's ability to correctly reproduce parameters near the surface, does not implicate that the model provides correct data necessary for driving an RCM. For instance, the GCM, which shows the best agreement with observed parameters near the surface, differs the strongest from reference data over the lateral boundary. This leads to the conclusion that GCMs as drivers for regional climate models should not only be selected based of the quality near the surface, but also based on the quality of upper air parameters, particularly over the lateral boundary.

Zusammenfassung

Im Jahr 2013 wird der fünfte Sachstandsbericht des Intergovernmental Panel on Climate Change (IPCC) erscheinen. Die darin enthaltenen Daten globaler Klimamodelle (GCMs) werden seit Februar 2011 im fünften Coupled Model Intercomparison Project (CMIP5) zusammengetragen. Um von der großräumigen Auflösung von GCMs ($\approx 150 \text{ km} \times 150 \text{ km}$) zu regionalen Prognosen des Klimawandels zu gelangen, werden unter dem Coordinated Regional Climate Downscaling Experiment – kurz CORDEX und im Fall von Europa EURO-CORDEX – Daten aus mehreren GCMs aus CMIP5 mittels regionaler Klimamodelle (RCMs) regionalisiert.

Diese Diplomarbeit evaluiert die unterschiedlichen CMIP5 Modelle hinsichtlich ihrer Fähigkeit, den Zustand des Klimas zwischen 1961 und 2000 zu reproduzieren und korrekte Daten bereitzustellen, die für das Betreiben eines RCMs nötig sind. Zu diesem Zweck wurden die von den GCMs modellierte bodennahe Lufttemperatur, der Niederschlag und der Luftdruck auf Meereshöhe über der Landfläche Europas, sowie die Lufttemperatur, spezifische Luftfeuchtigkeit und horizontale Windkomponenten, wie sie von RCMs übernommen werden, also dreidimensional auf verschiedenen Druckebenen in einem Europa umschließenden Gebiet (laterale Grenzregion), analysiert. Hierfür verwendete Methoden umfassten räumliche Verteilungen, Jahresgänge und jeweilige Abweichungen von diesen, Quantile-Quantile-Plots, Trends und interannuale Variabilität sowie einen Model Performance Index. Als Referenzen dienten die bodennahen Parameter aus dem European high-resolution gridded data set (E-OBS) und die Parameter aus dem European re-analysis data set (ERA-40) auf Druckebenen. Die Analyse zeigt eine gute Übereinstimmung modellierter Bodenfelder mit den verwendeten Beobachtungsdaten, während die Parameter der lateralen Grenzregion stärker abweichen. Die Ergebnisse deuten darüber hinaus an, dass die Fähigkeit eines Modells bodennahe Parameter korrekt zu modellieren nicht automatisch bedeutet, dass es korrekte Parameter, die für das Betreiben eines RCMs benötigt werden, bereitstellt. Beispielsweise weicht jenes Modell, welches die größte Übereinstimmung mit beobachteten bodennahen Parametern hat, am meisten von den Referenzdaten in der lateralen Grenzregion ab. Dies führt zum Schluss, dass GCMs als Antrieb für regionale Modelle nicht nur nach der Qualität ihrer bodennahen Parameter, sondern auch nach Parametern welche die freie Atmosphäre beschreiben, insbesondere in der lateralen Grenzzone, für Regionalisierungen ausgewählt werden sollten.

1 Introduction

Climatic conditions sketch themselves responsible for a variety of societal developments. Both, deciding on the success of human sprawl on earth, and further encouraging technical developments in a response to challenging conditions, the climate's influence on mankind can hardly be neglected [Toynbee 1949]. With increasing spread, number and productivity of human activity in the form of entropy creating creatures, that to a great extent utilize the discharge of energy stored in fossil fuels and shape the earth's surface according to their demand, humanity is facing a similar challenge again, an increasingly warming climate. To be better prepared and to get a grasp on how big or fatal upcoming changes will be in terms of money, quality of life or even human deaths, climate modelling poses a useful tool. Several efforts are undertaken by scientists and modelling groups on the whole planet to promote projections of the changing conditions. These efforts include amongst many others estimations of the models' reliability and a breaking down of the global change on the regional level that directly affects everyday life. Evaluations of a Global Climate Model (GCM)'s ability to drive Regional Climate Models (RCMs) mainly incorporate variables near the surface. But variables that are actually forwarded in the regionalisation process are variables on pressure levels. This missing connection is the motivation behind this thesis, which aims at determining if current evaluation processes are to be extended for logical reasons by assessments of variables that are actually forwarded in the regionalisation process. An evaluation undertaken by Prein [2009] of Coupled Model Intercomparison Project (CMIP)3 data shows discrepancies between a GCM's ability to model parameters near the surface and parameters on pressure levels over Europe. This thesis on the other hand aims at examining if a global models ability to reproduce correct climate variables on the ground is equivalent to its ability to provide correct driving data to drive a regional model over the lateral boundary. Hence, the main research question is as follows:

Do GCMs that show good results in remodelled ground parameters
also provide good driving data for a Regional Climate Model
(RCM) over the lateral boundary?

This first chapter will clarify important and necessary terms, and present mayor lines of argumentation in relation to the assessment as well as actual scientific results. The second chapter will present the research domain, assessed variables, used data sets and applied methodologies. This will be followed by a presentation, discussion and summarization.

1.1 The Climate

The word ‘climate’ has been used frequently in the recent past. Especially the projected and in the meanwhile observable climate change has been subject to public debate and encouraged an even more reckless use of the term what lead to a multiplication of associated meanings. This makes it necessary to define what the climate is and what it is not in the course of this thesis. As the Intergovernmental Panel on Climate Change (IPCC) puts it in their Fourth Assessment Report (AR4) [Baede 2007]:

Climate in a narrow sense is usually defined as the average weather, or more rigorously, as the statistical description in terms of the mean and variability of relevant quantities over a period of time ranging from months to thousands or millions of years. The classical period for averaging these variables is 30 years, as defined by the World Meteorological Organization (WMO). The relevant quantities are most often surface variables such as temperature, precipitation and wind. Climate in a wider sense is the state, including a statistical description, of the climate system.

The components of the climate system are the atmosphere, the hydrosphere, the cryosphere, the pedosphere, and the biosphere [Hantel 2001]. These components and their related processes are partly represented in Global Climate Models (GCMs). Because of its own internal dynamics and of external forcings the climate system is not static, it is exposed to constant change. The main external forcings are solar radiation, volcanic eruptions, and anthropogenic forcing in the form of emitted greenhouse gases and land use change. If statements about the present climate are made, it is necessary to have robust observations at hand. By contrast if claims on future climate are to be made, one has to draw on GCMs to get realistic estimations. A GCM is [Baede 2007]:

a numerical representation of the climate system based on the physical, chemical, and biological properties of its components, their interactions and feedback processes, and accounting for all or some of its known properties. The climate system can be represented by models of varying complexity, that is, for any one component or combination of components a spectrum or hierarchy of models can be identified, differing in such aspects as the number of spatial dimensions, the extent to which physical, chemical or biological processes are explicitly represented, or the level at which empirical parameterizations are involved.

Climate change science is one of the fastest developing scientific disciplines in the last 50 years. Since 1951 scientific literature concerning the field has doubled every 11 years [Somerville et al. 2007].

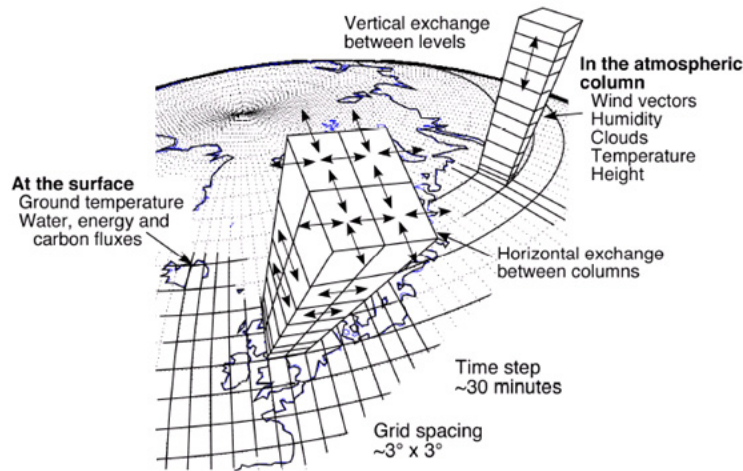


Figure 1.1: Schematic illustration of a GCM's operating principle [McGuffie and Henderson-Sellers 2005].

1.2 Climate Models

Generally there are two main kinds of dynamic climate models in respect of the modelled region. The Global Climate Models (GCMs) look at the climate from a global perspective while Regional Climate Models (RCMs) seek to resolve the climate and possible changes in specific areas more accurately.

1.2.1 Globale Climate Models (GCMs)

GCMs are based on fundamental principles of physics, the conservation of mass, energy, and momentum. Conservation of mass says, that the mass inside a certain volume can only change through in- and outflows at the boundary of the volume or via sources and sinks. Conservation of energy is described by the first law of thermodynamics, energy can only be transformed, and it is not possible to generate nor destroy it. Finally conservation of momentum accounts, according to the equation of motion (Navier-Stokes), for magnitude and direction of velocity in reference to present forces (gravity, pressure gradient, force of inertia, and Coriolis force). Out of these fundamental principles the basic equations are derived. In order to make these non-linear partial differential equations feasible for a climate model, they have to be simplified and solved numerically. Therefore the equations are discretised in space and time. Temporal resolution of a GCM is in relation to its spatial resolution in order to resolve relevant processes like circulation systems. A rule of thumb is, that if spatial resolution is halved, time steps have to be halved as well [von Storch, Güss and Heimann 1999]. A schematic illustration is presented in Figure 1.1.

An other example of the progression of climate science is visible in model complexity (see Figure 1.2). Over the last decades more and more relevant processes have been integrated in climate models to provide a more realistic and consistent picture of the climate system and its possible changes. Generally state of the art GCMs couple atmospheric and oceanic processes, and are therefore referred to as Atmosphere-Ocean General Circulation Models (AOGCMs). Up to what extent relevant aspects are included in a climate model depends on the different models but in general there is a trend toward the integration of more processes. Bolstered by an increase of computational capacities and resources not only model complexity increased but also the length of simulations and their spatial resolution. Figure 1.3 views the mean resolution of GCM short-term climate simulations used in the past four IPCC Assessment Reports. Long-term climate simulations were normally performed with the previous report generation's resolution [Somerville et al. 2007]. The horizontal resolution of state of the art GCMs evaluated in this thesis is around 180 km.

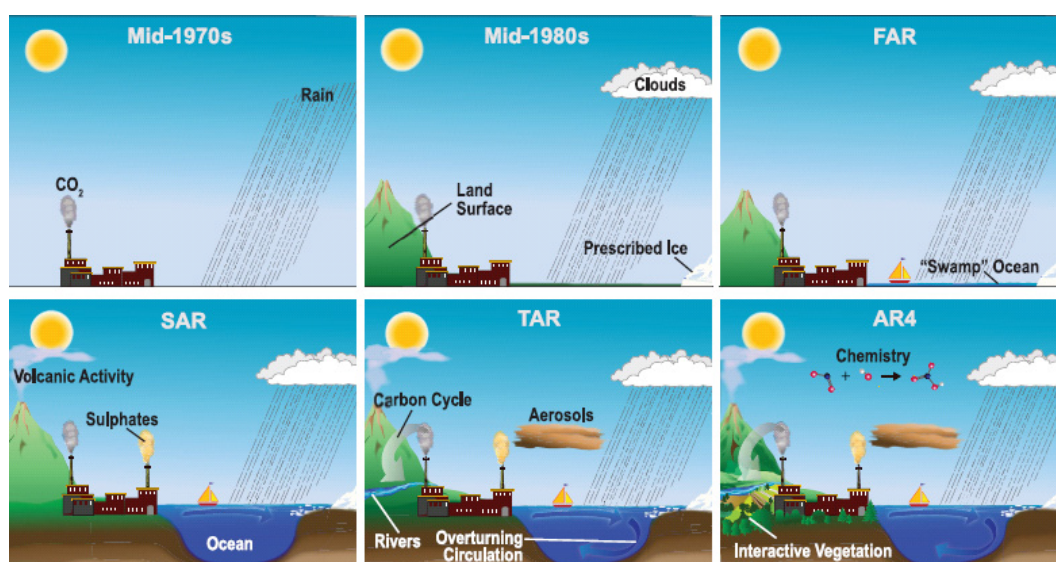


Figure 1.2: Climate models and the increase of included processes with time. (IPCC's First Assessment Report (FAR) 1990, Second Assessment Report (SAR) 1996, Third Assessment Report (TAR) 2001, and Fourth Assessment Report (AR4) 2007) [Somerville et al. 2007].

1.2.2 Regional Climate Models (RCMs)

Giorgi and Mearns [1991] mention in the early nineties three methodologies within regional climate change simulations. Purely empirical approaches are seeking to gain information by looking at instrumental records of the recent

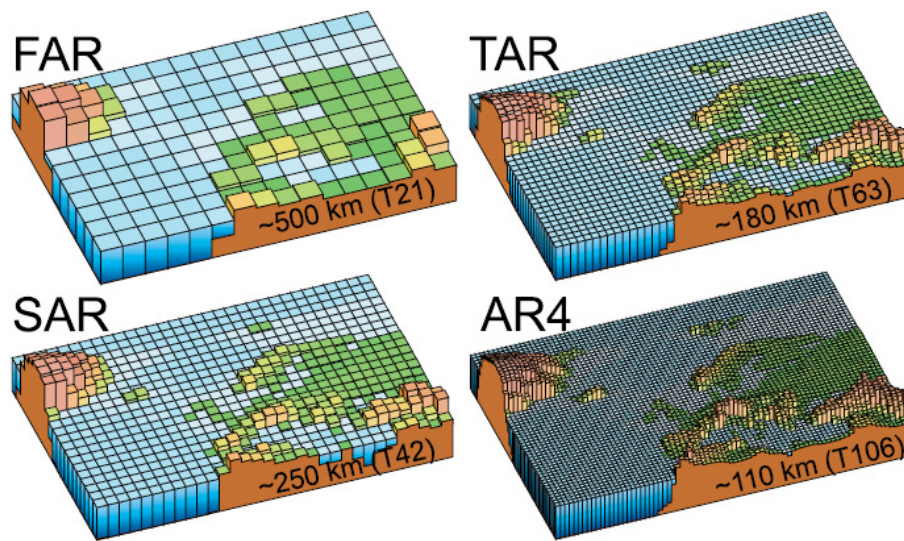


Figure 1.3: GCMs and the increases of spatial resolution with time. ((IPCC's First Assessment Report (FAR) 1990, Second Assessment Report (SAR) 1996, Third Assessment Report (TAR) 2001, and Fourth Assessment Report (AR4) 2007) [Somerville et al. 2007].

past or at paleoclimatic analogues. Semi empirical approaches are using information of coarse resolution global circulation models and set it in an empirically derived relationship with local surface variables. And modelling approaches try to overcome deficiencies of the former empirical approaches, which are not expected to produce accurate quantitative estimates of a nondeterministic and nonlinear regional climate.

A similar differentiation originates from the concept of downscaling, a concept describing a way of obtaining information on regional scales from a GCM. Within downscaling two main approaches are distinguished [Rummukainen 2010]:

- Statistical downscaling seeks to obtain regional information by identifying statistical relationships between large scale climate patterns.
- Dynamical downscaling describes the process of deriving regional climate information via physical-dynamical relationships. The regional climate is modelled based on large-scale climate conditions usually provided by a GCM.

Before formulating the various kinds of RCMs it is useful to name some of the reasons why regional climate modelling is undertaken. GCMs have one big shortcoming that make regional modelling a necessary asset in climate science. Their resolution is far too coarse to obtain climate information on regional and local scale. RCMs in contrast work on a finer resolution and therefore are able to

resolve climate processes not represented in global models. Wang et al. [2004] mention the following examples to highlight the usefulness of RCMs:

- Land-atmosphere interactions: RCMs are better in resolving land surface heterogeneities and in representing associated feedback processes with the atmosphere.
- Topographic effects on regional climate: Regional climate may be orographically forced and regulated, and needs to be resolved accordingly.
- Effect of land use change on regional climate: High resolution RCMs are able to incorporate spatially highly inhomogeneous land use changes.

Because of their potential to resolve land-sea contrast, complex topography, and land use more accurately, e.g., near costal regions or mountains, RCMs are able to improve the information content that would have been obtained from GCMs simulations alone [Laprise 2006]. In a further step data produced by RCMs is used by other modelling groups focusing on various aspects of climate change and its consequences in the field of impact assessment or resource management (e.g., agriculture, risk assessment, hydrology, and alike) [Finger, Hediger and Schmid 2011; Wang et al. 2004].

Classification of RCMs

Within dynamical downscaling one can distinguish further between high resolution regional models or nested limited-area models, that model the climate for a specific region, and variable resolution or stretched-grid global models, that model the climate over the entire globe, but get into more detail by clinching their grid over the area of interest¹. The former approach allots some assets over the latter, since it is less computational demanding and RCMs can be combined with various GCMs in order to account for uncertainty among projections of future climate [Laprise 2006; Rummukainen 2010], but has to manage the transmission of data on relatively big time steps between the two models and their different resolutions.

A nested RCM requires information at its lateral boundaries to integrate large scale circulations to the region of interest. Therefore RCMs can be subdivided into two different modes how the information flow from the GCM to the RCM is managed. RCMs are realized by nesting them, either in a **one-way** or an interactive **two-way** mode into a global climate model. To dump it down, nesting means a regional climate model is run within a GCM over a limited

¹A promising approach is the model for prediction across scales (MPAS) that uses an icosahedral (hexagonal) mesh, which gets more dense over areas of interest or key areas crucial to model outcomes and may show a complex shape (e.g., mountain ranges) [Skamarock et al. 2011].

area. The GCM provides the initial conditions for the area within the RCM, and beyond that, drives the RCM by distributing boundary conditions over the lateral boundary at the rim of the RCM over the modelled time span. In the two-way mode the RCM affects the GCM at the lateral boundary by handing over meteorological properties itself, while in the one-way mode the information flows unidirectional from the GCM to the RCM. The two way nesting approach has the benefit that systematic errors due to the underrepresentation of a region, that affects the global climate, can be reduced by feeding back small scale information to the large scale and by an increased update frequency². Conversely higher computational resources are needed since a GCM and RCM have to be modelled simultaneously, which is why the implementation of the two way nesting mode has been limited in recent years. In further consequence of the thesis, RCMs mean one-way nested RCMs.

An RCM's initial and lateral boundary conditions

When a RCM is initialized, data provided from a GCM or reanalysis data sets is applied to the regional domain, these are the **initial conditions**. Usually the first days of a regional climate model's simulation are neglected in order to give the model's atmosphere the possibility to spin-up [Giorgi and Mearns 1999]. When incorporating soil temperature profiles longer spin-up time of up to several years is necessary [De Ridder 2008].

The **lateral boundary** encloses the RCM. Information of the GCM is accumulated over a boundary relaxation or adjustment zone, to allow for a smoother transition between the regional climate simulation and the lateral boundary conditions. The term nudging describes how the lateral boundary zone is applied to the RCM. The size of this relaxation zone varies from case to case, but is typically 4-10 RCM grid points in diameter [Rummukainen 2010; Wang et al. 2004]. This relaxation zone ensures that model solutions of the RCM match the data from the large-scale driving field on the inflow and the outflow side of the RCM domain. Often it is referred to Davies in this context, who stated the purpose of his lateral boundary treatment as follows: "It should be capable of transmitting smoothly into and out of the limited domain the large scale flow resolved by, and implicit in, the external boundary data. It should also adequately represent the outgoing gravity waves and fine-mesh-scale meteorological flow inherent in the initial data for the limited domain or generated in situ during the time integration" [Davies 1975, cf. 406].

²Lorenz and Jacob [2005] could show the broad benefits of a two way nesting approach on modelling results on a global scale, by applying a RCM over the broader Indonesian region, that is characterized by vast numbers of small islands, that are insufficiently resolved in a GCM. This approach also benefits from the small update frequency (24 min) between GCM and RCM.

In his 2 dimensional model a parabolic relaxation coefficient was used and the relaxation zone was five grid points wide. All sighted literature applied procedures similar to Davies', generally using an exponential weighting term that ranges from 1 at the innermost to zero at the outermost grid point in the buffer or relaxation zone. It was shown that noise can be reduced via a broader buffer zone. Generally modellers try to minimize effects due to the lateral boundary conditions on the model solutions. This may be achieved by a relatively large RCM domain, and by ensuring that the region of interest is relatively far away from the lateral boundaries [Giorgi and Mearns 1999; Wang et al. 2004]. An other prominent nudging technique is the spectral nudging [von Storch, Langenberg and Feser 2000]. Large scale information of the GCM is truncated in terms of high frequency parts and the field of the regional model is fitted to this information unto a certain height, the weighting decreases with decreasing height.

The needed information is given over in the form of meteorological variables from GCMs or reanalysis data sets. Giorgi and Mearns [1991] identify wind components, temperature, water vapor, and surface pressure as the needed information for a one-way nesting to be realized, while Rummukainen [2010] further adds sea-surface temperature and sea ice to the list of key variables.

As mentioned earlier RCMs are driven by global climate data to ensure that global circulation patterns are present in the simulations. This leads to no or few deviation of large-scale circulations simulated in the RCM from global data in particular in the middle to upper troposphere [Giorgi and Mearns 1999]. On the other side if major storm tracks are misplaced in the global data they will be misplaced in the RCM as well. If the RCM is driven by incorrect data sets this will be reflected in the model results. The quality of the RCM output is therefore strongly dependent on the driving data provided by the GCM in general [Giorgi and Mearns 1991]. This phenomenon is called the **garbage in garbage out** problem³. To overcome this issue there have evolved two approaches, in the case of different GCM simulations being available. Giorgi and Mearns [1999] suggest that in order to obtain the best results from a RCM the one GCM simulation should be selected as driving data, that shows the best performance over the modelled region. In addition the selection of the driving data should be dependent upon the GCM's ability to provide accurate boundary conditions [Wang et al. 2004]. Another way to account for deficient climate change signals projected by GCMs is to incorporate different GCMs as drivers in a RCM study [Rummukainen 2010].

³Though RCMs are capable to reduce small-scale errors in regions with land-sea contrast or orographic forcings, errors do not get significantly amplified nor corrected by RCMs.

1.3 Evaluation of GCMs in the Context of Regional Climate Modelling

In this subsection literature about four main aspects, which are of some relevance, are presented. It begins with an overview over various reanalysis data sets. The second part will concentrate on various facets of the role of the lateral boundary. This is followed by a review of some projects concentrating on combinations of various GCMs and RCMs. In a last part, different ways of assessing model performance are discussed.

1.3.1 Evaluations Based on Reanalysis Data

In order to determine which global model provides the most accurate data, one has to draw on the past to compare the models with a reference, often provided by reanalysis data. This data sets assimilate measurements of various sources (e.g. weather balloons, radiosondes, etc.) in a three dimensional state often on a Gaussian grid. Between different reanalysis data sets there do exist several discrepancies. E.g., ECMWF reanalysis and NCEP/NCAR show significant differences (especially for the water vapor flux and lower-atmospheric circulation) concerning Asian summer monsoon and its interannual and intraseasonal variabilities [Wang et al. 2004]. To give an general overview on the validity of these data sets, Reichler and Kim [2008b] performed an assessment of common global reanalyses, by calculating the root mean square errors and using available observations as reference. European re-analysis data set (ERA-40) was attested to perform “consistently well, and in most quantities better than any other product”, with the exception of tropical precipitation rate (pr). In consequence of its good performance concerning the physic quantities (18 quantities accounting for thermodynamic state and radiative energy) and because of the lack of available observations ERA-40 was selected to be the reference for the evaluation of the upper air dynamic quantities (see Figure 1.4).

Indications of an excessive warming trend in the lower troposphere in ERA-40 data were found by Bengtsson, Hagemann and Hodges [2004]. They estimated that a more credible warming trend lies about 40 % under the trend pretended by the reanalysis data. Furthermore they pointed out that there is a great deal of uncertainty when calculating trends from reanalysis data and discourage from trend calculations based on ERA-40.

Dessler and Davis [2010] showed significant differences in trends calculated from various reanalysis data sets (ERA-40, ERA-interim, Japanese Reanalysis (JRA), National Centers for Environmental Prediction/Nation Center for Atmospheric Research (NCEP/NCAR), Modern Era Retrospective-Analysis for Research and Applications (MERRA); see Figure 1.5). A study by Santer et al. [2000] shows trend discrepancies between various satellite (MSUb, MSUc, MSUd), radiosonde (HadRT1.1, HadRT1.2) and reanalysis (ERA, NCEP) data sets in magnitude,

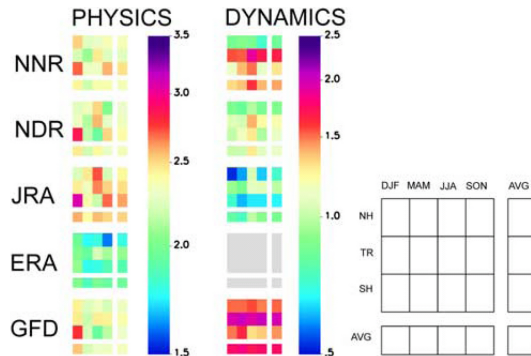


Figure 1.4: Root mean square errors of different reanalyses (National Centers for Environmental Prediction(NCEP)/Nation Center for Atmospheric Research (NCAR) Reanalysis (NNR), NCEP/Department of Energy reanalysis (NDR), Japanese Reanalysis (JRA), ERA-40 and the coupled climate model GFDL CM2.1) over 1979 to 1999. For the physics quantities available observations were used for validation and for dynamics ERA-40. Errors are presented by season and region (NH 30°N to 90°N, Tropics (TR) 30°S to 30°N, SH 90°S to 30°S) or as corresponding averages [Reichler and Kim 2008b].

direction and significance even for the time period 1979 to 1993 that was covered by satellite measurements. Because of the difficultness to obtain reliable trend estimates from noisy time series, as well as assessing their corresponding statistical significance, one cannot tell whether the observed trends do differ from zero nor from model estimations, since confidence intervals of the trend estimates are quite broad.

1.3.2 Evaluations of the Lateral Boundary Conditions

There have been a number of undertakings to account for the role of the initial and lateral boundary conditions in driving a RCM [Amengual et al. 2007; Diaconescu, Laprise and Sushama 2007; Marbaix et al. 2003; Wu, Lynch and Rivers 2005; Zhong et al. 2009]. All leading to the assumption that the quality of the boundary forcings plays a key role for making credible projections in regional climate modelling.

The role of different spatial (1°, 2°, and 3° and temporal (12, 24, and 48 hours on 1° spatial resolution) resolutions of provided lateral boundary conditions was evaluated by Amengual et al. [2007]. Model runs of the HIRLAM mesoscale model over Europe were evaluated concerning heavy rainfall events over Mediterranean Spain. Finer resolution showed no clear improvement of the model outcome, while shorter time steps led to an improvement. This lets assume that model outcome is relatively insensitive to spatial resolution of the lateral boundary fields and hence the resolution of the driving GCM.

Zhong et al. [2009] performed a study on the buffer zone's width (5 to 20 RCM

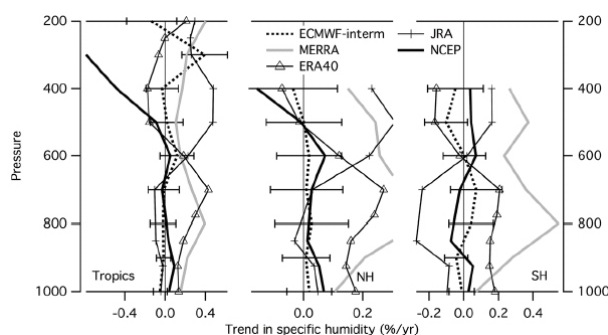


Figure 1.5: Specific humidity (hus) trends of different reanalyses over 1979 to 2010 (1989 for ERA-interim) for the tropics (20°S to 20°N), northern (20°N to 50°N) and southern (20°S to 50°S) hemisphere. Trends are expressed as a percentage of averaged hus values. The bars indicate the 95 % confidence interval of ERA-interim [Dessler and Davis 2010].

grid points) for east Asia during summer monsoons using reanalysis data. They showed that a broader buffer zone is only better for upper tropospheric low-frequency circulation systems, while circulations in the middle and lower troposphere as well as a precipitation patterns are not reproduced accordingly within the same setting. They state that the broader the buffer zone “the lower the correlation coefficient of the precipitation pattern between simulation and observation” [Zhong et al. 2009, cf. 1036].

A direct assessment of the impact of perturbed lateral boundary conditions and initial conditions on simulation biases was undertaken by Wu, Lynch and Rivers [2005] applying the Mesoscale Model (MM5) over a domain covering Alaska and western Canada. The lateral boundary conditions were distributed by four reanalysis data sets, all of them treated with four different interpolation procedures giving overall 16 different driving sets. In a second step initial or boundary conditions or both were perturbed. With simulation length the impact of biases in initial conditions decreased, while there was no clear trend for biases in the lateral boundary conditions. Overall the perturbed lateral boundary conditions contributed more to the total uncertainty than perturbed initial conditions. Precipitation and boundary height showed more sensitivity in concern of biases in the driving data than others (e.g., surface energy fluxes, air temperature). Nevertheless the four different driving data sets contributed the most to the uncertainty of the simulations.

The Big-Brother Experiment mimicked errors of a GCM by driving a RCM (Canadian RCM, CRCM) over a larger eastern America domain [Diaconescu, Laprise and Sushama 2007]. Lateral boundary conditions were on the one hand provided by a RCM simulation that has been driven with reanalysis data, and on the other hand by other RCM simulations that have been driven with the same reanalysis data, but have been perturbed with errors of adjustable magni-

tude. The impact of this set up was assessed by controlling for mean sea level pressure, temperature at 850 hPa, and precipitation in February, and showed a linear dependence between errors at the lateral boundary conditions and the perturbed driving data. The RCM did not significantly amplify nor correct these errors present in the driving data, but did correct some small-scale errors in regions with land-sea contrast or orographic forcing. However the authors speculated that RCMs may be less dependent on erroneous driving data in the summer seasons, but state, “that the quality of lateral boundary data plays a critical role in regional climate modelling, highlighting the need for good lateral boundary conditions and hence the necessity for a credible coupled GCM simulation to drive an RCM” [Diaconescu, Laprise and Sushama 2007, cf. 349].

To sum up, the quality of the lateral boundary conditions is crucial when regionalising global climate data. Further it is dependent on applied implementation procedures, and should be delivered on fine temporal scales. In comparison the lateral boundary contribute much more and continuously to model outcomes compared to the initial conditions.

1.3.3 Coordinated Regional Downscaling

To get a grasp on regional climate change several efforts have been undertaken to elevate regional climate modelers intercomparison and to foster modelers knowledge transfer, to obtain regional information on climate change from a variety of different modeler groups and to overcome the issue of what GCM should be used to drive which RCM [Laprise 2006]. For Europe the following projects have focused on this issue:

The Modelling European Regional Climate, Understanding and Reducing Errors (MERCURE, 1997 to 2000) project concentrated on strengths and weaknesses of nested RCMs [MERCURE 2002].

As Extension the Prediction of Regional scenarios and Uncertainties for Defining European Climate change risks and Effects (PRUDENCE, 2001 to 2004) analysed the projected climate changes for the end of the century. In course of this project 10 RCMs (some of them multiple times) were driven by three GCMs modelling two different IPCC AR4 scenarios. The aim of the project was to derive regional climate scenarios for Europe, while regarding for uncertainty induced by choice of RCM, scenario, driving GCM, and sampling uncertainty. Out of all components boundary forcings, ergo the choice of the GCM, were identified to contribute the most to the overall uncertainty [Déqué et al. 2007]. The driving GCM showed a dominant effect on the regional modelled temperature in spring, autumn, and winter and on precipitation in spring and summer [Christensen and Christensen 2007]. Model validation was conducted by comparing the models ability to simulate the past mean climate and interannual variability with ERA-40 [Jacob et al. 2007].

Also the ENSEMBLES project (2004 to 2009) focused on probabilistic esti-

mations of uncertainties, that arise by the use of multiple GCMs and RCMs [Linden and Mitchell 2009].

A quite new established framework that seeks to provide the most accurate climate projections on regional basis in a similar way is the Coordinated Regional Climate Downscaling Experiment (CORDEX) [Giorgi, Jones and Asrar 2009]. The European domain of the EURO-CORDEX subdivision is subject to this thesis (see Section 2.1).

1.3.4 Model Performance Metrics

Since the quality of lateral boundaries conditions directly affects the quality of the RCM results and are provided by various GCMs for projections of the future climate, it is necessary to evaluate global models with respect to their quality. How this evaluation should be carried out and what aspects are accounting for model quality is frequently debated in scientific literature.

Giorgi and Mearns [2002] approached this issue via their ‘Reliability Ensemble Averaging’ (REA), by a combination of model performance, in terms of the model bias, and model convergence, in terms of the models agreement on future climate, into one single index.

Räisänen [2007] notes three main lines of evidence when examining model reliability: “the skill of models in simulating present day climate ..., intermodel agreement in future climate change, and the ability of models to simulate climate changes that have already occurred.” [Räisänen 2007, cf. 2]. While present biases in simulations of the present climate indicate a deficient representation of some processes in a model and may directly distort feedback processes, he criticizes the rejection or down weighting of model in terms of their agreement on the future climate change.

Model validation itself holds several complications within. Because of the highly complex manner of the climate it is difficult to identify model errors and quality factors that account for a good simulation. To evaluate climate models it is furthermore necessary to compare simulations against past or present day observed climate, since such records cannot be made available for the future. But present day observations (sometimes even the same) were used in model development, evaluation, and ranking or posterior weighting [Knutti et al. 2010]. Moreover, past observations tend to hold a large amount of uncertainty and are sometimes weak in reliability for all wanted aspects of present day climate [Reichler and Kim 2008a].

Despite these controversies, if performance and to a certain extend reliability of GCM simulations by a comparison with the present climate is to be assessed, an incorporation of observational data is unavoidable. Various research projects

tried to catch model quality in terms of agreement with empirical data in different ways.

Ulden and Oldenborgh [2006] evaluated 23 coupled GCMs (CMIP3) in respect of their ability to reproduce sea level pressure patterns (reference ERA-40). While most models showed a high pattern correlation, only five models performed good at all latitudes when testing for explained spatial correlation.

By quantifying the skill of CMIP3 GCMs Maxino et al. [2008] accounted for model performance. They calculating a normalized skill score, which compared entire probabilistic density functions to observed ones, for the parameters temperature and precipitation and their maximum and minimum values over the Murray-Darling Basin in Australia,

In attempt to rank 24 GCMs from the IPCC AR4 Errasti et al. [2011] accounted for the seasonal cycle and probabilistic density functions of sea-level pressure (psl), surface air temperature (tas), and precipitation rate (pr) over the Iberian Peninsula and tested for correlation with ERA-40.

In an inquiry on the model selection of GCMs for driving RCMs Pierce et al. [2009] applied 42 performance metrics (based on seasonal means and standard deviations over different time spans as well as amplitude and phase of the annual harmonic) assessing temperature and precipitation indices of 21 GCMs over the western United States during January to March. The evaluated period ranged from 1960 to 1999, the evaluated models consisted of GCMs from the CMIP3 ensemble. The spatial mean square error was transformed into a skill score accounting for spatial biases, spatial correlations, and spatial standard deviations. They stated that in their application a selection of climate simulations based on their quality does not produce systematic differences in detecting and attributing climate change and highlighted the importance of using an ensemble of GCMs to reduce effects of internal climate variability. Furthermore the multimodel ensemble average performed superior in comparison to the single models. This fact was ascribed to “the cancelation of offsetting errors” [Pierce et al. 2009, cf. 8442].

Another study focused on interannual variability and potential predictability of temperature at 850hPa, geopotential at 500hPa, and stream function at 300hPa of a atmospheric model intercomparison project models between 1979 and 1988. The variability was divided in forced (by prescribed SST and SIC evolution) and weather noise. There was a wide variation over the different GCMs concerning their ability to simulate observed interannual variability and little connection between other model characteristics and the corresponding ability to simulate observed variability [Zwiers and Kharin 1998].

In an attempt to visualize model improvement within the different CMIPs, Reichler and Kim [2008a] designed a new measurement, a Model Performance Index (MPI) which can be easily depicted, regards present errors in the GCM remodelled climate state and furthermore allows for an incorporation of different

variables (see Subsection 2.6.5).

A similar MPI based on root mean square errors was developed by Gleckler, Taylor and Doutriaux [2008] and used in an assessment of CMIP3 models addressing more than 20 different variables. They acknowledged that, though capturing model performance in general, the index simplifies the complexities of climate models and information on the characteristics of simulated fields is not adequately attended for. In addition a model variability index, consisting of variance ratios, was introduced, but it featured only small or no correlations with the MPI. They noted that the relative ranking of models tends to be almost independent of the choice of reference data, internal variability, and the resolution of the regridded data, a model may only be moved “up or down in the ranking by several slots” [Gleckler, Taylor and Doutriaux 2008, cf. 18], although model indexes covering for interannual variability are only weakly correlated with indexes of mean climate performance.

Generally it can be said, that a model’s ability to simulate one aspect of climate processes and phenomena quite well does not automatically mean other aspects are represented in similar quality.

2 Research Domains, Variables, Data Sets, and Methods

In this chapter a specification of the variables used in the assessment, over which region they are provided, what data sets are used, and what methods will be applied to them in order to get a grasp on model performance is discussed. Figure 2.1 gives a first overview of the just mentioned decisive points and shows the different work packages that had to be processed in the course of this thesis. A clarification of the mentioned aspects in more detail is presented in this section.

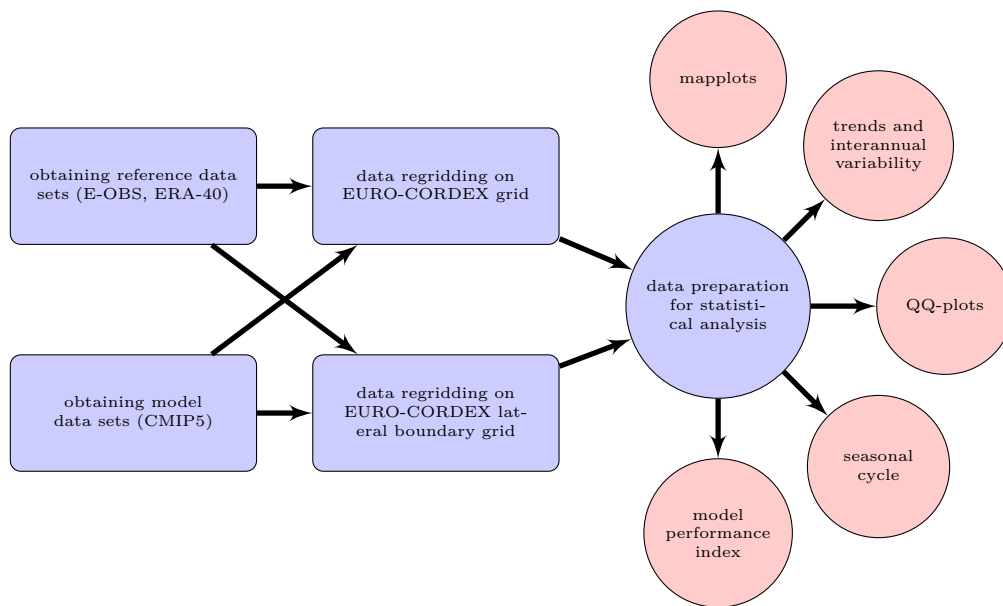


Figure 2.1: Flow diagramm of the approach used in the evaluation.

2.1 Research Domain

To obtain relevant information on future climate, data from Global Climate Models (GCMs) is used to drive Regional Climate Models (RCMs) (see Chapter 1). Because of the limitations of GCMs the World Climate Research Programme (WCRP) formed the Task Force on Regional Climate Downscaling (TFRCD) in December 2008, with the purpose of developing a framework to

evaluate and improve Regional Climate Downscaling (RCD) in the course of the Fifth Assessment Report (AR5) and beyond. As a first action TFRCD initialized the Coordinated Regional Climate Downscaling Experiment (CORDEX) framework to pool international regional climate modelers efforts [Giorgi, Jones and Asrar 2009]. To achieve this Coordinated Regional Climate Downscaling Experiment (CORDEX) designed a set of experiments concerning specific terrestrial regions. The EURO-CORDEX [Gobiet, Jacob and Community 2012] “is the European branch of the CORDEX initiative and will produce ensemble climate simulations based on multiple dynamical and empirical-statistical downscaling models forced by multiple global climate models from the Coupled Model Intercomparison Project Phase 5 (CMIP5)”[cf. EURO-CORDEX 2012]. The so called CORDEX domains encompass almost all land areas of the world and include South, Central and North America, Africa, West, East and Central Asia, Australasia, Antarctica, the Arctic, and the Mediterranean, as well as a European domain [ipsl 2012]. This very same European domain is subject to this thesis (Figure 2.2).

The domain was further divided into two sub domains, Northern Europe (NEU) and Southern Europe (SEU) which are separated by the 48° north circle of latitude. This segmentation is done referring to Intergovernmental Panel on Climate Change (IPCC) Fourth Assessment Report (AR4)’s classification of the two regions Northern Europe (NEU) and Southern Europe (SEU), ranging from 10°W to 40°E and 48°N to 75°N, and 10°W to 40°E, 30°N to 48°N, respectively [Hegerl et al. 2007]. Since this classification is stated on a non rotated grid in contrast to the research domain and therefore the two IPCC domains are not congruent with the CORDEX region, 48°N was chosen to be the boundary between the two domains NEU and SEU. Ground parameters presented in Table 2.1 were analysed over this two sub domains and over the entire EURO-CORDEX domain as well. The remaining variables were assessed over the lateral boundary enclosing the EURO-CORDEX domain. A more detailed description of the lateral boundary can be found in Section 2.5.

2.2 Variables

In the course of the evaluation of Global Climate Model (GCM)s and their ability to reproduce the past climate state and further drive a Regional Climate Model (RCM) different relevant climate variables have been assessed. In a preliminary examination of the EURO-CORDEX region’s past climate state the variables surface air temperature (tas), precipitation rate (pr) and sea-level pressure (psl) have been included. In addition air temperature (ta), specific humidity (hus), eastward wind (ua) and northward wind (va) are evaluated in this study. Those are the components of the basic set of boundary conditions necessary to operate a regional model [Giorgi and Mearns 1991; Rummukainen

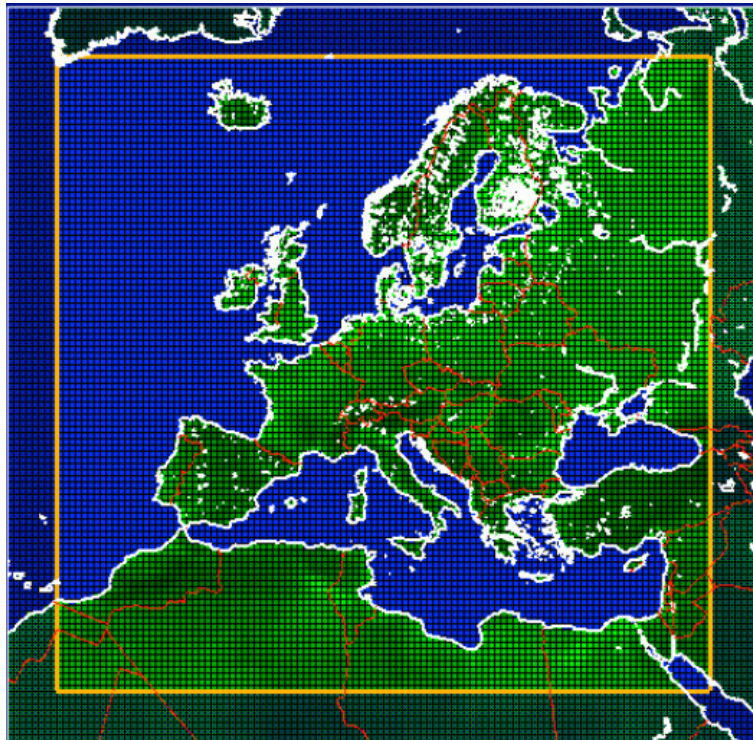


Figure 2.2: The EURO-CORDEX domain (rotated north pole at 162°W 39.25°N , top left corner at 331.79°W 21.67°N).

2010]. This four variables were included on four pressure levels in the analysis of the EURO-CORDEX region lateral boundary. In addition also sea surface temperature and sea ice belong to the boundary conditions, but were not accounted for in this evaluation. All used variables were provided on monthly mean basis. The following paragraphs describe the variables being used in the assessment in more detail and presents relevant aspects.

2.2.1 Air Temperature (t_a)

One of the most easily tangible variables, that moreover directly affects every day human live, is air temperature. It is a state variable and base unit of the international units system (SI-system) and has the unit Kelvin (K), although the use of the Celsius Scale ($^{\circ}\text{C}$) is more common in the field of climate science. As the state of every gas also the state of the air is described by the three variables temperature T , pressure p and density ρ . These variables are contextualized by the ideal gas law (Equation 2.1, V denotes the volume, n the number of moles, m the mass, M the molar mass and R is the ideal gas constant ($R = 8.3144 \text{ J/mol}\cdot\text{K}$)). A change in temperature is hence a change in

Table 2.1: Overview of the climate variables and corresponding units, pressure level and reference data set used in the evaluation.

	Variable	Unit	Pressure Level	Reference data
tas	surface (2m) air temperature	K	ground	E-OBS
pr	precipitation rate	kg/m ² ·s	ground	E-OBS
psl	sea-level pressure	Pa	ground	E-OBS
ta	air temperature	K		ERA40
hus	specific humidity	kg/kg	300 hPa, 500 hPa,	ERA40
ua	eastward wind	m/s	700 hPa, 850 hPa	ERA40
va	northward wind	m/s		ERA40

pressure if the ratio $\frac{V}{n}$ stays constant [Kraus 2004].

$$p \cdot V = n \cdot R \cdot T = \frac{m}{M} \cdot R \cdot T \quad (2.1)$$

Different forms of energy are a prerequisite for all processes that take place in the more or less open climate system. Besides radiation there exist two other important mechanisms. One is transportation of water vapor carrying energy in form of latent heat, the other is transportation of sensible heat. Ta is accounting for the latter and is often referred to as unordered motion of particles. It can be affected by several factors such as radiation ratios and surface properties, heat conductivity of the uppermost soil layer, altitude, topography, wind and advection, or cloud conditions. In the troposphere ta decreases almost linearly with a temperature gradient of between 6 K and 10 K (depending on moistness) per 1000 m till the tropopause [Etling 2008; Liljequist and Cehak 1994; von Storch, Güss and Heimann 1999].

2.2.2 Precipitation Rate (pr)

Precipitation is defined as water or ice particles which reach the surface. They are generated via condensation or sublimation in the atmosphere, reach the surface. Water droplets and ice crystals forming a cloud are ranging from 1 μm to 100 μm in diameter. By collisions, coalescence, and diffusion from droplets to ice particles (Bergeron-Findeisen-process) water drops form and start to rain out when reaching a diameter greater than 100 μm . Precipitation events can be observed near fronts, areas of convergence, in the case of convections and as a result of orographically forced rising air. Furthermore, it can occur in manifold forms basically determined by drop size and aggregate state, and may comprehend fog, dew and alike. The precipitation rate is measured in mass per area over time kg/(m²·s) [Kraus 2004; Liljequist and Cehak 1994; von Storch, Güss and Heimann 1999].

2.2.3 Sea-Level Pressure (psl)

Because of the earth's gravitation air exerts a force on the subjacent area, this force is called the air pressure. On a certain altitude its magnitude is determined by the total weight of all gas and liquid material located above. Air is compressible, that means its density declines with altitude since fewer and fewer air exerts force on the subjacent layer. Analogously, air pressure decreases with altitude exponentially. The barometric height formula, if integrated over height z and pressure p , allows to determine air pressure on any given altitude, which is in the course of this thesis the mean sea level [Kraus 2004; Liljequist and Cehak 1994].

$$\frac{\partial p}{\partial z} = -\frac{p \cdot M}{R \cdot ta} \cdot g \quad (2.2)$$

2.2.4 Specific Humidity (hus)

Humidity indicates the amount of water vapor in the air. Without water vapor there would be no clouds, precipitation, fog, dew and alike. Water vapor itself contributes to the total air pressure. This partial pressure of water vapor can be described by the ideal gas law (Equation 2.3). The amount of water vapor, that can be found in a certain volume of air, is limited by the saturation vapor pressure that rises with increasing temperature ($e^* = e^* \cdot ta$). It is defined as the relation of the mass of water vapor (ρ_V) to the mass of the moist air (ρ_m) and hence has the unit kg/kg [Kraus 2004].

$$e = \rho_V \cdot R_V \cdot ta \quad (2.3)$$

$$q = \frac{\rho_V}{\rho_m} = \frac{\rho_V}{\rho_{dA} + \rho_V} = \frac{\frac{e}{R_V \cdot ta}}{\frac{p-e}{R_L \cdot ta} + \frac{e}{R_V \cdot ta}} \quad (2.4)$$

2.2.5 Horizontal Wind Components

Motion in the atmosphere is essentially driven by the regional unbalance of energy supply and removal. Winds transport latent and sensible heat over various planetary circulation systems from the tropics to colder areas in direction of the poles. The research domain stretches from approximately 15°N to 75°N (Figure 2.2). At the southern end it overlaps with the tropical zone, a region dominated by northeasterly trade winds. This planetary circulation zone is separated by the tropical belt of high pressure at around 30°N from the prevailing westerlies located further north [Liljequist and Cehak 1994].

Meteorological elements (ε) are field quantities, which means, they are functions of and changing with the four field coordinates x, y, z , and t (Equation 2.5). The

motion of an air particle is described by its velocity, that means by the distance s it covers within the time t (Equation 2.6). \vec{i} , \vec{j} , and \vec{k} are the unit vectors in the three spatial directions. Building the total differential allows us to account for the different wind components ua , va and wa accounting for wind motions in the corresponding directions east, north, and vertical (Equation 2.7) [Kraus 2004].

$$\left. \frac{\partial \varepsilon}{\partial x} \right|_{y,z,t} \quad \left. \frac{\partial \varepsilon}{\partial y} \right|_{x,z,t} \quad \left. \frac{\partial \varepsilon}{\partial z} \right|_{x,y,t} \quad \left. \frac{\partial \varepsilon}{\partial t} \right|_{x,y,z} \quad (2.5)$$

$$\vec{v} = \frac{d\vec{s}}{dt} = \frac{dx}{dt}\vec{i} + \frac{dy}{dt}\vec{j} + \frac{dz}{dt}\vec{k} \quad (2.6)$$

$$ua = \frac{dx}{dt} = \vec{v} \cdot \vec{i} \quad va = \frac{dy}{dt} = \vec{v} \cdot \vec{j} \quad wa = \frac{dz}{dt} = \vec{v} \cdot \vec{k} \quad (2.7)$$

2.3 Global Climate Models (GCMs)

Coupled Model Intercomparison Project (CMIP)5 is the fifth project of the CMIP project series managed by the Program for Climate Model Diagnosis and Intercomparison (PCMDI) initiated by the World Climate Research Programme (WCRP)'s Working Group on Coupled Modelling (WGCM) in 1995. The program is funded by the World Meteorological Organization (WMO), the International Council for Science (ICSU), and the Intergovernmental Oceanographic Commission (IOC) of UNESCO. The program was initiated to foster communication within the international climate modelling groups and to obtain data on comparable basis (data format NetCDF) by prescribing various experiments of interests.

In the course of the upcoming IPCC fifth assessment report, CMIP5 GCMs will be a main source for presented climate projections. An overview of realised experiments is given in Figure 2.3. The standard set of model simulations aims at evaluations of model performances (how good the GCMs simulate the recent past); at projections of the future climate, further divided into the near term (until 2035) and the long term (until 2100 and beyond); and at getting a grasp on factors responsible for differences between the different model projections¹. Of particular interest to this thesis is the 'Historical' experiment which spans from 1850 to at least 2000. It is forced by naturally and anthropogenically induced observed atmospheric composition changes, solar forcings, emissions of short-lived species as well as aerosols or their precursors, and land use changes.

¹[CMIP5 website 2012]

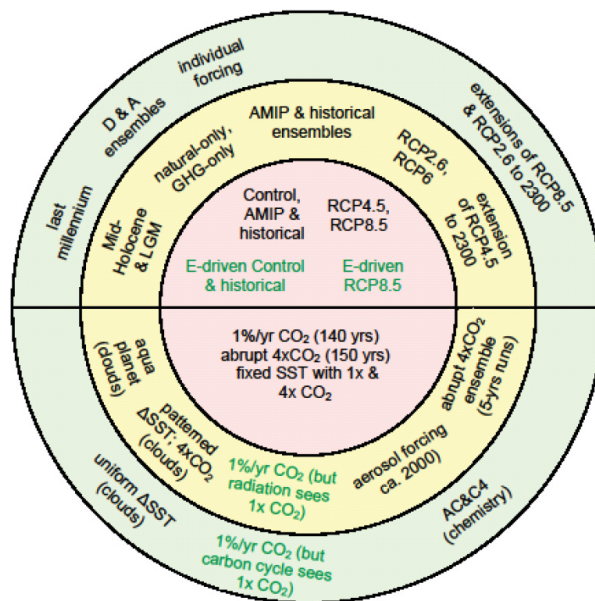


Figure 2.3: Schematic summary of the CMIP5 long-term experiments. The colors indicate different tiers, whereas the central red circle indicates the core experiments. Further, there is a division between experiments that can be compared with observations or are providing projections (located in the upper half of the circle), and experiments that aim at improving the knowledge of the climate system and model behavior (located in the lower half) [Stouffer, Taylor and Meehl 2011].

Only the time period of January 1961 to December 2000 will be processed, since robust observations have to be available in order to conduct the intended analysis [Taylor, Stouffer and Meehl 2012]. Since February 2011 first model output has been made available on Earth System Grid (ESG) data portals of CMIP5 participants. Data that has been made available until 31st January 2012 was included in the analysis. This includes 91 model runs of 21 GCMs distributed by 13 modelling groups. An overview of the analyzed models is given in Table 2.2. The Number of total runs indicates how many different data sets of a model were available. This may have different reasons. Most of the time the different runs are so-called different realizations, that are a consequence of small changes in the GCM's initial conditions. Another reason may be a variation in the perturbed physics of a model². All downloaded values are monthly mean averages.

²see also the CMIP5 Data Reference Syntax (DRS) and Controlled Vocabularies on http://cmip-pcmdi.llnl.gov/cmip5/docs/cmip5_data_reference_syntax.pdf (11 April 2012)

Table 2.2: Model overview of CMIP5 GCMs [CMIP5 website 2012].

Modelling Center	Institution	Country	Model	N total runs	spatial Res. [lat \times lon]	Reference
BCC	Beijing Climate Center	CHN	bcc-csm1-1	3	$2.8125^\circ \times 2.8125^\circ$	bcc.cma.gov.cn
CCCma	Canadian Centre for Climate Modelling and Analysis	CAN	CanESM2	5	$2.8125^\circ \times 2.8125^\circ$	www.cccma.ec.gc.ca
CNRM-CERFACS	Centre National de Recherches Meteorologiques	FR	CNRM-CM5	9	$1.4063^\circ \times 1.4063^\circ$	www.cnrm.meteo.fr
CSIRO-QCCCE	Commonwealth Scientific and Industrial Res. Org.	AUS	CSIRO-Mk3-6-0	10	$1.875^\circ \times 1.875^\circ$	[Rotstayn et al. 2010]
INM	Inst. for Numerical Math.	RUS	inmcm4	1	$1.5^\circ \times 2^\circ$	[Volodin, Dianskii and Gusev 2010]
IPSL	Institute Pierre-Simon Laplace	FR	IPSL-CM5A-LR	5	$1.875^\circ \times 3.75^\circ$	icmc.ipsl.fr
			IPSL-CM5A-MR	1	$1.2587^\circ \times 2.5^\circ$	icmc.ipsl.fr
MIROC	Atmosphere and Ocean Research Institute (The University of Tokyo) and others	JAP	MIROC-ESM	3	$2.8125^\circ \times 2.8125^\circ$	[Watanabe et al. 2011]
			MIROC4h	3	$0.5625^\circ \times 0.5625^\circ$	[Sakamoto et al. 2012]
			MIROC5	4	$1.4063^\circ \times 1.4063^\circ$	[Watanabe et al. 2011]
			MIROC-ESM-CHEM	1	$2.8125^\circ \times 2.8125^\circ$	[Watanabe et al. 2011]
MOHC	Met Office Hadley Centre	UK	HadGEM2-ES	4	$1.2414^\circ \times 1.875^\circ$	[Jones et al., Martin et al., Collins et al. 2011]
			HadGEM2-CC	3	$1.2414^\circ \times 1.875^\circ$	
MPI-M	Max-Planck-Inst. for Meteorology	GER	MPI-ESM-LR	3	$1.875^\circ \times 1.875^\circ$	[Roeckner et al. 2006]
MRI	Meteorological Research Institute	JAP	MRI-CGCM3	5	$1.125^\circ \times 1.125^\circ$	[Yukimoto et al. 2011]
NASA-GISS	NASA Goddard Institute for Space Studies	USA	GISS-E2-H	5	$2^\circ \times 2.5^\circ$	www.giss.nasa.gov
			GISS-E2-R	16	$2^\circ \times 2.5^\circ$	www.giss.nasa.gov
NCC	Norwegian Climate Centre	NOR	NorESM1-M	3	$1.875^\circ \times 2.5^\circ$	met.no
NOAA-GFDL	Geophysical Fluid Dynamics Laboratory	USA	GFDL-CM3	5	$2^\circ \times 2.5^\circ$	nomads.gfdl.noaa.gov
			GFDL-ESM2M	1	$2^\circ \times 2.5^\circ$	nomads.gfdl.noaa.gov
			GFDL-ESM2G	1	$2^\circ \times 2.5^\circ$	nomads.gfdl.noaa.gov

2.4 Observational Data Sets

Two different observational data sets were selected as reference, that cover the evaluation period from 1 January 1961 to 31 December 2000. The European high-resolution gridded data set (E-OBS) provides reference data for the ground parameters, while the European Centre for Medium-Range Weather Forecasts (ECMWF) 40 years re-analysis (ERA-40) accounts for variables assessed in the evaluation of the lateral boundary on pressure levels.

2.4.1 European High-Resolution Gridded Data Set (E-OBS)

The E-OBS provides high resolution land only gridded data for *tas*, *pr*, and *psl*. Overall 2192 stations have been combined to the most comprehensive data set over Europe and the Mediterranean. All processed data series have undergone quality control and homogeneity assessment, and are available in form of grid box averages to allow for easy comparison with RCMs. Four different spatial resolutions are available, whereupon a $0.22^\circ \times 0.22^\circ$ rotated pole grid resolution on monthly basis was used in the assessment. E-OBS is subject to ongoing improvements. The newest version (E-OBS v5) spans from January 1950 to June 2011 [Besselaar et al. 2011; Haylock et al. 2008; Klok and Klein Tank 2009].

Table 2.3: E-OBS number of stations

climate variable	number of stations
<i>tas</i>	1233
<i>pr</i>	2052
<i>psl</i>	416

2.4.2 European Centre for Medium-Range Weather Forecasts (ECMWF) 40 years re-analysis data set (ERA-40)

The 40 years European re-analysis data set (ERA-40) of the ECMWF combines various meteorological observations from September 1957 to August 2002. Considered data was gathered by a variety of systems including sondes, balloons, ships, aircrafts, satellites, and buoys (cf. Table 2.4). As one can see the number of considered observational systems as well as the number of records have increased with time, as observational density and new ways of conceiving atmospheric parameters (e.g., via satellites) have developed (cf. Figure 2.5). The aggregated data was assimilated applying the ECMWF data assimilation and forecasting system using a vertical resolution of 60 levels with an almost

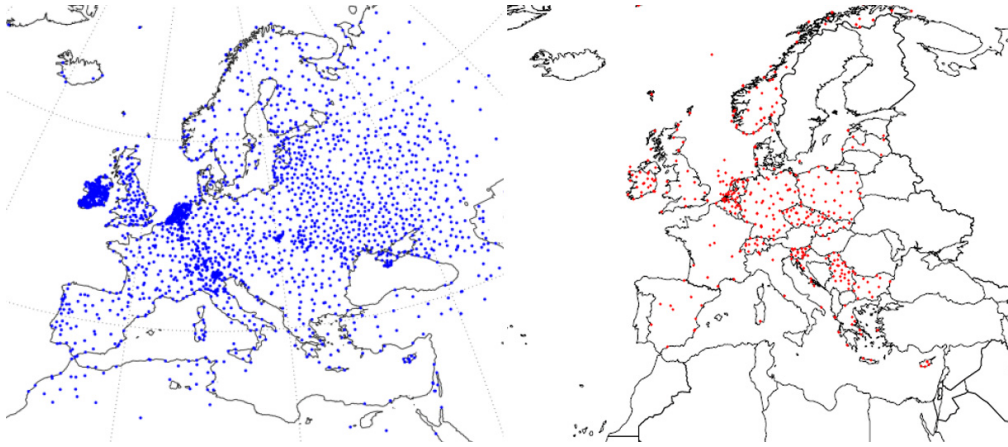


Figure 2.4: E-OBS station network. To the left: tas and pr as far as 2007 [Klok and Klein Tank 2009]. To the right: psl as far as 2011 [Besselaar et al. 2011].

uniform spacing of about 125 km and a T159 spectral model resolution on a regular Gaussian grid [Uppala et al. 2005]. The variables ta, hus, ua, and va

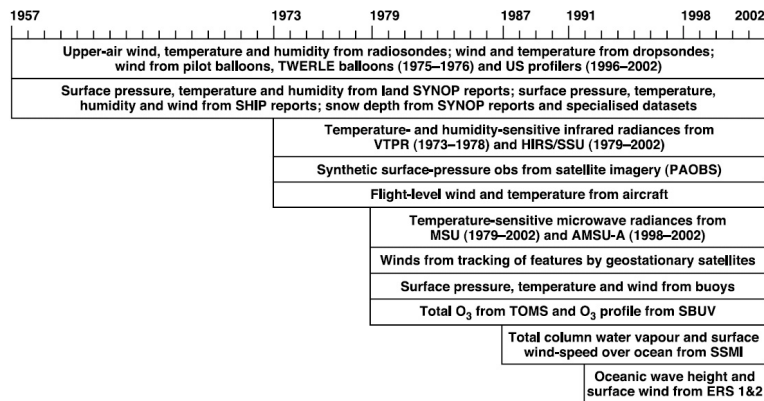


Figure 2.5: Chronology of observation types assimilated in ERA-40 from 1957 to 2002 [Uppala et al. 2005].

were evaluated against ERA-40 data provided on a $1.125^\circ \times 1.125^\circ$ Gaussian grid and on the pressure levels of 300 hPa, 500 hPa, 700 hPa, and 850 hPa.

2.5 Regridding and Data Processing

All GCM and ERA-40 data sets are given on regular Gaussian grid. Their resolution ranges from 0.5625° to 3.75° . The E-OBS data sets are given on a very fine $0.22^\circ \times 0.22^\circ$ rotated grid (rotated North Pole at 162°W 39.25°N). To conduct an intercomparison of climate data, it has to have the very same resolution,

Observation type	1958–66	1967–72	1973–78	1979–90	1991–2001
SYNOP/SHIP	15 313	26 615	28 187	33 902	37 049
Radiosondes	1 821	2 605	3 341	2 274	1 456
Pilot balloons	679	164	1 721	606	676
Aircraft	58	79	1 544	4 085	26 341
Buoys	0	1	69	1 462	3 991
Satellite radiances	0	6	35 069	131 209	181 214
Satellite winds	0	0	61	6 598	45 671
Scatterometer	0	0	0	0	7 575
PAOBs	0	14	1 031	297	277

Table 2.4: Average daily counts of various types of observation supplied to the ERA-40 data assimilation, for five selected periods [Uppala et al. 2005].

and moreover, grid points have to be located on the very same position. For the analysis of the ground parameters GCM data has been regridded in bilinear form to the rotated E-OBS grid. To control for regridding errors, averages over 10×10 grid points were generated leading to a rotated $2.2^\circ \times 2.2^\circ$ resolution. Since E-OBS only accounts for land surface parameters, grid points covered by more than 50 percent of sea were excluded from the subsequent analysis. In Figure 2.6 an overview of the processed grid points is given.

The same resolution and rotated grid was used in the evaluation of the lateral boundary. The lateral boundary was therefore split up into four sub segments, one located at each side of the EURO-CORDEX region: the left (western), top (northern), right (eastern) and the bottom (southern) segment. The upper segment is slightly shifted from all others to guarantee that the evaluated lateral boundary band is not overlapping with the EURO-CORDEX region (cf. Figure 2.6).

All used values are monthly mean values. Though driving data to RCMs is normally provided on much smaller time scales, it has several reasons monthly mean values were consulted. The amount of data and calculatory needs would have increased disproportional, and moreover adequate data on 6 hour basis was not available at the time the analysis was conducted.

2.6 Methods

This section presents the used methods in the course of the analysis. Except for the map plots, which were only used for an assessment of the ground parameters, all listed methods were applied to the two different sets of parameters.

2.6.1 Map Plots

The map plots included in this thesis show the EURO-CORDEX domain and are presenting the absolute values of the observation, as well as the absolute values of a model and its deviations from the observation over the four meteorological

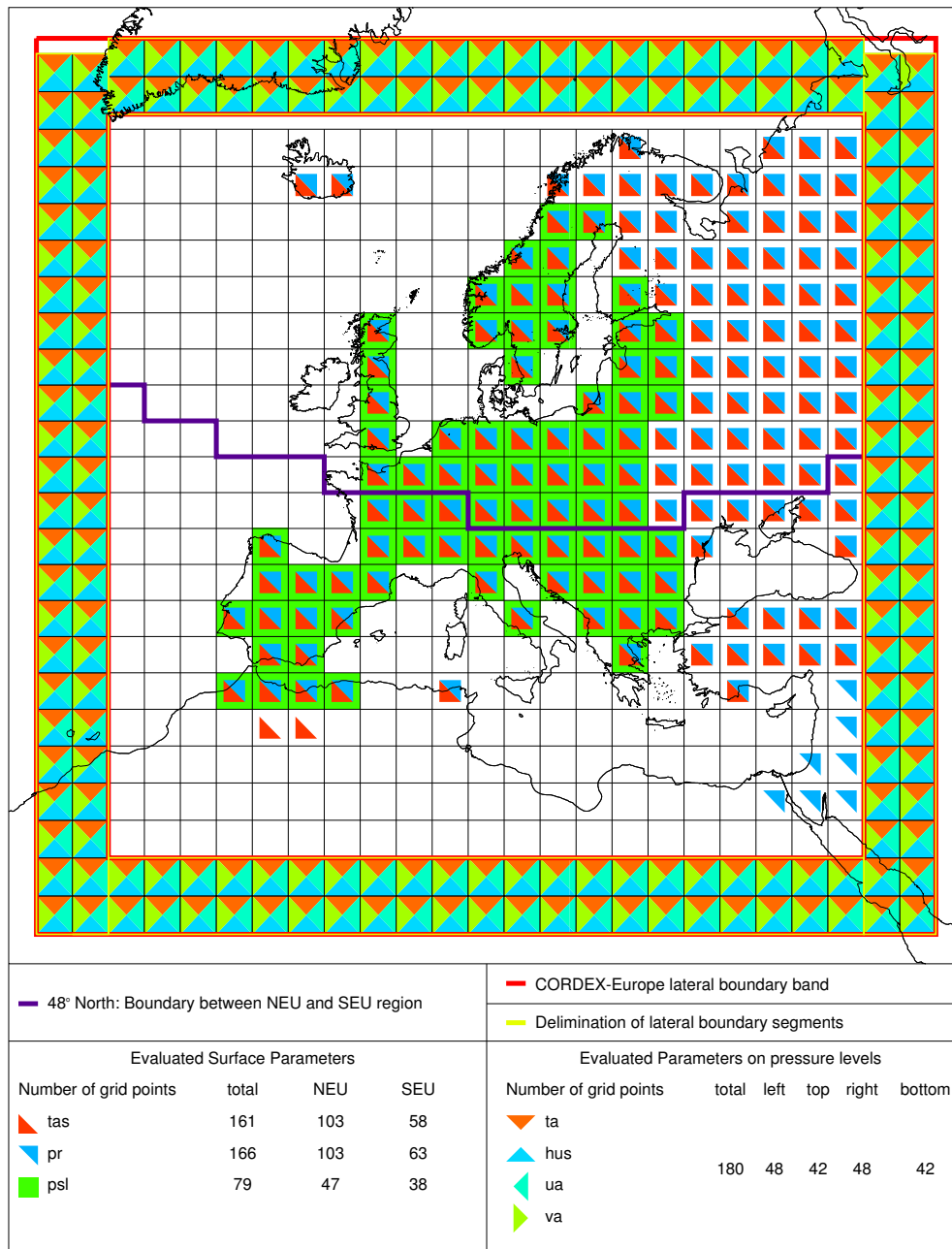


Figure 2.6: Evaluated variables on gridpoint basis over the EURO-CORDEX domain and its corresponding lateral boundary. Blue and red triangles, and green squares inside the EURO-CORDEX region represent available data for tas, pr, and psl, respectively. The blue line represents the boundary between the regions of NEU and SEU, and is located at 48°N. The parameters, ta, hus, ua, and va, included in the analysis of the lateral boundary are illustrated by triangles in the corresponding colors red, blue, turquoise, and green.

seasons of December, January and February (DJF), March, April and May (MAM), June, July and August (JJA) and September, October and November (SON). Also displayed are the seasonal and annual mean and bias values, as well as the maximum and minimum seasonal and annual bias values on grid point basis for the particular model.

2.6.2 Seasonal Cycle

The seasonal cycle plots show the temporal progression of a parameter throughout the year. Presented plots in Chapter 3 use the monthly mean values averaged over the evaluation period of 40 years. Also contained in the plots are the yearly mean values of the parameters. Bias plots of the seasonal cycle are included in the analysis as well, and display deviations from the observations over the year.

2.6.3 Quantile-Quantile (QQ) Plots

Quantile-Quantile (QQ) plots are probability plots and compare two cumulative distribution functions with each other, by plotting the corresponding quantiles. This method allows for a graphical determination whether two data sets share a common distribution. A perfect fit of the two cumulative distributions would mean that the quantiles lie at the same position and a diagonal would be displayed. In the presented QQ plots one dimension represents the position of the 5 % quantiles of the reference data set, while the other represents the 5 % quantiles of the evaluated models [Wilks 2006].

Figure 2.7 presents a QQ plot for the GFDL-CM3 (red) and the MIROC5 (green) models 5 % to 95 % quantiles compared to the E-OBS observational data set of sea-level pressure (psl). The quantiles of the MIROC5 model are located to the upper left of the diagonal at the lower end of the distribution, and to the lower right at the upper end of the distribution (e.g., 5 % quantile of E-OBS approximately at 1006.5 hPa and at approximately 1010 hPa for MIROC5). This lets us draw the following conclusions: The distribution of the values of the MIROC5 model is narrower than of E-OBS and even more clinched at the lower tail because of the slope of the curve. In contrast the distribution of the GFDL-CM3 model psl values is broader than of the observation, the lower tail values are located under, the upper tail values above the diagonal.

2.6.4 Trends and Interannual Variability

A linear relationship between a dependent and an independent variable can be described by a simple linear regression. The independent variable is often referred to as the predictor x (e.g., the time), and the dependent as predictand y (e.g., a climatic variable). As shown in Figure 2.8 a linear regression delineates this relationship by a single straight line, that minimizes the error for predictions

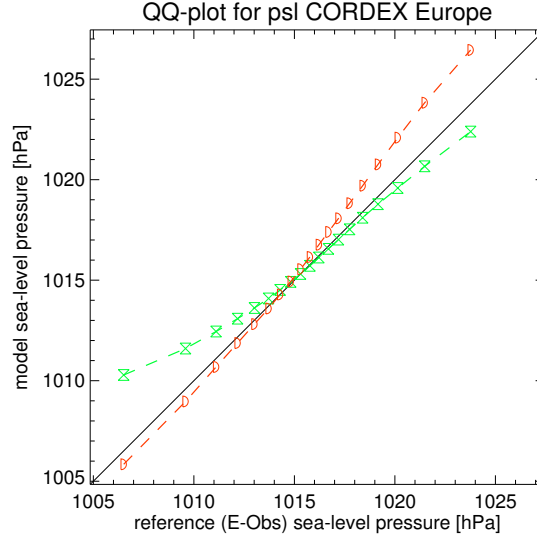


Figure 2.7: A Quantile-Quantile plot.

of y . For the linear regressions applied in this thesis the least square or ordinary least squares regression, that uses the squared-error criterion to determine the least error, is used, as the investigated period is a rather short one. A feature of this method is that small discrepancies between the points and the line have a rather small impact on the regressions slope, while large discrepancies provoke substantial changes [Wilks 2006]. For processed variables their annual mean values were used in the calculation of the linear regression line and its components. Generally the regression line is given by the relationship,

$$\hat{y} = a + bx. \quad (2.8)$$

The errors to be minimized are the vertical distances between the regression line and the data points defined as

$$e_i = y_i - \hat{y}(x_i). \quad (2.9)$$

The regression equation is generated by combination of Equation 2.8 and 2.9.

$$y_i = \hat{y}_i + e_i = a + bx_i + e_i \quad (2.10)$$

Solving for the squared errors yields

$$\sum_{i=1}^n (e_i)^2 = \sum_{i=1}^n (y_i - \hat{y}_i)^2 = \sum_{i=1}^n (y_i - [a + bx_i])^2, \quad (2.11)$$

which derivatives with respect to a and b are zeroed in to minimize the squared error.

$$\frac{\partial \sum_{i=1}^n (e_i)^2}{\partial a} = \frac{\partial \sum_{i=1}^n (y_i - a - bx_i)^2}{\partial a} = -2 \sum_{i=1}^n (y_i - a - bx_i) = 0 \quad (2.12a)$$

$$\frac{\partial \sum_{i=1}^n (e_i)^2}{\partial b} = \frac{\partial \sum_{i=1}^n (y_i - a - bx_i)^2}{\partial b} = -2 \sum_{i=1}^n [x_i (y_i - a - bx_i)] = 0 \quad (2.12b)$$

$$\sum_{i=1}^n y_i = n \cdot a + b \sum_{i=1}^n x_i \quad (2.13a)$$

$$\sum_{i=1}^n x_i y_i = a \sum_{i=1}^n x_i + b \sum_{i=1}^n (x_i)^2 \quad (2.13b)$$

By rearranging Equation 2.12a and 2.12b the normal equations 2.13a and 2.13b are obtained. Solving for the intercept a and the slope b yields:

$$b = \frac{\sum_{i=1}^n [(x_i - \bar{x})(y_i - \bar{y})]}{\sum_{i=1}^n (x_i - \bar{x})^2} = \frac{n \sum_{i=1}^n (x_i \cdot y_i) - \sum_{i=1}^n x_i \sum_{i=1}^n y_i}{n \sum_{i=1}^n (x_i)^2 - (\sum_{i=1}^n x_i)^2} \quad (2.14a)$$

$$a = \bar{y} - b\bar{x} \quad (2.14b)$$

One obstacle of the ordinary least squares regression is that in total the errors equal zero $\sum_{i=1}^n e_i = 0$. The minimized errors scatter around the regression line (Equation 2.9). This conditional distribution of the residuals can be described by the standard error [Wilks 2006].

$$s_e^2 = \frac{1}{n-2} \cdot \sum_{i=1}^n e_i^2 = \frac{1}{n-2} \cdot \sum_{i=1}^n [y_i - \hat{y}(x_i)]^2 \quad (2.15)$$

In the course of this thesis the standard error is the interannual variability since the predictor equals subsequent years. By this means statements about the

climatic trends can be extended by statements about the climatic variability.

$$\text{Variability} = \sqrt{s_e^2} \quad (2.16)$$

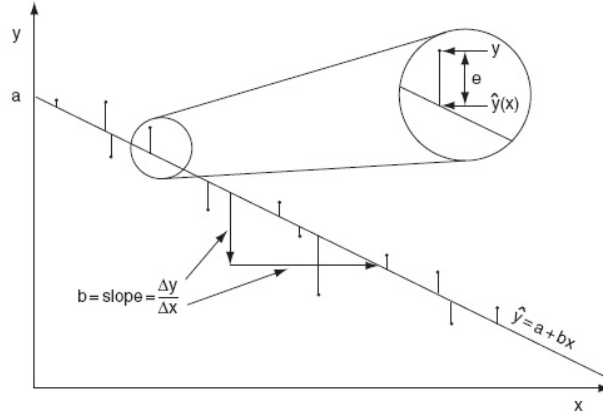


Figure 2.8: Schematic illustration of simple linear regression [Wilks 2006].

2.6.5 Model Performance Index (MPI)

There have been several attempts to get a grasp on model performance [Gleckler, Taylor and Doutriaux 2008; Pierce et al. 2009; Reichler and Kim 2008a]. One of the most simple and comprehensible, in that sense that it enables for the combination of spatial fits of different climate variables into a single index, is the Model Performance Index (MPI) developed by Reichler and Kim [2008a] to analyze models of the CMIP3 project in climatological terms. In the course of this thesis CMIP5 model performance was evaluated with this approach for the set of discussed climate variables (cf. Section 2.2).

To obtain the Model Performance Index (MPI) the normalized error variance e_{vm}^2 is calculated for each model (m) and variable (v) in a first step. It is the total of the squared grid point differences between the models and observations climatology normalized by the corresponding grid points' (n) interannual variance (Equation 2.17). \bar{s}_{vmn} denotes the simulated climatology of a climate model, \bar{o}_{vn} the observed climatology and σ_{vn} the interannual variance.

$$e_{vm}^2 = \sum_n (w_n (\bar{s}_{vmn} - \bar{o}_{vn})^2 / \sigma_{vn}^2) \quad (2.17)$$

$$I_{vm}^2 = e_{vm}^2 / \overline{e_{vm}^2}^{\text{CMIP5}} \quad (2.18)$$

$$I_m^2 = \overline{I_{vm}^2}^v \quad (2.19)$$

By normalizing the individual error variances over the ensemble (CMIP5 models) mean error variances, the Model Performance Index (MPI) I_m^2 is obtained. The normalization ensures an intercomparability of the different MPIs, which now vary evenly around one. Since more than one climate variable was analyzed in this way, the mean MPI is calculated by averaging the MPIs of individual parameters and pressure levels.

Robustness of the MPI

Quantitative estimates of the MPIs robustness have been realized by bootstrapping. The I^2 is a singular value varying around one. Since it captures the mean climatology of the various variables a certainty range can be calculated via bootstrapping. Bootstrapping was developed to allow for numerical estimations of the standard error of a parameter, no matter how complicated its mathematical formulation. The bootstrap sample is a random sample of n parameters \mathbf{x}^* drawn from \hat{F} with replacement. That means that the bootstrap sample is not assembled by data of the actual data set \mathbf{x} itself, but resampled by randomly drawn versions of \mathbf{x} . Because of this, various combinations of \mathbf{x} can appear in the bootstrap sample. A data value \mathbf{x} may be included not at all or several times in the bootstrap sample. Applying the function of the MPI s to the bootstrap sample yields a bootstrap replicate of I^2 .

$$\hat{F} \rightarrow (x_1^*, x_2^*, \dots, x_n^*) \quad \mathbf{x}^* = (x_1^*, x_2^*, \dots, x_n^*) \quad (2.20)$$

$$\hat{I}^{2*} = s(\mathbf{x}^*) \quad (2.21)$$

Repeating this bootstrapping several times, randomly drawing B independent bootstrap samples yields just as many bootstrapped I^2 . To obtain estimations of a standard error between 25 and 200 bootstraps are replicated, to ensure a more precise estimation, B was set to 1000 for determinations of the MPIs. The standard error $se_f(\hat{I}^2)$ can be easily estimated via the standard deviation of the single bootstraps. $\hat{I}^{2*}(\cdot)$ is the mean MPI [Efron and Tibshirani 1993].

$$\hat{I}^{2*}(b) = s(\mathbf{x}^{*b}) \quad b = 1, 2, \dots, B \quad (2.22)$$

$$\hat{se}_B = \left(\sum_{b=1}^B [\hat{I}^{2*}(b) - \hat{I}^{2*}(\cdot)]^2 / (B - 1) \right)^{1/2} \quad (2.23)$$

To put it in other words, the climate is defined as the average weather over a rather long time span. By averaging a meteorological variable the mean climate state is obtained. To derive a range of the climate state it is derived by randomly selecting various years within the research period with replacement.

3 Results

The results chapter presents findings that were obtained by applying the methods discussed in Section 2.6. Continuing the line of this thesis the findings should provide information concerning the quality of evaluated Global Climate Model (GCM) simulations with respect to drive one way nested Regional Climate Models (RCMs). This is accounted for in terms of the model performance over the EURO-Coordinated Regional Climate Downscaling Experiment (CORDEX) lateral boundary and should contribute to an expansion of model selection solely based on performance over ground parameters. Therefore the results section contains a part concentrating on evaluated surface variables and another part focusing on an assessment of variables on pressure levels representing possible lateral boundary conditions (see Table 2.1).

Presented figures will most of the time contain ensemble averages if multiple realizations of a model have been made available. This serves illustrative purposes only, since otherwise a plot would contain 91 different model realizations and can be justified by the similarity of projections from a model's different realizations. If runs of different perturbed physics were performed by a model, they were treated separately. E.g., the MRI-CGCM3 model distributed two perturbed physics ensembles labeled MRI-CGCM3_p1 and MRI-CGCM3_p2 in the following analysis.

Not all the plots that were produced in the course of the thesis, especially the map figures and figures that consider every model realizations, are presented in this document. For a full consultation please make use of the accompanying compact disc.

3.1 Evaluation of Surface Parameters over Europe

This section presents results of the evaluation of the variables surface air temperature (tas), precipitation rate (pr) and sea-level pressure (psl) over Europe for areas where European high-resolution gridded data set (E-OBS) reference data was available and over the two subregions Northern Europe (NEU) and Southern Europe (SEU). In a first consideration the variables are assessed separately via mapplots and figures of the seasonal cycles, quantiles, slope of the trend and interannual variability. The final section seeks to present a multiple parameters evaluation via the Model Performance Index (MPI).

3.1.1 Surface Air Temperature (tas)

Spatial patterns of tas of the Multimodel Mean (MMM) are shown in Figure 3.1. Negative biases can be found over northern Europe for every season and are strongest during winter. Generally positive biases are predominant over south and middle Europe especially in the summer and winter period.

The models show only small deviations with the observed seasonal cycle over Europe and the two subregions (see Figure 3.2). Over SEU more models show a warm bias, while over NEU the contrary is the case. The model biases generally lie between ± 2 °C, do not exceed ± 3 °C and show a tendency to be bigger during the winter month (see Figure 3.3).

Regarding the distribution of values the Quantile-Quantile (QQ) plot implies only small deviations between the models and the reference. At the upper tail of the distribution models tend to be warmer than the reference. At the lower tale the opposite is the case for the whole domain and over NEU. Over SEU models reproduce too warm temperatures (see Figure 3.4). Put in other words, for the whole European domain and over NEU a stretching of the MMM's data distribution with longer tails at both ends of the distribution is the case, while a skewing of the distribution to the left can be observed over SEU.

The trend between 1961 and 2000 reproduced by the MMM is about 0.002 °C/year larger than the observation. The models scatter around the reference slope of 0.022 °C/year at around ± 0.015 °C/year. Both E-OBS and the MMM show a stronger warming trend over NEU than SEU (see Figure 3.5). Regarding the temperature's interannual variability yields a good agreement over SEU, while it is underrepresented over NEU by most of the Global Climate Models (GCMs).

3.1.2 Precipitation Rate (pr)

The ensemble MMM shows a strong positive bias over Europe. In the mean the models simulate 10.48 mm/month more precipitation than recorded by observations. The bias is weakest in summer and strongest in spring. Figure 3.6 also shows a strong negative bias in winter at Mediterranean coastal regions of North Africa, Levant and Turkey and at regions near the Atlantic namely northern Spain, the British Islands and Norway.

3.1 Evaluation of Surface Parameters over Europe

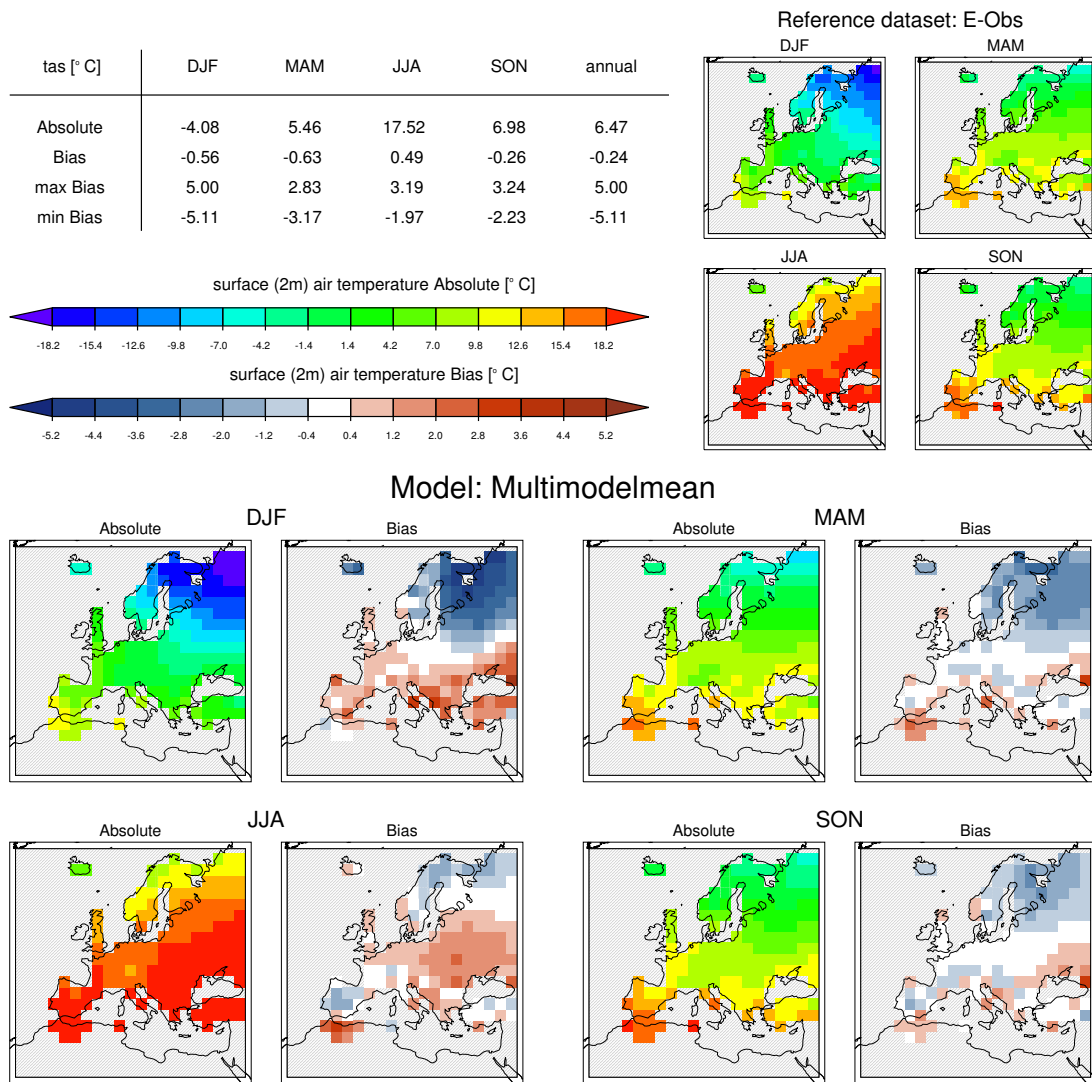


Figure 3.1: Mapplots of absolute and bias values of CMIP5 ensemble MMM of the tas over Europe between 1961 and 2000. As reference data serves E-OBS v5.

3 Results

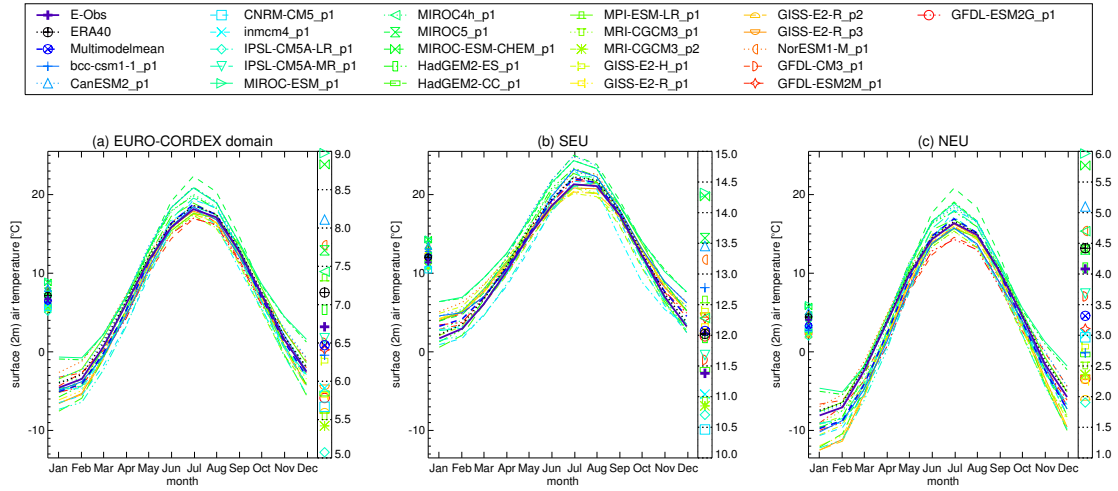


Figure 3.2: Seasonal cycle of tas of the CMIP5-ensemble for (a) the EURO-CORDEX domain (b) SEU and (c) NEU between 1961 and 2000.

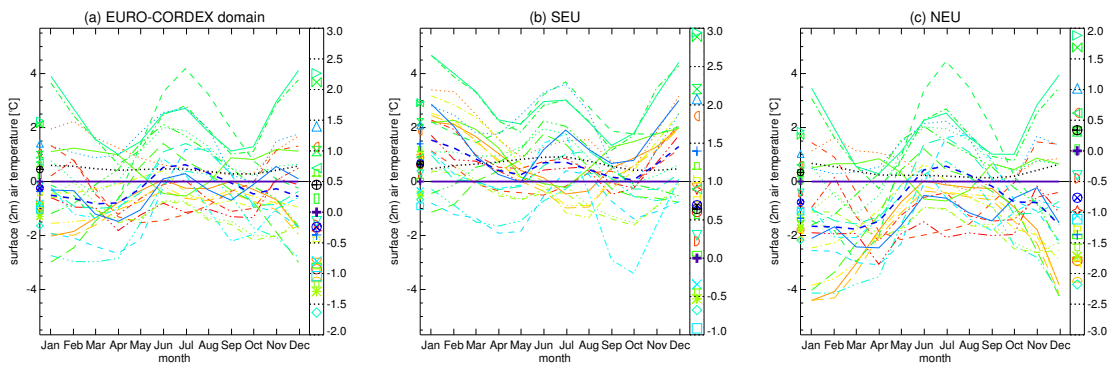


Figure 3.3: Bias in the seasonal cycle of tas of the CMIP5 ensemble for (a) the EURO-CORDEX domain (b) SEU and (c) NEU between 1961 and 2000 in reference to E-OBS. The legend is the same as in Figure 3.2.

3.1 Evaluation of Surface Parameters over Europe

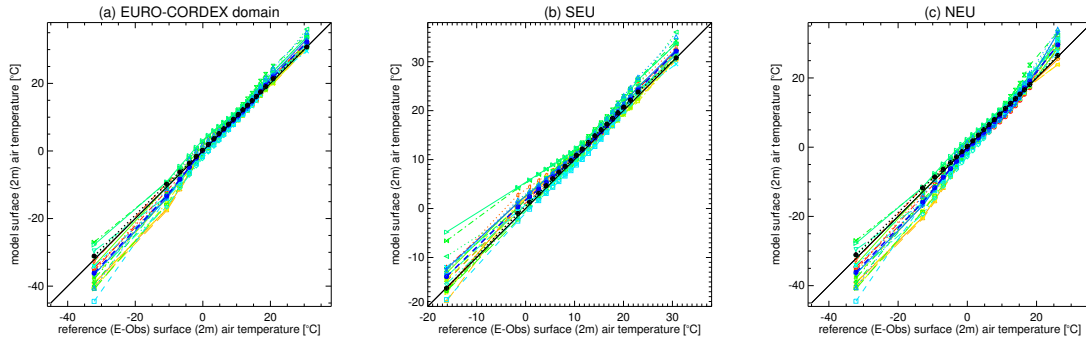


Figure 3.4: QQ plot of t_{as} of the CMIP5-ensemble for (a) the EURO-CORDEX domain (b) SEU and (c) NEU between 1961 and 2000 in reference to E-OBS showing the 5 % quantiles. The legend is the same as in Figure 3.2.

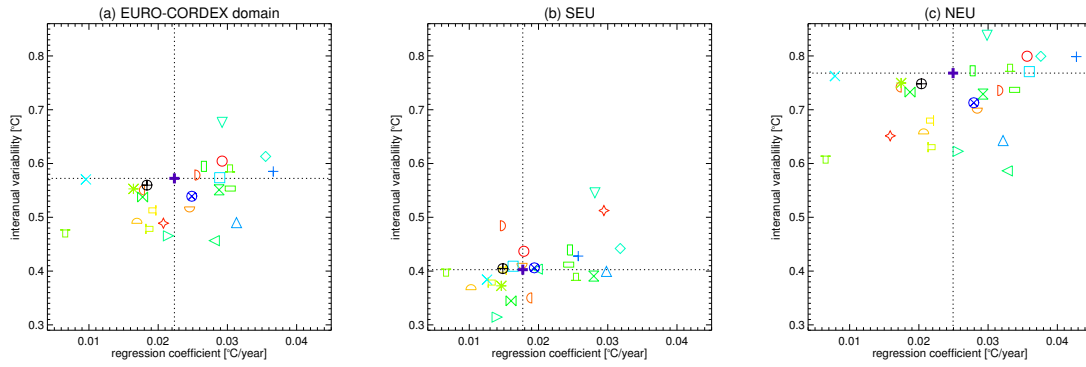


Figure 3.5: Scatter plot of slope and interannual variability based on linear regression for t_{as} of the CMIP5-ensemble for (a) the EURO-CORDEX domain (b) SEU and (c) NEU between 1961 and 2000 in reference to E-OBS. The legend is the same as in Figure 3.2.

3 Results

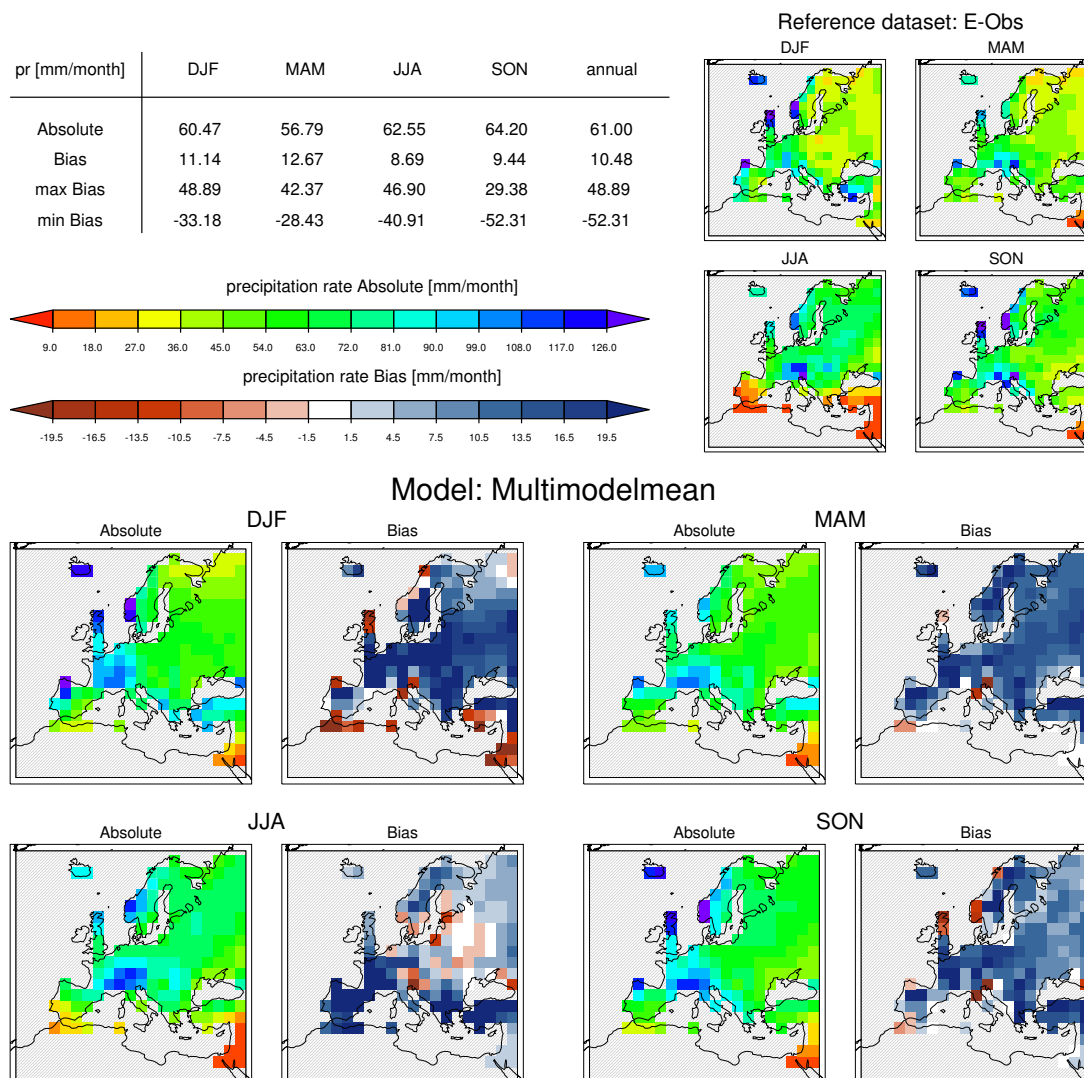


Figure 3.6: Mapplots of absolute and bias values of CMIP5 ensemble MMM of the pr over Europe between 1961 and 2000. As reference data serves E-OBS v5.

In the mean the models follow the shape of the observed seasonal cycle well (see Figure 3.7). During summer the models differ more from observational data in SEU, while for the rest of the year a higher bias can be noted over NEU. European re-analysis data set (ERA-40) captures around 8 mm/month less precipitation than E-OBS. Almost no model shows a negative bias (see Fig-

3.1 Evaluation of Surface Parameters over Europe

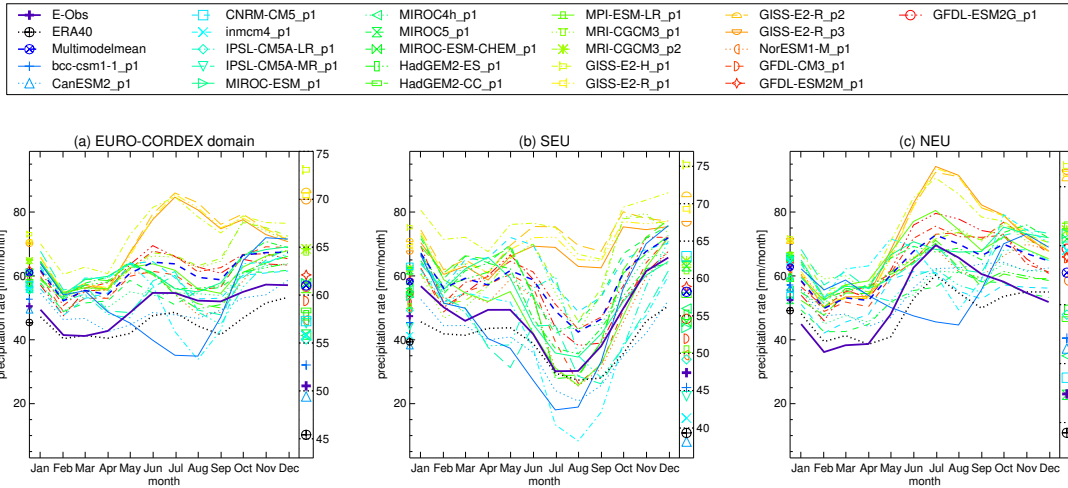


Figure 3.7: Seasonal cycle of pr of the CMIP5-ensemble for (a) the EURO-CORDEX domain (b) SEU and (c) NEU between 1961 and 2000.

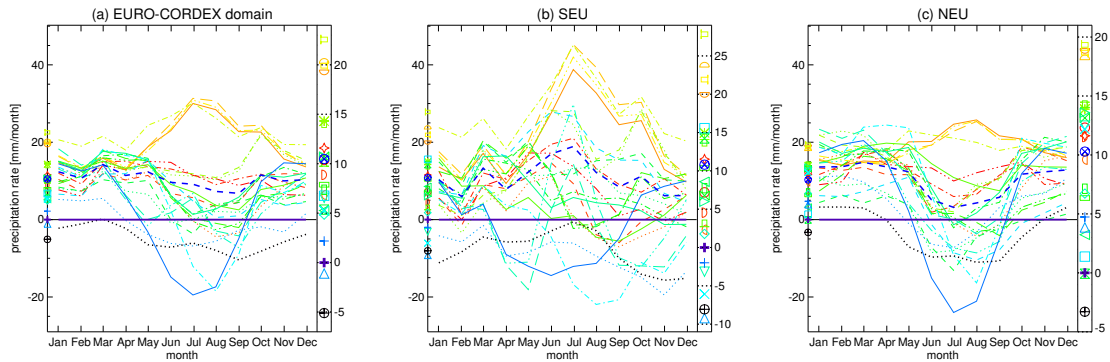


Figure 3.8: Bias in the seasonal cycle of pr of the CMIP5-ensemble for (a) the EURO-CORDEX domain (b) SEU and (c) NEU between 1961 and 2000 in reference to E-OBS. The legend is the same as in Figure 3.7.

ure 3.8). Overall the two models GISS-E2-H and GISS-E2-R show the strongest deviations, with a positive bias of about 20 mm/month.

The finding of too wet CMIP5 models is also visible in the QQ plots in Figure 3.9. At the lower to middle parts of the distributions, the global models quantiles are showing more precipitation, while for the maximum value all models except for GISS-E2-H feature a too small extreme. The models show deficiencies in modelling month of high precipitation.

The GCMs correctly model the trend in precipitation and its interannual variability for the European domain with the trend of the ensemble mean and E-OBS both located at about $+0.02$ mm/(month · year) and their corresponding interannual variability at around 22 mm/(month · year). But when setting the focus on the two subdomains, some model shortcomings are visible. While for SEU E-OBS shows a clear negative trend of about -0.125 mm/(month · year) the MMM is located at about -0.035 mm/month. Two models, namely GFDL-ESM2M and IPSL-CM5A-MR capture this negative trend quite good, but their interannual variability clearly exceeds the observed one of 3.5 mm/(month · year). Trend evaluation for NEU features the contrary. While E-OBS shows a positive trend of about 0.11 mm/(month · year), the MMM is located around 0.05 mm/(month · year). Some models show model the trend evolution considerably well for this region (see Figure 3.10).

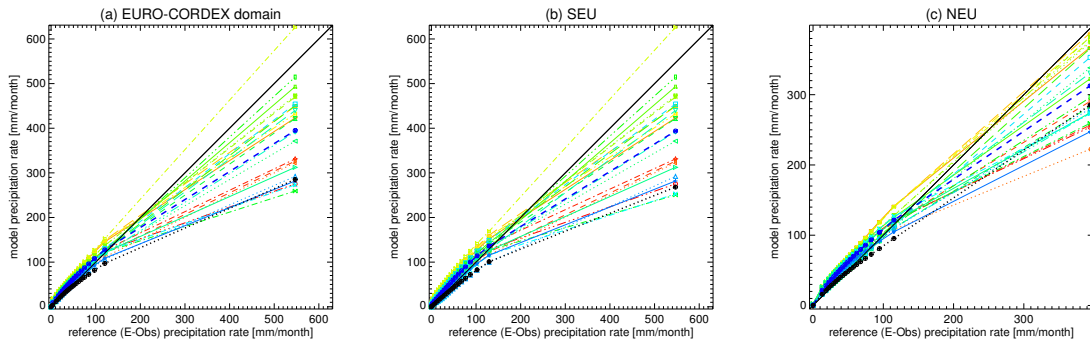


Figure 3.9: QQ plot of pr of the CMIP5-ensemble for (a) the EURO-CORDEX domain (b) SEU and (c) NEU between 1961 and 2000 in reference to E-OBS showing the 5 % quantiles. The legend is the same as in Figure 3.7.

3.1.3 Sea-Level Pressure (psl)

In the mean the E-OBS observations geographical pattern of psl is reproduced by the ensemble MMM. Biases are strongest in winter, quite low in spring and summer and vanishingly low during autumn (-1.32 hPa, -0.63 hPa, -0.4 hPa and -0.13 hPa; -0.42 hPa for the whole year). Except for summer a negative

3.1 Evaluation of Surface Parameters over Europe

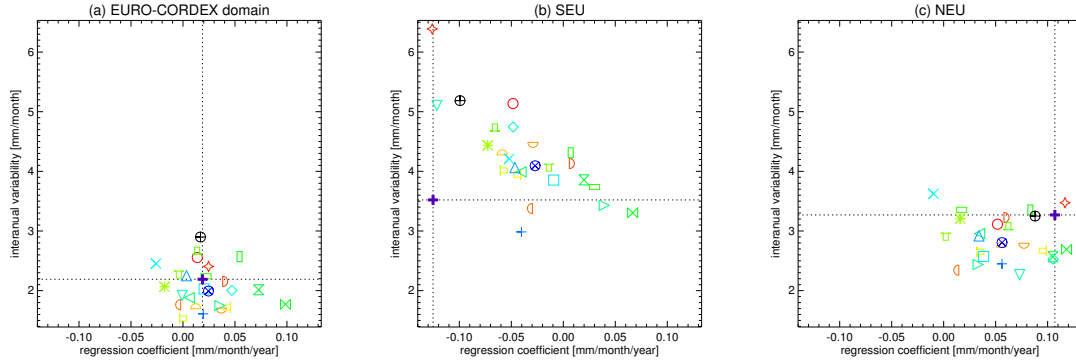


Figure 3.10: Scatter plot of slope and interannual variability based on linear regression for pr of the CMIP5-ensemble for (a) the EURO-CORDEX domain (b) SEU and (c) NEU between 1961 and 2000 in reference to E-OBS. The legend is the same as in Figure 3.7.

bias exists over central Europe, while over northern Europe, especially in summer, and over Spain, particularly pronounced in winter, a positive bias prevails (see Figure 3.11).

Considering the seasonal cycle visible in Figure 3.12 the shape is reproduced well by the MMM over the whole Europe domain and most notably over SEU. For NEU there are some minor deviations, namely a small negative bias over the winter half and a positive bias over the summer half of the year. In the mean the models spread quite uniformly around E-OBS (± 3 hPa). Strongest deviations are found during the winter month (see Figure 3.13).

Over the whole EURO-CORDEX domain a compression of the psl quantiles in relation to E-OBS is the case for the majority of the models as indicated in Figure 3.14. This skewing of the distribution to the right concerns all models and gets more pronounced over SEU. Nevertheless the MMMs distribution is almost congruent with the observations also concerning the extreme quantiles over NEU.

The good representation of NEU by the model's ensemble mean proceeds for the trend's slope and interannual variability (see Figure 3.15). Both nearly do not differ from E-OBS and are located at -0.005 hPa/year and 0.95 hPa/year, respectively. Over SEU E-OBS shows a positive trend of almost 0.03 hPa/year while the MMM shows no trend and all models being quite distant from E-OBS in the scatter plots. For the whole domain this differences are softened mainly due to the good performance of the models over NEU.

Nevertheless it should be noted that there are stronger deviations between E-OBS and ERA-40 than there are between E-OBS and the MMM. ERA-40 deviates from E-OBS regionally and temporally, with a prevailing strong negative bias over northern Europe especially in winter and a positive bias over

3 Results

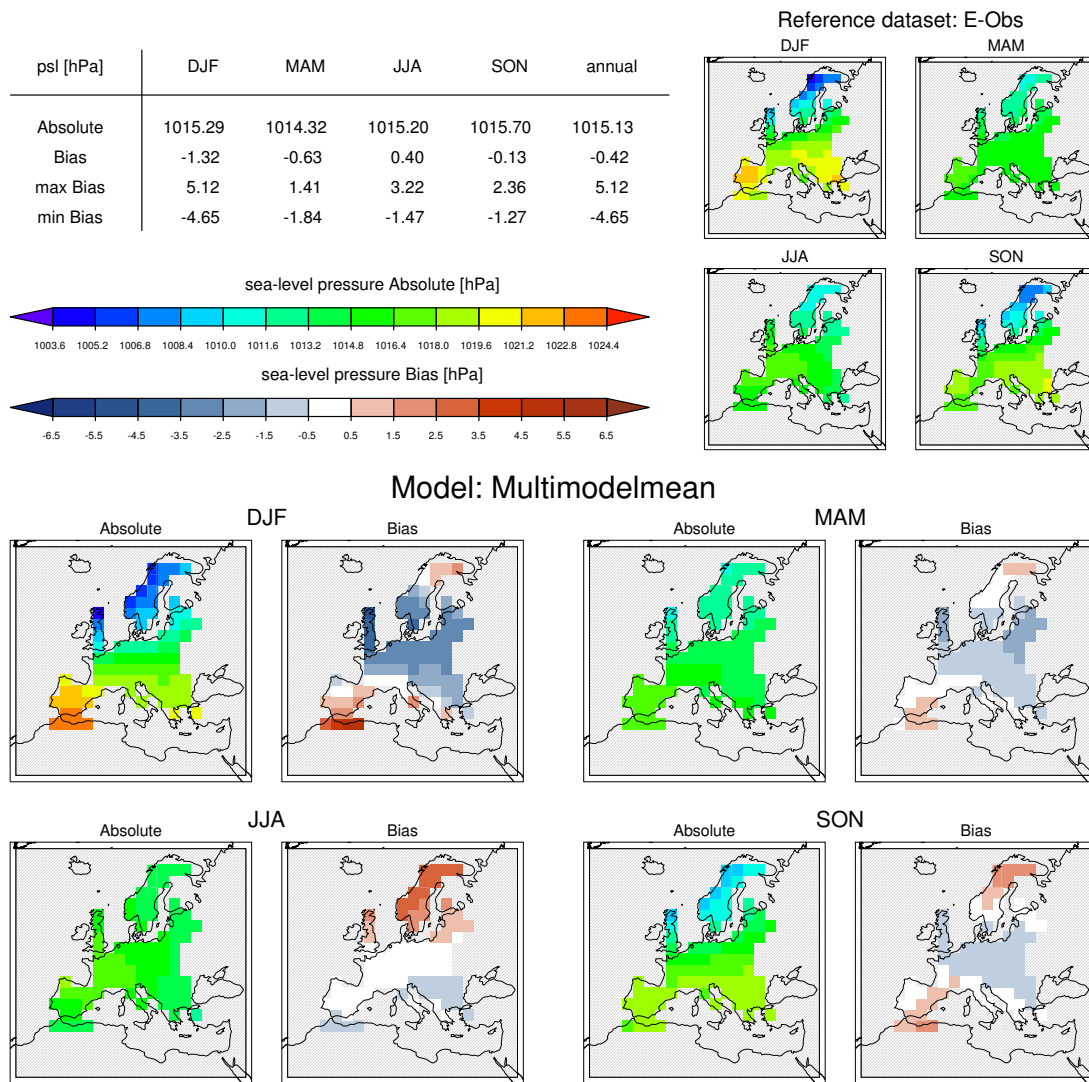


Figure 3.11: Mapplots of absolute and bias values of CMIP5 ensemble MMM of the psl over Europe between 1961 and 2000. As reference data serves E-OBS v5.

3.1 Evaluation of Surface Parameters over Europe

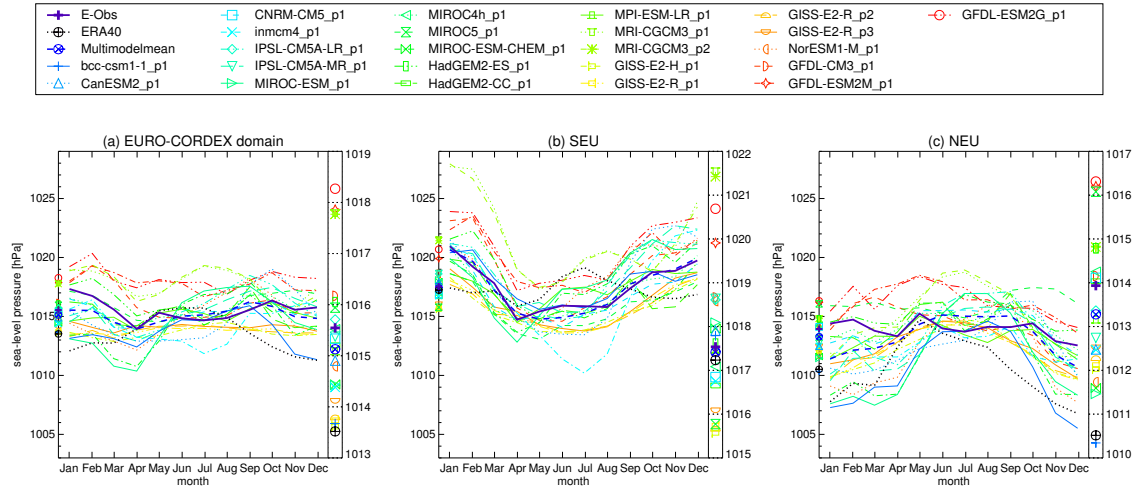


Figure 3.12: Seasonal cycle of psl of the CMIP5-ensemble for (a) the EURO-CORDEX domain (b) SEU and (c) NEU between 1961 and 2000.

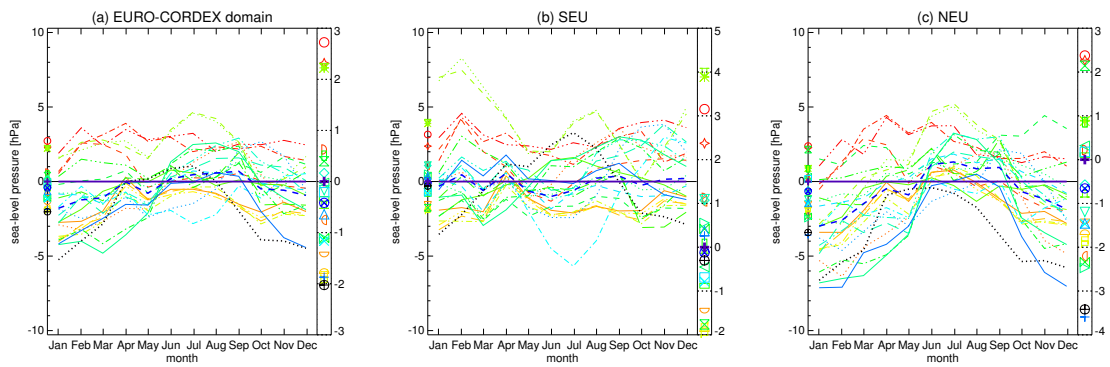


Figure 3.13: Bias in the seasonal cycle of psl of the CMIP5-ensemble for (a) the EURO-CORDEX domain (b) SEU and (c) NEU between 1961 and 2000 in reference to E-OBS. The legend is the same as in Figure 3.12.

3 Results

southern Europe particularly in summer. Also the seasonal cycle shows only poor agreement between the two with a strong negative bias in the winter half year over NEU and SEU and a positive bias over SEU in summer. ERA-40 quantiles are furthermore clinched together in the middle section of the distribution, especially over SEU. The slope of trend of ERA-40 is negative, while for E-OBS it is positive (both have the same magnitude of ± 0.01 hPa/year). While over SEU they show a sign of similarity they are more dislodged over NEU. Furthermore, ERA-40 shows a higher interannual variability than E-OBS over northern and southern Europe.

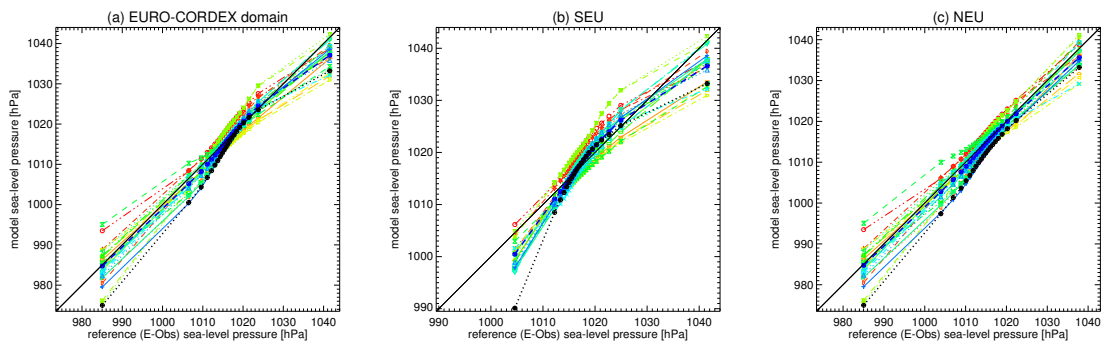


Figure 3.14: QQ plot of psl of the CMIP5-ensemble for (a) the EURO-CORDEX domain (b) SEU and (c) NEU between 1961 and 2000 in reference to E-OBS showing the 5 % quantiles. The legend is the same as in Figure 3.12.

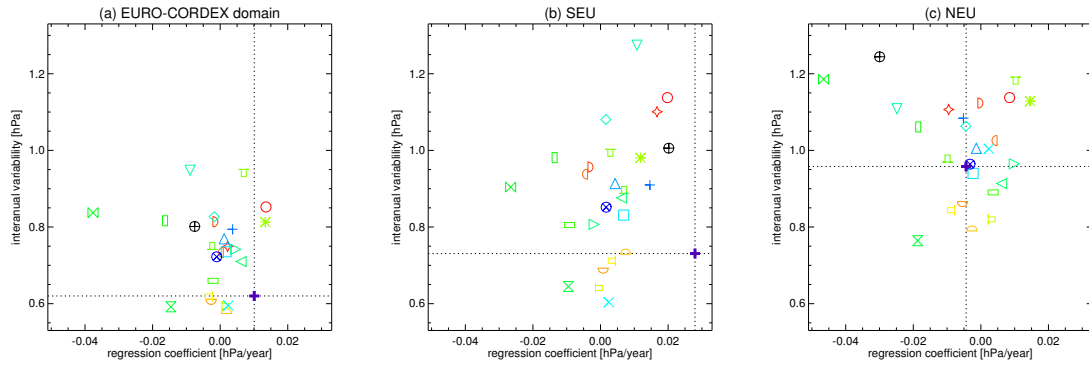


Figure 3.15: Scatter plot of slope and interannual variability based on linear regression for psl of the CMIP5-ensemble for (a) the EURO-CORDEX domain (b) SEU and (c) NEU between 1961 and 2000 in reference to E-OBS. The legend is the same as in Figure 3.12.

3.1.4 Combined treatment of the ground parameters

Figure 3.16 shows the MPI for ground parameters. The top three performing models in terms of the MPI for tas are GFDL-CM3, IPSL-CM5A-MR and HadGEM2-ES, for pr MIROC4h, CanESM2 and CanESM2 and for psl HadGEM2-ES, MIROC4h and HadGEM2-CC. If the particular MPIs are averaged over all parameters the best reproductions of the climate state are made by MIROC4h, HadGEM2-ES and GFDL-CM3. In the mean the ensemble MMM is the fourth best. Interestingly the MMM does not achieve the best results for a single parameter. ERA-40 performs best for tas and pr while its performance is very poor for psl.

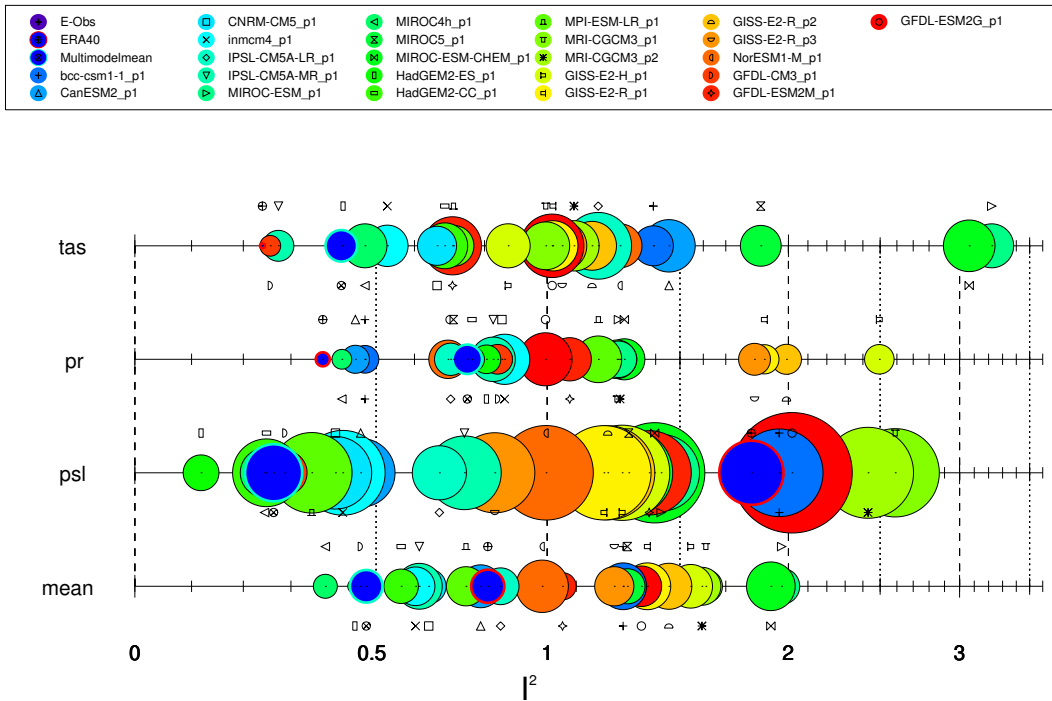


Figure 3.16: MPI of and the mean over all ground parameters of the CMIP5-ensemble for the EURO-CORDEX domain between 1961 and 2000. The circles account for the 80 % confidence interval.

3.2 Evaluation of Parameters over the Lateral Boundary

The lateral boundary evaluated in this section of the thesis is the lateral boundary of the EURO-CORDEX domain (see Section 2.1). A basic set of driving conditions, namely air temperature (t_a), specific humidity (h_{us}), eastward wind (u_a) and northward wind (v_a) are evaluated in terms of their ability to reproduce the seasonal cycle of ERA-40, similarity of their distributions by comparing the location of the quantiles and their capability to reproduce a similar trend and interannual variability on the four pressure levels 850 hPa, 700 hPa, 500 hPa, and 300 hPa and the four segments of the lateral boundary. An assessment via the MPI seeks to account for model performance on the variable level over the lateral boundary as a total. In a final assessment the performance of the models over the different parameters is combined.

3.2.1 Air Temperature (t_a)

As visible in Figure 3.17 the models are generally too warm at lower heights (850 hPa and 700 hPa), while they are too cold on 300 hPa (except for the bottom segment). E.g., over the Atlantic on 850 hPa the coldest model is still 1.3 °C warmer than ERA-40. The model spread is substantial and ranges from 4 °C to almost 7 °C. Concerning the shape of the seasonal cycle a description according to the different segments is beneficial. For the left segment the models cycle tends to be too shallow. The models show a strong positive bias on 850 hPa that turns into a negative bias on 300 hPa almost linearly over the different pressure levels (see Figure 3.18). Deviations from ERA-40 are strongest in winter, except for 300 hPa where they are peaking in June. Though not as strong as for the left segment, also for the top segment the seasonal cycle is represented too flat. The MMM has a positive bias on 700 hPa and 850 hPa of around 1.5 °C, almost no bias on 500 hPa and a negative bias of 2 °C on 300 hPa. For the right segment the picture turns in that sense, that the seasonal cycle of the MMM is too strong for 850 hPa and 700 hPa while it is in good agreement on 500 hPa and 300 hPa. For the bottom segment biases are positive on all pressure levels. While the shape of the seasonal cycle matches quite well between ERA-40 and the ensemble mean at 850 hPa, it is becoming increasingly flat for the latter with higher altitude.

Figure 3.19 presents the models 5 % quantiles in opposition to ERA-40 quantiles. In the mean the models distribution of temperature values is compressed at the lower to middle part while it is stretched at the upper tail for the left segment and on 850 hPa, 700 hPa, and 300 hPa. For the same segment but on 500 hPa the distribution is generally clinched and shows shorter tails. Over the top segment there is a slight stretching present till the median on 850 hPa, followed by a clinching till the 90 % quantile and a stretching onwards to the end of the distribution. On 700 hPa the MMM's distribution of t_a values is

3.2 Evaluation of Parameters over the Lateral Boundary

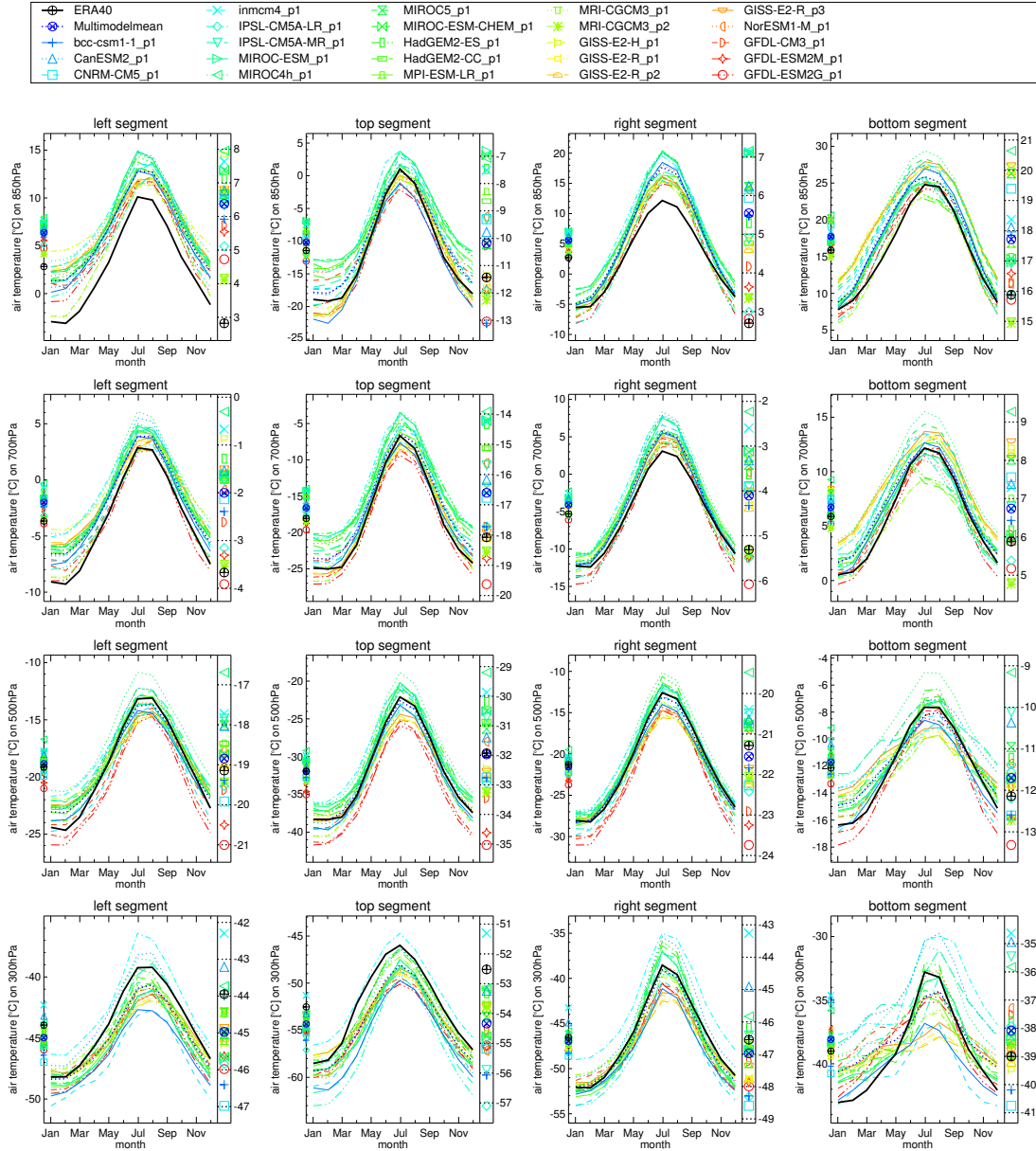


Figure 3.17: Seasonal cycle of t_a of the CMIP5-ensemble for the EURO-CORDEX lateral boundary between 1961 and 2000. The lines account for the different pressure levels, 850 hPa, 700 hPa, 500 hPa, and 300 hPa from top to bottom. The rows denote for the four segments left, top, bottom, and right from left to right.

3 Results

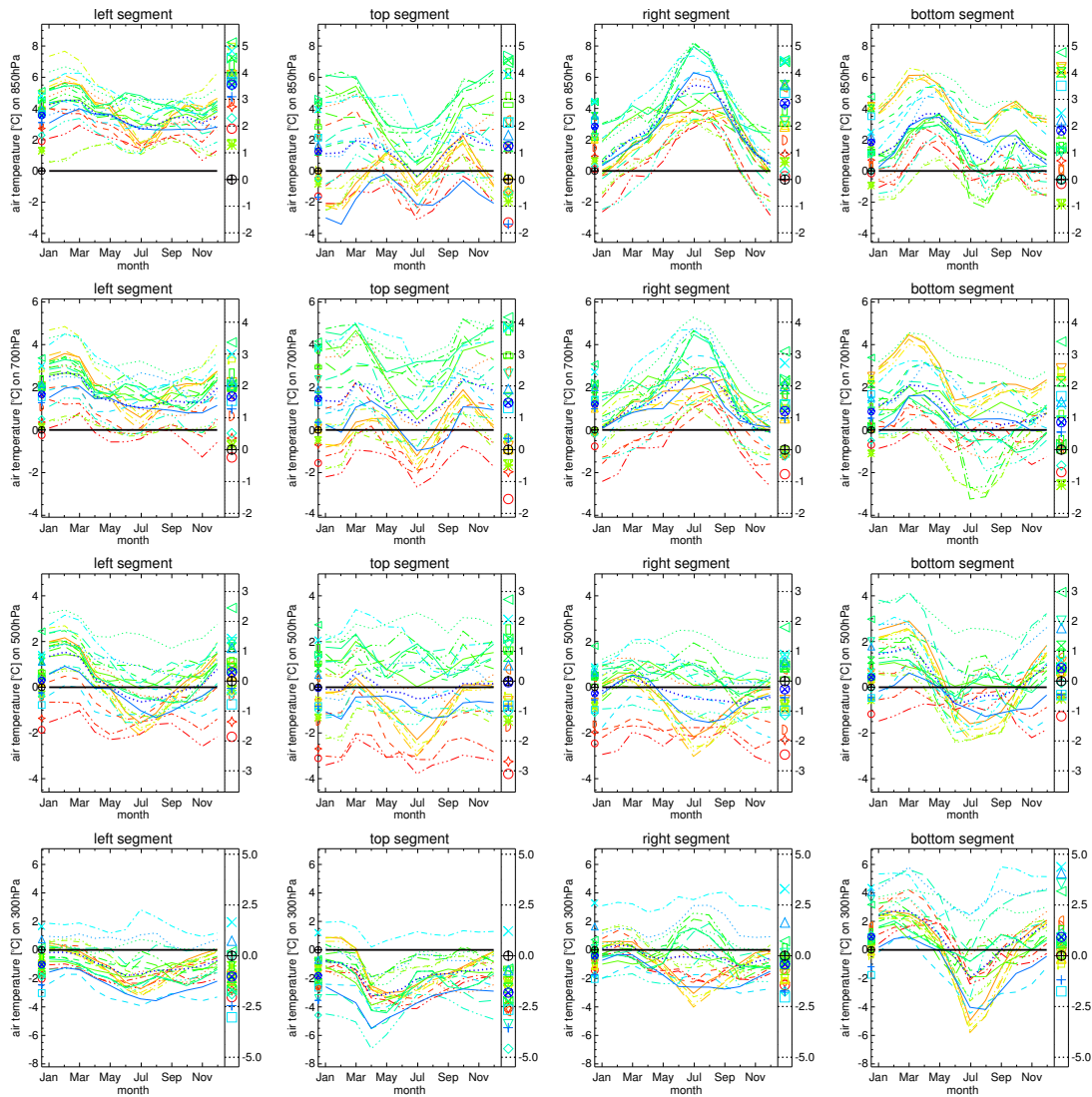


Figure 3.18: Bias in the seasonal cycle of t_a of the CMIP5-ensemble for the EURO-CORDEX lateral boundary between 1961 and 2000. The lines account for the different pressure levels, 850 hPa, 700 hPa, 500 hPa, and 300 hPa from top to bottom. The rows denote for the four segments left, top, bottom, and right from left to right. The legend is the same as in Figure 3.17.

generally clinched, while on 500 hPa the allocation of the quantiles is quite similar. On 300 hPa a clinching till the median is observable. Over the right lateral boundary model quantiles are generally located further apart than the reference ones on 850 hPa and 700 hPa. While the form of the distribution matches quite well on 500 hPa and 300 hPa till the 50th percentile, the upper half of the distribution is compressed till the 75 % quantile and stretched onwards to the maximum values. This issue is more pronounced on 300 hPa. For the part of the lateral boundary mainly located over the Sahara (bottom segment) the quantiles on 850 hPa are located further apart from one another, than it is the case for ERA-40, till the median and closer together onwards unto the maximum. For 700 hPa the distributions of the MMM and the reference match quite well. The same is the case on 500 hPa and 300 hPa until the 25 % quantile, but this connection is replaced by a clinching till the top end of the distributions. Results concerning the linear trend in ERA-40 are not in favour of the CMIP5 models (see Figure 3.20). This issue may be a result of incorrect reference data of ERA-40 and is discussed in more detail in Section 4.1. Nevertheless in the following main results of the MMM performance will be discussed in this paragraph. Throughout the different pressure levels over the left segment the ensemble mean shows a trend between 0.017 °C/year and 0.018 °C/year, while ERA-40 indicates a negative trend for the three higher pressure levels and a stronger positive trend on 300 hPa than the models. Except for 300 hPa, interannual variability of the models is higher than suggested by the reference. At least for the top segment there are some models suggesting a similar trend to the reference on 850 hPa and 300 hPa. On 850 hPa ERA-40 indicates a trend of around 0.009 °C/year while the MMM shows a stronger trend of 0.013 °C/year. On 700 hPa, 500 hPa and 300 hPa the MMM shows a trend of 0.019 °C/year, 0.018 °C/year and 0.007 °C/year while ERA-40 reports -0.002 °C/year, -0.01 °C/year and -0.002 °C/year, respectively. There are also mayor discrepancies concerning the interannual variability except for 850 hPa. A similar conclusion can be drawn for the right segment, where the reference recognizes almost no warming on all pressure levels (slope located around 0 °C/year) while the MMM indicates a positive trend of 0.02 °C/year. For the interannual variability thow the two are in better agreement. For the bottom segment the following can be registered. On 850 hPa the interannual variability is in good agreement, while the MMM shows a trend of around 0.02 °C/year in contrast to ERA-40 that indicates a trend of 0.002 °C/year. On 700 hPa, 500 hPa, and 300 hPa the MMM's trend still is around 0.02 °C/year, while ERA-40 shows less or even a negative trend and a stronger variability.

3 Results

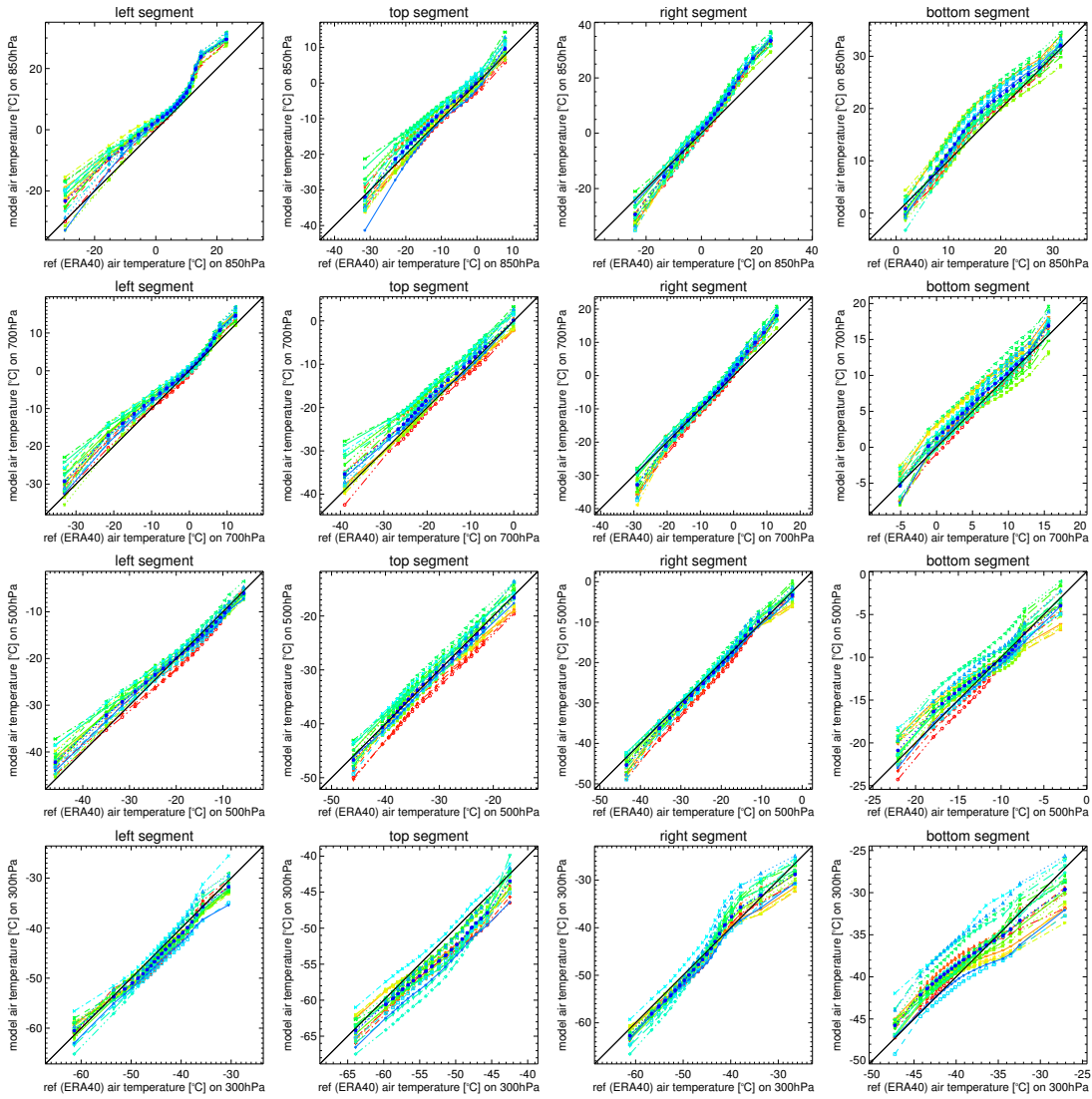


Figure 3.19: QQ plot of t_a of the CMIP5-ensemble for the EURO-CORDEX lateral boundary between 1961 and 2000 in reference to ERA-40 showing the 5 % quantiles. The lines account for the different pressure levels, 850 hPa, 700 hPa, 500 hPa, and 300 hPa from top to bottom. The rows denote for the four segments left, top, bottom, and right from left to right. The legend is the same as in Figure 3.17.

3.2 Evaluation of Parameters over the Lateral Boundary

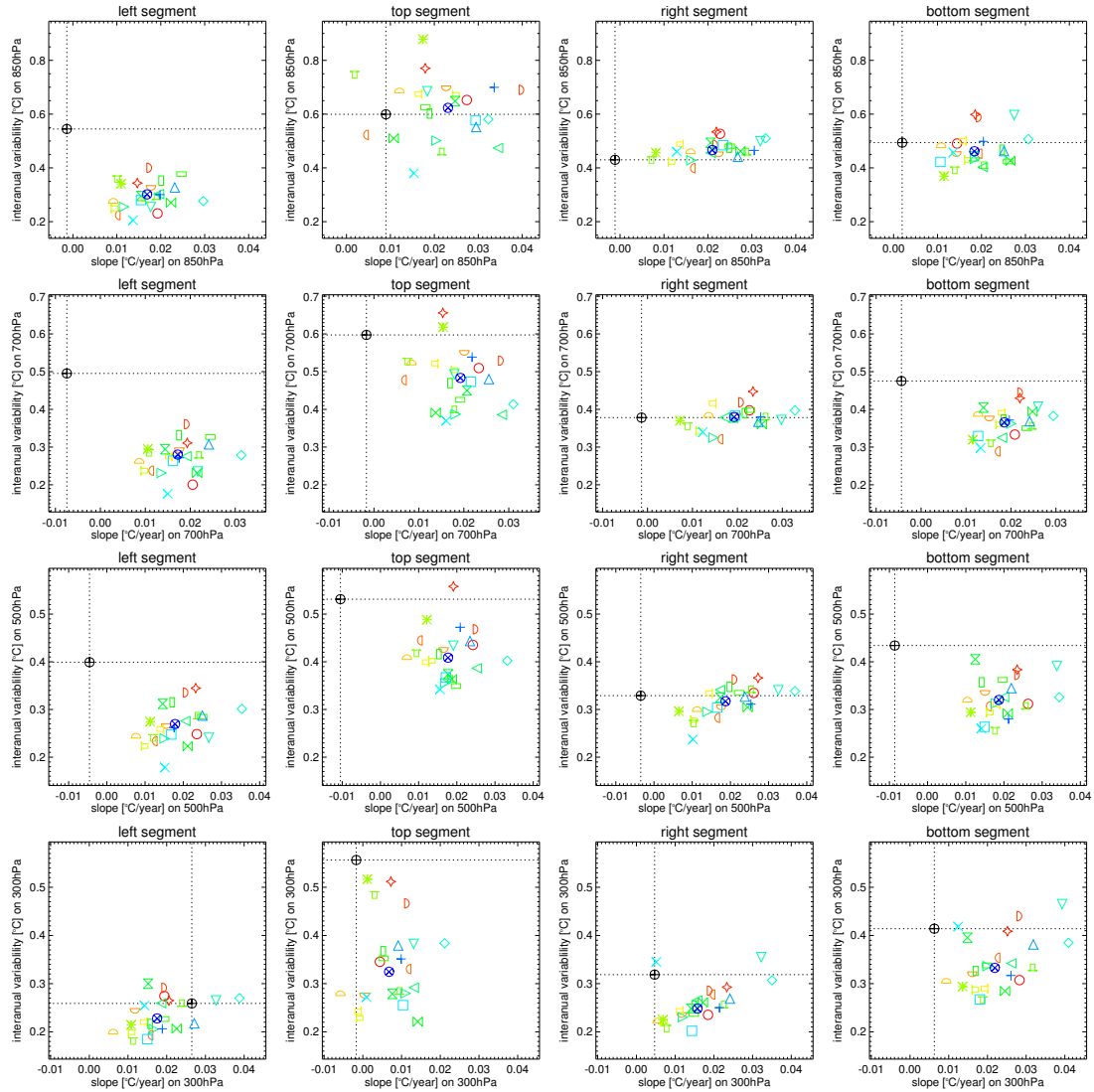


Figure 3.20: Scatter plot of slope and interannual variability based on linear regression for t_a of the CMIP5-ensemble for the EURO-CORDEX lateral boundary between 1961 and 2000. The lines account for the different pressure levels, 850 hPa, 700 hPa, 500 hPa, and 300 hPa from top to bottom. The rows denote for the four segments left, top, bottom, and right from left to right. The legend is the same as in Figure 3.17.

Summarising the results mentioned above we can state that the models show a warm bias on higher pressure levels with strongest deviations during summer over the right segment and during winter over the bottom segment, while a cold bias is found on 300 hPa. The MMM's distribution is very fragmented in terms of the various segments and pressure levels, what makes generalisations a difficult endeavour. While ERA-40 shows a negative or no temperature trend over most segments and especially in the lower to middle troposphere, the single models as well as the MMM deviate strongly from this behaviour and show a positive trend. However, interannual variability is in some places reproduced acceptable.

Figure 3.21 presents an integrated assessment of t_a on all pressure levels employing the MPI yields as the top three performing models in terms of the MPI on 300 hPa MRI-CGCM3_p1, MRI-CGCM3_p2 and GISS-E2-R_p3; on 500 hPa bcc-csm1-1, NorESM1-M and GISS-E2-R_p3; on 700 hPa MRI-CGCM3_p2, MRI-CGCM3_p1 and IPSL-CM5A-LR; and on 850 hPa MRI-CGCM3_p2, MRI-CGCM3_p1 and GFDL-ESM2G. An averaging over the different pressure levels yields that the two different realizations of perturbed physics of the MRI-CGCM3 model perform best in terms of the applied MPI. In quite a distance the NorESM1-M Model achieves the third best results. Although always located close to the best performers, the MMM does only achieve the best results on 500 hPa. In the mean it is located between the second and third best model.

3.2 Evaluation of Parameters over the Lateral Boundary

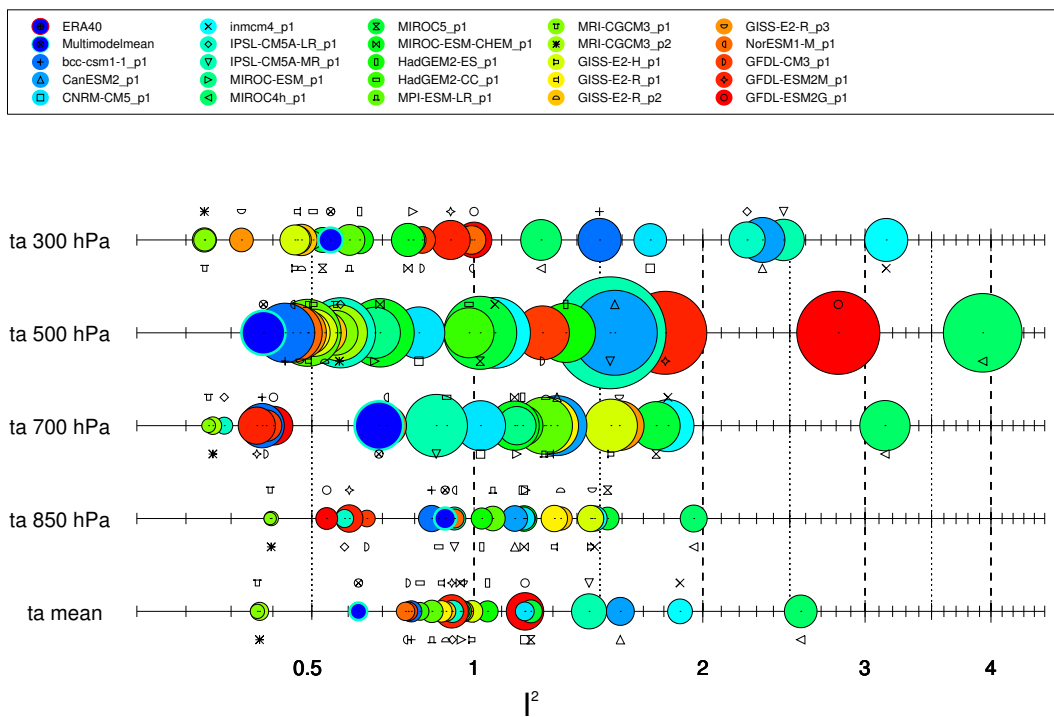


Figure 3.21: MPI of and the mean over all pressure levels of t_a of the CMIP5-ensemble for the EURO-CORDEX lateral boundary between 1961 and 2000. The circles account for the 90 % confidence interval.

3.2.2 Specific Humidity (hus)

The CMIP5 models are too dry in terms of hus as visible in Figure 3.22. Over the Atlantic ocean (left segment) the shape and amplitude of the seasonal cycle is reproduced quite well by the models. Except for 850 hPa, where the MMM shows a negative bias of -0.6 g/kg, only small biases are present. On 300 hPa ERA-40's seasonal cycle shows a longer phase of higher humidity than the MMM. For the top segment ERA-40's seasonal cycle is also reproduced quite well by the mean of the models in terms of the general shape on 850 hPa, 700 hPa and 500 hPa. On 300 hPa the MMM is too dry, with the peak of hus reaching 0.07 g/kg in July while ERA-40 presents 0.09 g/kg. The models are too wet on 850 hPa and 700 hPa and too dry on 300 hPa, while on 500 hPa no bias can be noted. For the right segment the following aspects can be listed. The MMM is too dry on 850 hPa especially during summer with a bias of -0.5 g/kg. On 500 hPa and 300 hPa it is slightly dryer. The form of the modelled seasonal cycle is too flat on 850 hPa and 300 hPa, while it is more profound than ERA-40 for 700 hPa and 500 hPa. Like for the left flank the seasonal cycle shows a longer phase of higher humidity than the observation on 300 hPa. For 700 hPa the two seasonal cycles match almost perfectly. Highest model spread can be noted for the bottom flank likely attributable to its location over the tropical zone. On this flank also the biggest biases can be found for hus. In Figure 3.23 it is visible, that in the mean the models are -1 g/kg dryer than the reference on ERA-40 on 850 hPa, -0.5 g/kg on 700 hPa and 0.023 g/kg wetter on 300 hPa. The shape of the seasonal cycle is only reproduced poorly with a mismatching location of yearly peaks and minima on all pressure levels.

According to the QQ plots the distribution of hus values for the MMM over the left segment on 850 hPa are strongly clinched together for the whole distribution especially near the 25 % quantile with the exception of the extremes (see Figure 3.24). A clinching till the median followed by a stretching can be noted for 700 hPa. The distributions of quantiles for 500 hPa and 300 hPa match quite well with the observations except for the maximum value. For the top segment the distributions agree reasonably well on 850 hPa and 700 hPa and almost perfect on 500 hPa. On 300 hPa though a major clinching can be noted except for the maximum value which goes together with the reference. Also for the right segment distributions are in good agreement on 700 hPa, 500 hPa and 300 hPa with the exception for the upper tail. For 850 hPa a clinched MMM distribution is shown between the lower quartile and the 90 % quantile. The distributions for the bottom segment are in better agreement on 700 hPa and 500 hPa while for 300 hPa the quantiles of the MMM are further apart from one another than it is the case for the reference. Some clinching of the quantiles can be noted for 850 hPa.

Major discrepancies concerning the slope of the trend and interannual variability are found for hus visible in Figure 3.25. For the left seg-

3.2 Evaluation of Parameters over the Lateral Boundary

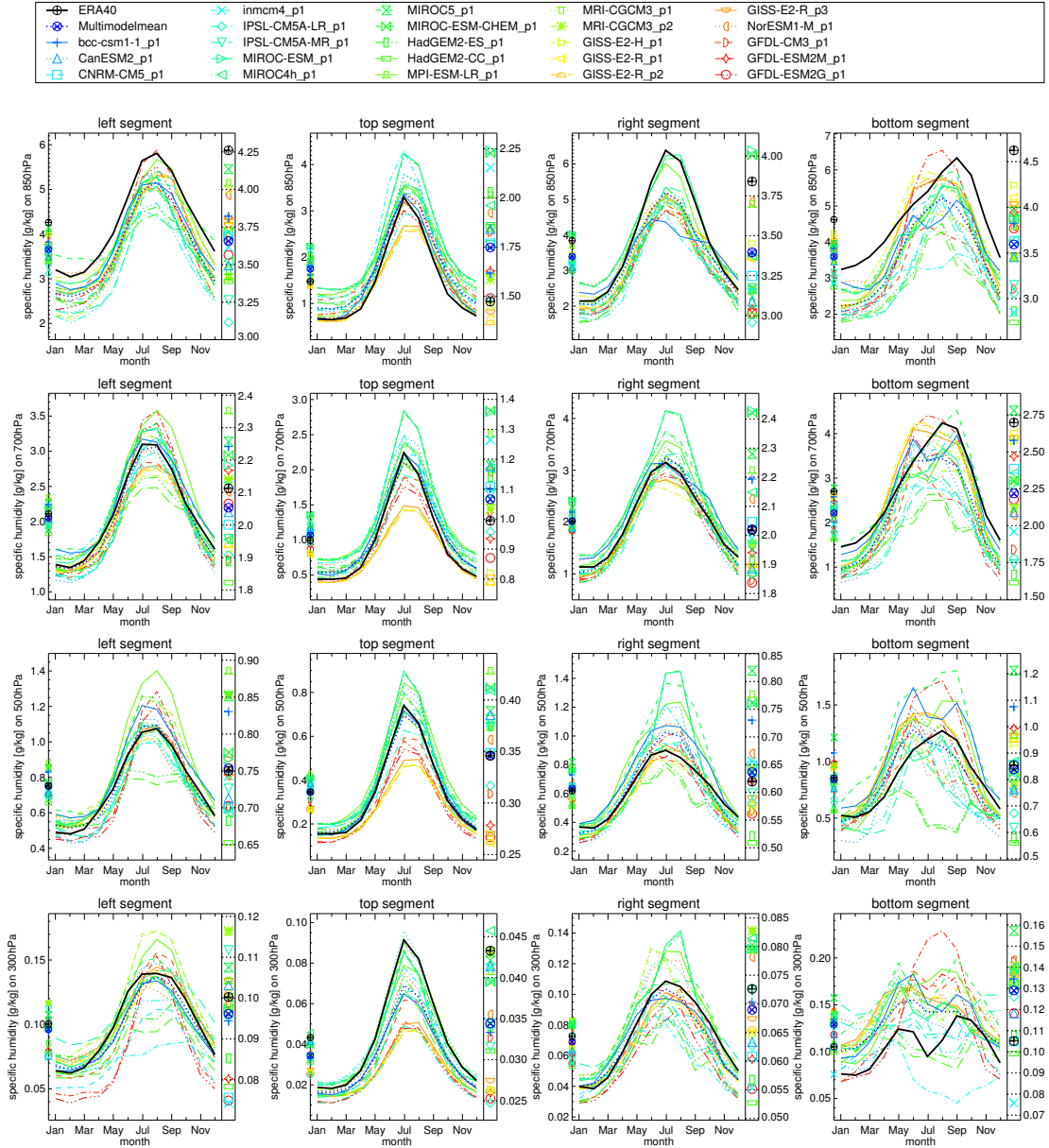


Figure 3.22: Seasonal cycle of hus of the CMIP5-ensemble for the EURO-CORDEX lateral boundary between 1961 and 2000. The lines account for the different pressure levels, 850 hPa, 700 hPa, 500 hPa, and 300 hPa from top to bottom. The rows denote for the four segments left, top, bottom, and right from left to right.

3 Results

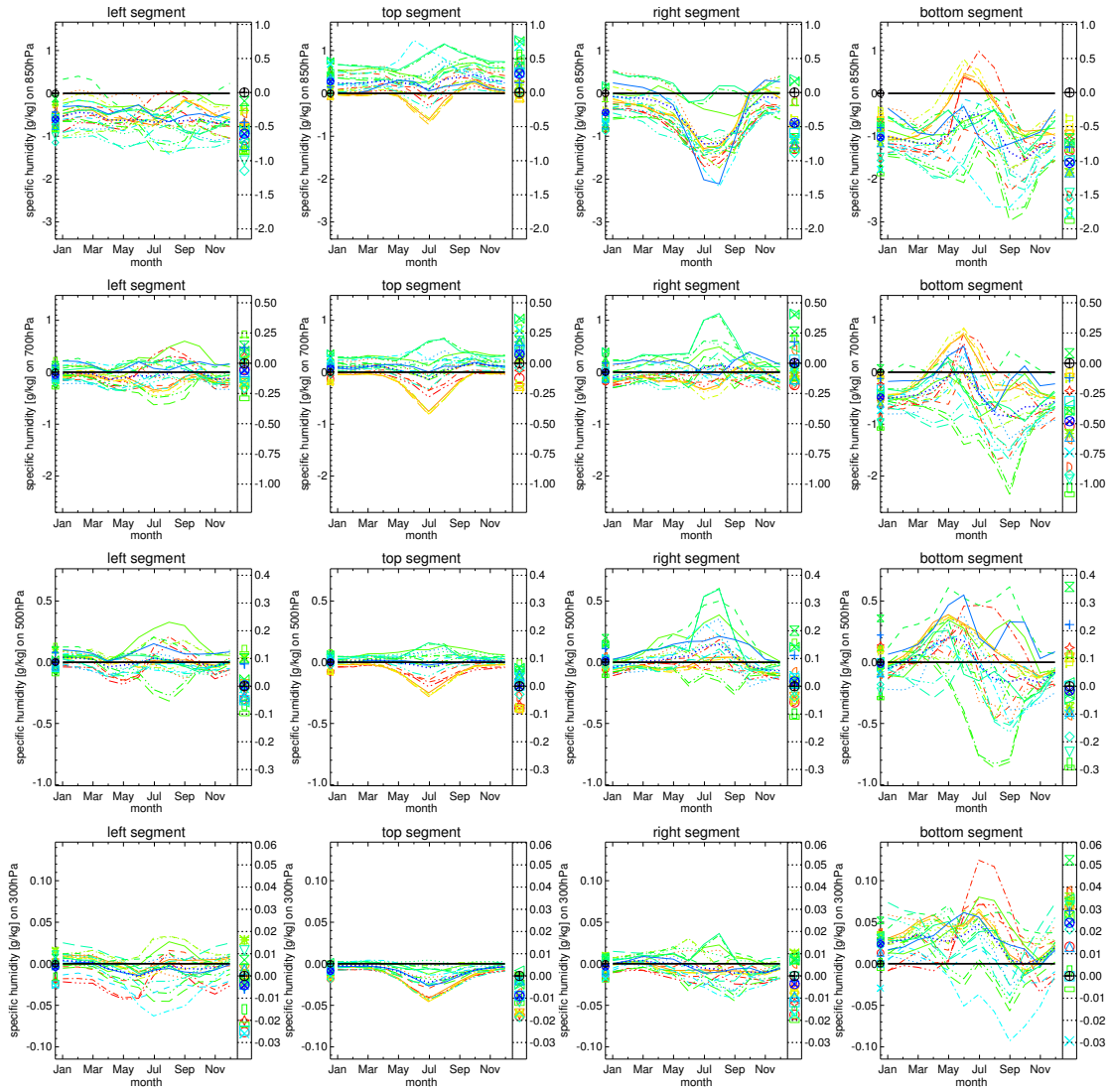


Figure 3.23: Bias in the seasonal cycle of hus of the CMIP5-ensemble for the EURO-CORDEX lateral boundary between 1961 and 2000. The lines account for the different pressure levels, 850 hPa, 700 hPa, 500 hPa, and 300 hPa from top to bottom. The rows denote for the four segments left, top, bottom, and right from left to right. The legend is the same as in Figure 3.22.

ment the trend of the models is generally lower than the trend shown by ERA-40; 0.003 g/(kg · year) compared to 0.007 g/(kg · year) on 850 hPa, 0.002 g/(kg · year) to 0.0075 g/(kg · year) on 700 hPa, 0.0011 g/(kg · year) to 0.002 g/(kg · year) on 500 hPa, only on 300 hPa the trends are matching. Concerning the interannual variability the models are in fair agreement on 850 hPa and 300 hPa, while they are too static on 700 hPa and 500 hPa. For the northern top segment trend dissimilarities persist but are now reversed. ERA-40's trend on 850 hPa is 0.001 g/(kg · year) while the MMM yields 0.003 g/(kg · year), on 700 hPa and 500 hPa the reference shows no trend while the models mean is 0.0017 g/(kg · year) and 0.006 g/(kg · year), on 300 hPa the trends are -0.0001 g/(kg · year) and 0.00006 g/(kg · year). Hus of the reference is more variable on 700 hPa to 300 hPa and more static on 850 hPa. Also for the right segment differences concerning the trend are quite high. While ERA-40 indicates a trend of 0.001 g/(kg · year) the MMM yields 0.0038 g/(kg · year) on 850 hPa. On 700 hPa they signal -0.0016 g/(kg · year) against 0.0021 g/(kg · year), respectively; on 500 hPa -0.001 g/(kg · year) and 0.0011 g/(kg · year) and on 300 hPa -0.00025 g/(kg · year) and 0.00015 g/(kg · year). The interannual variability is in good agreement with a tendency of the models being too static. For the bottom segment the models are in better agreement with the reference trend on 850 hPa and 700 hPa. Over all pressure levels on 500 hPa and 300 hPa trend discrepancies for hus are largest over the bottom segment with -0.0008 g/(kg · year) and 0.0014 g/(kg · year), and -0.00036 g/(kg · year) and 0.00027 g/(kg · year) for ERA-40 and the MMM, respectively. Again the models are generally too static concerning the interannual variability.

In summary it can be noted that when averaged over all segments of the lateral boundary the models show a negative bias for hus on 850 hPa and 700 hPa and a positive bias on 300 hPa. Except for the left segment of the lateral boundary the models show a stronger positive trend than the reference in the mean. Generally, the models are too static in terms of interannual variability. Also notably the lower the pressure level is the higher the spread of the models.

In terms of the MPI the models MRI-CGCM3_p2, MRI-CGCM3_p1 and CanESM2 perform best on 850 hPa; MRI-CGCM3_p2, CNRM-CM5 and MRI-CGCM3_p1 on 700 hPa; MRI-CGCM3_p2, MRI-CGCM3_p1 and GFDL-ESM2M on 500 hPa; and GISS-E2-R_p2, GISS-E2-R_p3 and GISS-E2-R_p1 on 300 hPa (see Figure 3.26). Averaging over the pressure levels attests MRI-CGCM3_p2 to perform best, MRI-CGCM3_p1 second best and CNRM-CM5 third best in terms of the MPI. The MMM does again not perform best for hus, although being ranked third in terms of the MPI.

3 Results

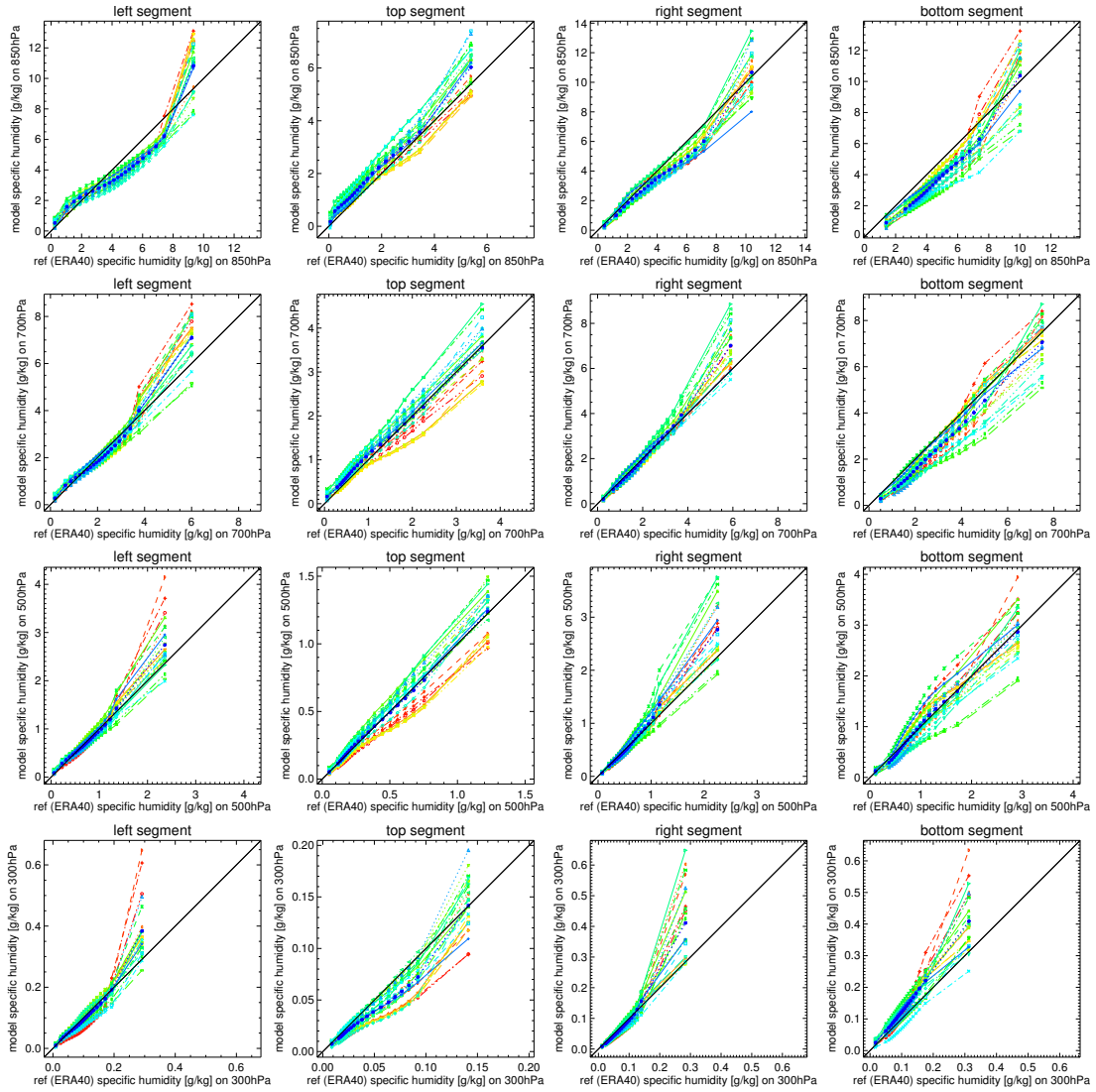


Figure 3.24: QQ plot of hus of the CMIP5-ensemble for the EURO-CORDEX lateral boundary between 1961 and 2000 in reference to ERA-40 showing the 5 % quantiles. The lines account for the different pressure levels, 850 hPa, 700 hPa, 500 hPa, and 300 hPa from top to bottom. The rows denote for the four segments left, top, bottom, and right from left to right. The legend is the same as in Figure 3.22.

3.2 Evaluation of Parameters over the Lateral Boundary

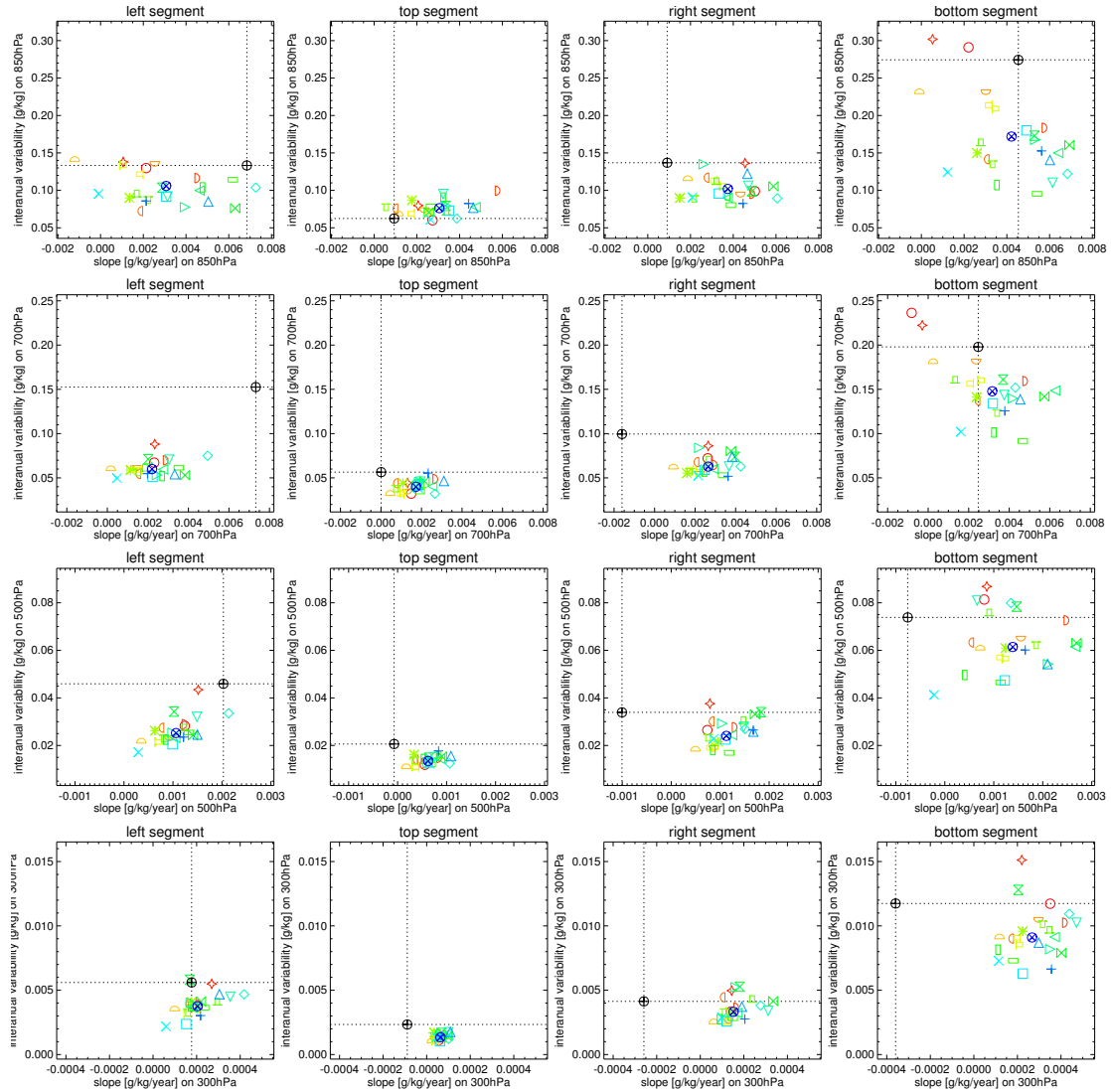


Figure 3.25: Scatter plot of slope and interannual variability based on linear regression for hus of the CMP5-ensemble for the EURO-CORDEX lateral boundary between 1961 and 2000. The lines account for the different pressure levels, 850 hPa, 700 hPa, 500 hPa, and 300 hPa from top to bottom. The rows denote for the four segments left, top, bottom, and right from left to right. The legend is the same as in Figure 3.22.

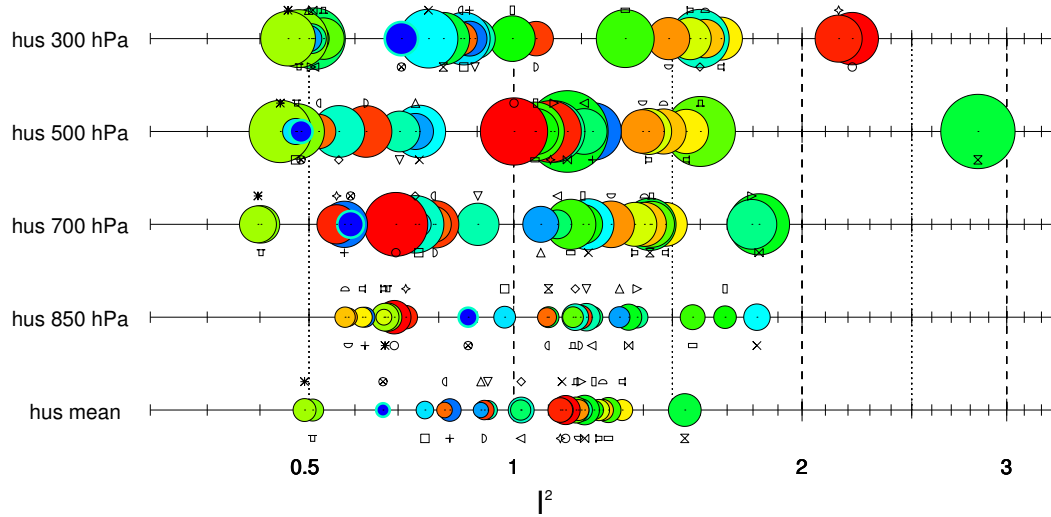


Figure 3.26: MPI of and the mean over all pressure levels of hus of the CMIP5-ensemble for the EURO-CORDEX lateral boundary between 1961 and 2000. The circles account for the 90 % confidence interval. The legend is the same as in Figure 3.21.

3.2.3 Eastward Wind (u_a)

While the model ensemble annual mean of u_a for the left segment is too small on 850 hPa, it turns out to be too big on 300 hPa as indicated in Figure 3.27. On 850 hPa the discrepancies prevail throughout the year, on 700 hPa the modelled wind is too weak predominantly from June to October, on 500 hPa the mean bias is vanishingly low while there exists an overestimation from November until May and an underestimation for the rest of the year, and on 300 hPa the modelled wind fits quite good for the summer months and is too strong for the other three seasons. Within the top segment the modelled u_a is too weak on all pressure levels. In the mean the seasonal cycle looks quite similar with strongest deviations in spring. For the right segment the following statements can be made. The basic shapes of the seasonal cycle of the MMM and ERA-40 look quite similar, while at the same time a strong overestimation of the wind is present, with the exception of 850 hPa where an underrepresentation is observed. Strongest deviations are visible for January to March on 700 hPa and above (see Figure 3.28). On 300 hPa the models low intensity timespan during the summer half year is too narrow. On 500 hPa and especially on 300 hPa all the single models indicate a stronger wind than ERA-40. For the bottom segment the modelled wind is too weak from 850 hPa to 500 hPa while it is too strong on 300 hPa. On 850 hPa and 700 hPa the modelled seasonal cycle is well below the reference throughout the year. Like for the right segment the mayor deficiencies evolve from an overestimation of wind speeds on 500 hPa and 300 hPa from January to March. Overall, the MMM in the bottom segment shows the biggest biases on all pressure levels except for 500 hPa, where biases are strongest over the right segment.

In relation to the reference the MMM distribution shows a longer tail at the lower end for 850 hPa and 700 hPa and a slight skew to the right on 500 hPa and 300 hPa over the left segment (see Figure 3.29). For the top segment longer tails at both ends of the ensemble mean's distribution are visible for 850 hPa and 500 hPa, a stretching of the quantiles from the lower tail till the median for 700 hPa and an overestimation of the maximum value for 300 hPa. Inspecting the QQ plots of the right segment yields a slight skew of the distribution to the right on 300 hPa and 500 hPa. On 700 hPa the MMM's distribution shows longer tails, and on 850 hPa a clinching of the quantiles till the lower quartile and a stretching onwards to the extremes. The strongest deviations from the ERA-40 distribution are visible for the bottom segment. Shorter tails are apparently present for the MMM's distribution on 850 hPa, while on 700 hPa and 500 hPa longer tails are shown. For 300 hPa the model ensembles distribution is strongly skewed to the right.

While ERA-40 shows a small positive trend for the left segment on all pressure levels the MMM shows a trend approximately $0.005 \text{ m}/(\text{s} \cdot \text{year})$ to $0.01 \text{ m}/(\text{s} \cdot \text{year})$ smaller located around $\pm 0 \text{ m}/(\text{s} \cdot \text{year})$ (see Figure 3.30).

Moreover, the models mean interannual variability is slightly lower than the one indicated by ERA-40. Over the top segment the picture reverses. The MMM now indicates an interannual variability being bigger than the one shown by the reference. On 850 hPa and 700 hPa ERA-40 indicates a trend around $-0.008 \text{ m}/(\text{s} \cdot \text{year})$ while the ensemble mean shows no trend on all pressure levels. On 500 hPa and 300 hPa reference and MMM agree with each other. ERA-40 trend's slope further increases constantly from $-0.002 \text{ m}/(\text{s} \cdot \text{year})$ on 850 hPa to $-0.015 \text{ m}/(\text{s} \cdot \text{year})$ on 300 hPa over the right segment. In contrast the MMM shows a trend of $0 \text{ m}/(\text{s} \cdot \text{year})$ on all levels. At least the interannual variability of models and reference is in better agreement. For the segment located over the Sahara ERA-40 again indicates a negative trend increasing with height from $-0.018 \text{ m}/(\text{s} \cdot \text{year})$ on 850 hPa to $-0.05 \text{ m}/(\text{s} \cdot \text{year})$ on 300 hPa. In comparison to the other segments, the bottom segment is the one showing the highest degree of variability. This relationship is reproduced well by the models, while the reproduced eastward wind fields are too static.

To sum up, biggest biases are found over the right segment. On the two pressure levels closer to the surface predominantly a negative bias is found, while on the uppermost a positive bias is found more frequently. The QQ plots show that the models' distributions are broader than the reference, leading to longer tails at both sides of the distribution. Trends are underestimated by the MMM for the lateral boundary zone located over the Atlantic, while they are overestimated for the rest. In the mean the models show almost no trend. Interannual variability on the other hand is underestimated for all segments except for the top one, where the contrary is the case. The ERA-40 data exhibits strong leaps in the seasonal cycle e.g., on 850 hPa which may emerge by the long shapes of the segments, since this behaviour is partly reproduced by the models.

Figure 3.31 shows the MPI for ua. In terms of the MPI the top three performers on 300 hPa are: CNRM-CM5, MPI-ESM-LR and MIROC-ESM-CHEM; on 500 hPa: MRI-CGCM3_p2, MRI-CGCM3_p1 and CNRM-CM5; on 700 hPa: MIROC5, MIROC4h and HadGEM2-CC; and on 850 hPa: MIROC4h, MIROC5 and CNRM-CM5. Averaging the MPI over the different pressure levels yields to the following ranking beginning with the best: CNRM-CM5, MIROC5 and MIROC4h. Again the MMM does not perform best on a single pressure level and is ranked third when averaging over all pressure levels.

3.2 Evaluation of Parameters over the Lateral Boundary

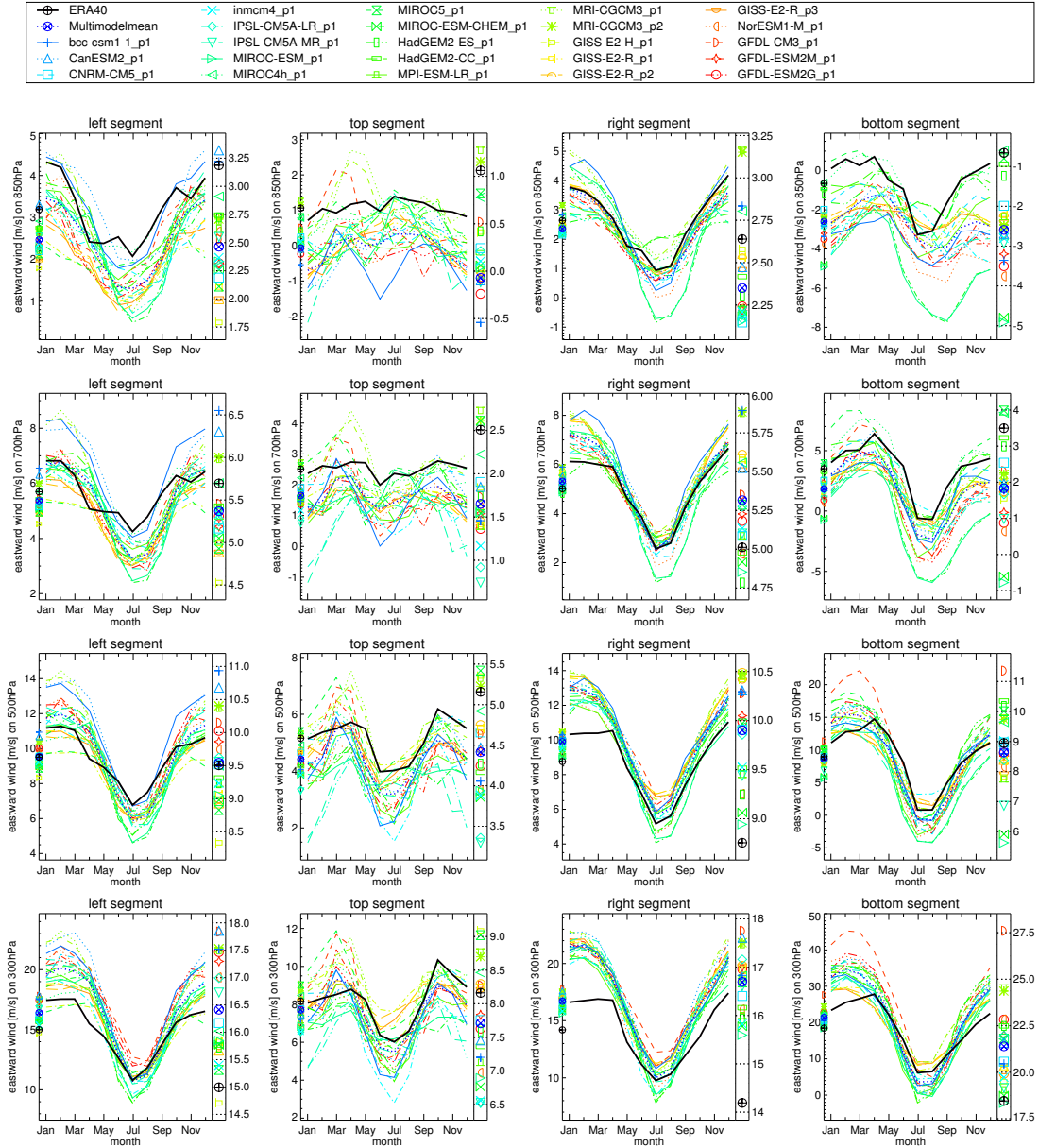


Figure 3.27: Seasonal cycle of u_a of the CMIP5-ensemble for the EURO-CORDEX lateral boundary between 1961 and 2000. The lines account for the different pressure levels, 850 hPa, 700 hPa, 500 hPa, and 300 hPa from top to bottom. The rows denote for the four segments left, top, bottom, and right from left to right.

3 Results

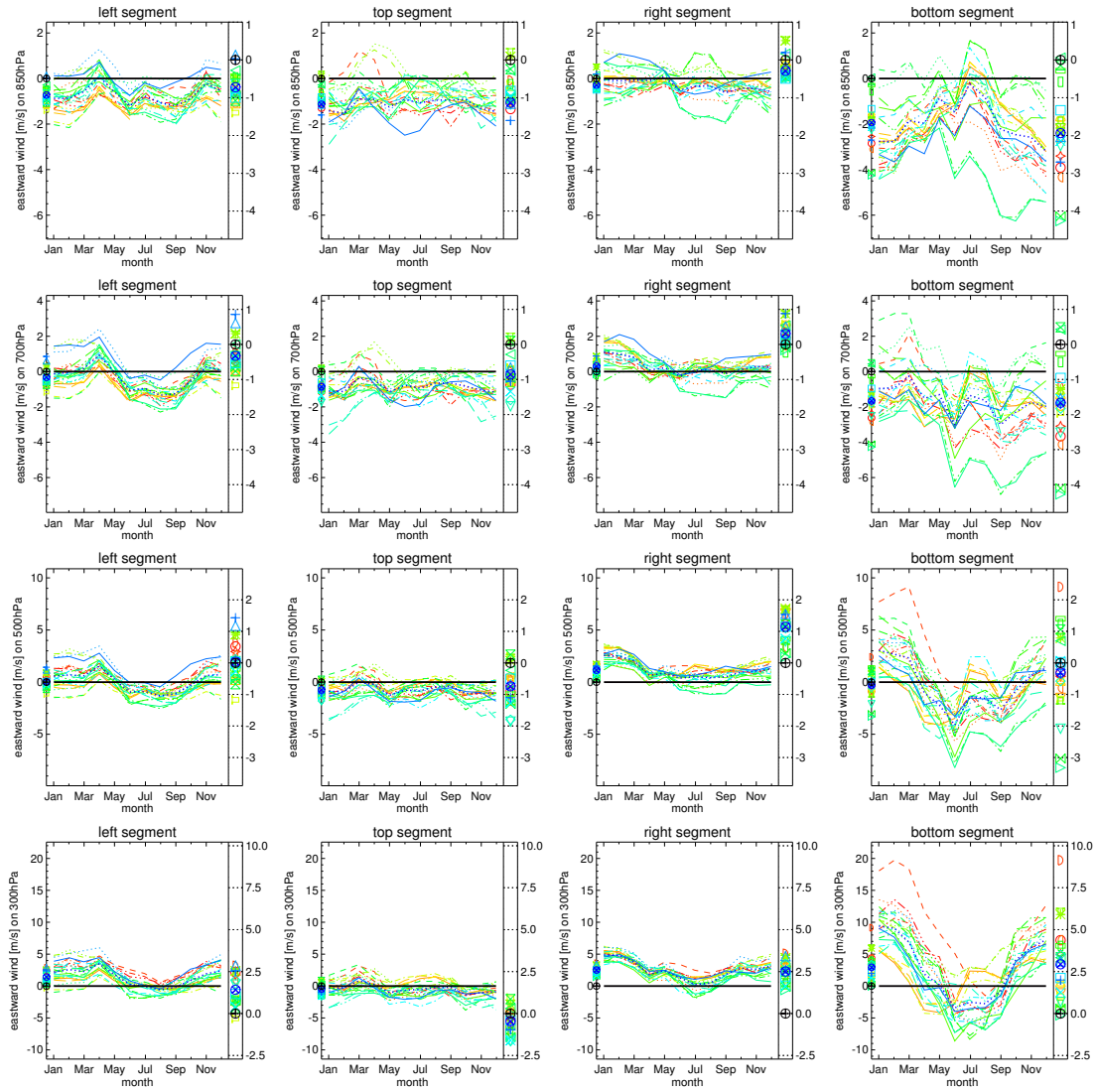


Figure 3.28: Bias in the seasonal cycle of u_a of the CMIP5-ensemble for the EURO-CORDEX lateral boundary between 1961 and 2000. The lines account for the different pressure levels, 850 hPa, 700 hPa, 500 hPa, and 300 hPa from top to bottom. The rows denote for the four segments left, top, bottom, and right from left to right. The legend is the same as in Figure 3.27.

3.2 Evaluation of Parameters over the Lateral Boundary

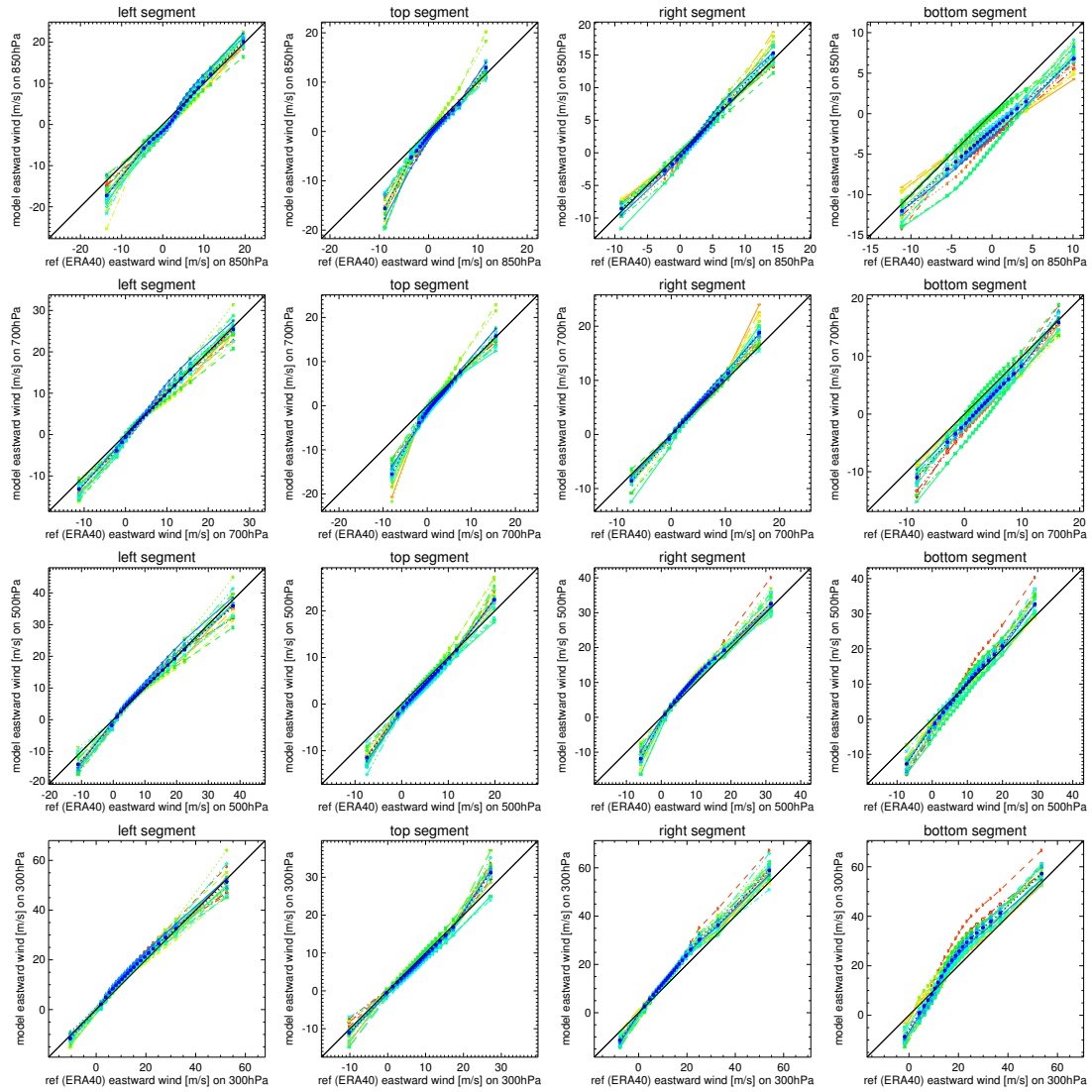


Figure 3.29: QQ plot of u_a of the CMIP5-ensemble for the EURO-CORDEX lateral boundary between 1961 and 2000 in reference to ERA-40 showing the 5 % quantiles. The lines account for the different pressure levels, 850 hPa, 700 hPa, 500 hPa, and 300 hPa from top to bottom. The rows denote for the four segments left, top, bottom, and right from left to right. The legend is the same as in Figure 3.27.

3 Results

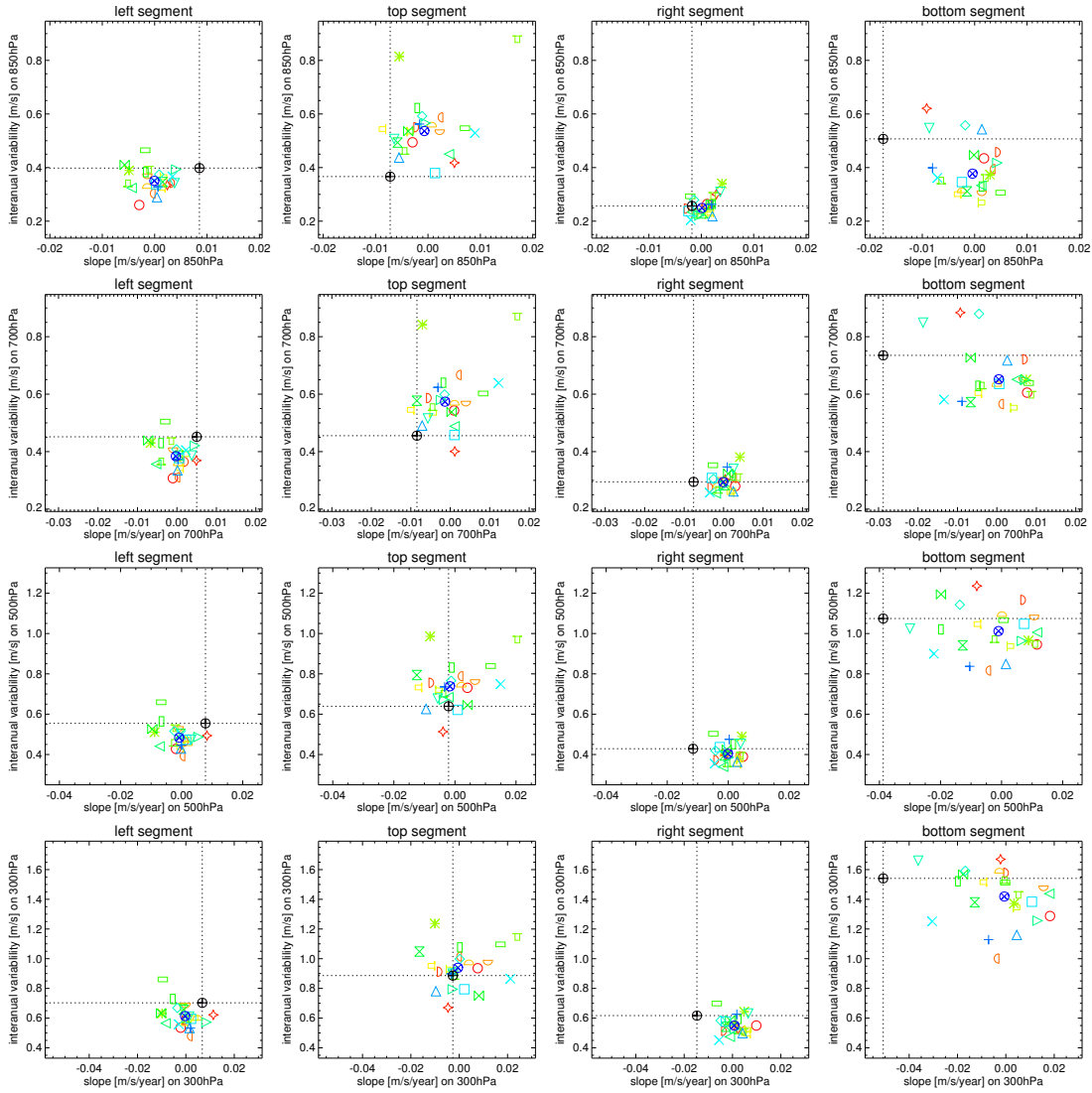


Figure 3.30: Scatter plot of slope and interannual variability based on linear regression for u_a of the CMIP5-ensemble for the EURO-CORDEX lateral boundary between 1961 and 2000. The lines account for the different pressure levels, 850 hPa, 700 hPa, 500 hPa, and 300 hPa from top to bottom. The rows denote for the four segments left, top, bottom, and right from left to right. The legend is the same as in Figure 3.27.

3.2 Evaluation of Parameters over the Lateral Boundary

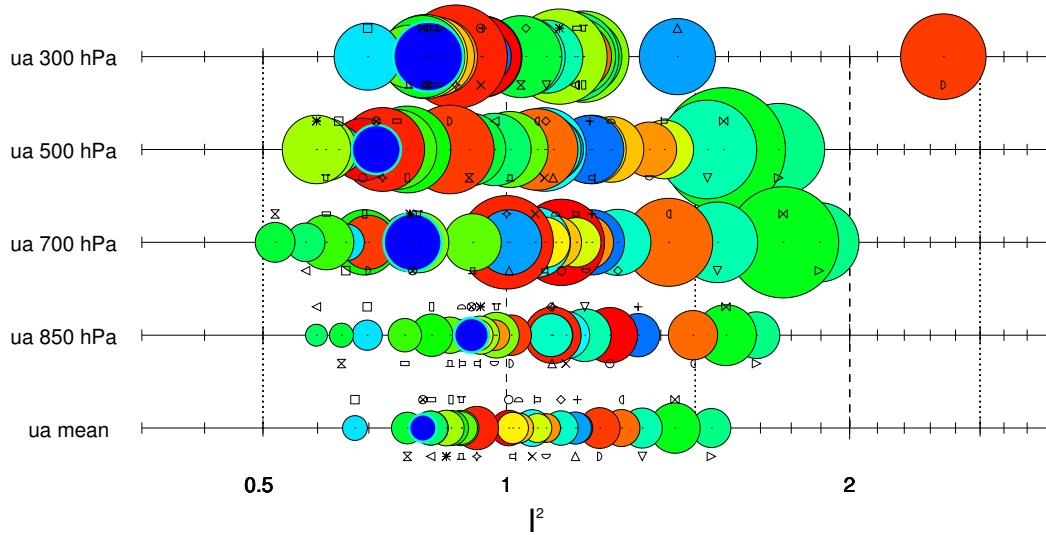


Figure 3.31: MPI of and the mean over all pressure levels of ua of the CMIP5-ensemble for the EURO-CORDEX lateral boundary between 1961 and 2000. The circles account for the 90 % confidence interval. The legend is the same as in Figure 3.21.

3.2.4 Northward Wind (v_a)

Monthly mean magnitudes of v_a are far weaker than their eastward counterpart. Also their seasonal cycle is less pronounced for the evaluated areas, characterized by multiple maximas and minimas.

A comparison of left segment's northward wind fields in Figure 3.32 and Figure 3.33 shows that the MMM has a negative bias on all levels compared to ERA-40. This arises mainly from discrepancies between November and April for 300 hPa to 700 hPa. On 300 hPa all single models show a negative bias. Over the top segment and the right segment the models show the strongest biases, although the general shape of the MMM seems to be in good agreement with the reference. On all pressure levels over the top segment all the models show a negative bias throughout the year. In contrast to ERA-40 that indicates a positive v_a the MMM displays negative annual v_a values. Biases between MMM and ERA-40 are from 850 hPa to 300 hPa -1.5 m/s, -1.3 m/s, -1.7 m/s and -2.2 m/s, respectively. Over the right segment the ensemble mean has positive biases throughout the year and the seasonal cycle shows major discrepancies concerning the position of maxima and minima. While ERA-40 shows a southward wind flow, the models indicate the opposite. Positive biases from 850 hPa to 300 hPa amount to 0.8 m/s, 1.5 m/s, 1.8 m/s and 1.9 m/s, respectively. Over the bottom segment the MMM has a negative bias on 850 hPa and 700 hPa and a positive one on the remaining two. While the shape of the seasonal cycle is reproduced in some aspects for 850 hPa, 700 hPa and 500 hPa there do exist major discrepancies on 300 hPa. On 850 hPa the biggest negative biases are found from June to October. Until 300 hPa this biases reduce further and the biggest positive biases are now found between December and March.

Comparing the distributions of the MMM and ERA-40 via the QQ plots yields that the ensembles mean distribution over the left segment features a longer tail at the lower end of the distribution (see Figure 3.34). On 700 hPa, 500 hPa and 300 hPa this observation continues and extends by shorter upper tail of the distributions that are skewed to the right. Aside from the before mentioned bias, the distribution on 850 hPa over the top segment shows longer tails. On 500 hPa and 300 hPa a longer tail at the lower end of the distribution is accompanied by a cinching of the quantiles beginning with the 10th percentile. The same finding is true for 700 hPa, but is extended by the models distribution return to the same maximum value as shown by ERA-40. Over the right segment a skewing of the MMM's distribution to the right is visible on 850 hPa, 700 hPa, 500 hPa and 300 hPa. Also the distributions on 850 hPa over the bottom segment show the same behaviour. The MMM features shorter tails at both sides of the distribution on 700 hPa, and a skewing to the left on 500 hPa. On 300 hPa the distributions of ERA-40 and the ensemble mean look quite similar, while the upper tail of the MMM is longer.

Concerning trend's slope and interannual variability presented in Figure 3.35 the following statements can be made. While the MMM indicates a trend around zero on all pressure levels over the left segment, ERA-40 shows a negative trend with increasing magnitude with height, ranging from -0.002 m/(s · year) on 850 hPa to -0.014 m/(s · year) on 300 hPa. The interannual variability is in good agreement over the left segment. Over the top segment the ensemble mean indicates a trend of approximately -0.001 m/(s · year) on all pressure levels, while ERA-40 indicates a positive trend between 0.008 m/(s · year) and 0.009 m/(s · year) and shows more variability than the MMM. Also over the right segment, trend discrepancies are relatively high. Again, the MMM shows almost no trend, with a trend's slope between ± 0.001 m/(s · year), while ERA-40 rates the slope at about -0.011 m/(s · year), -0.015 m/(s · year), -0.02 m/(s · year) and -0.021 m/(s · year) respectively from 850 hPa to higher altitudes. ERA-40 values show more variability than the models. For the bottom segment ERA-40 indicates a trend between 0.002 m/(s · year) and 0.005 m/(s · year) and the MMM a vanishingly weak negative trend, while the interannual variability between models and reference shows only small discrepancies.

Summarizing the results from above we can say that all models show a positive annual bias over the right segment and a negative annual bias over the top segment. For the top segment this underrepresentation of the northward air flow is present in every month of the year. A general skewing of the distributions to the right is observed. Like for *ua* the models show no trend of notable magnitude on all levels and segments of the lateral boundary and deviate strongly from the reference. There is a model tendency of under representing the interannual variability. Also for *va* ERA-40 and the models show strong leaps in the seasonal cycle.

The study of the MPI identifies MRI-CGCM3_p1, MRI-CGCM3_p2 and MPI-ESM-LR as the top three performers in descendent order on 300 hPa and 500 hPa (see Figure 3.36). On 700 hPa the best performing model is GFDL-ESM2G followed by MPI-ESM-LR and GFDL-ESM2M and on 850 hPa it is GISS-E2-R_p2 before GISS-E2-R_p1 and GISS-E2-H. In the mean over all pressure levels MPI-ESM-LR performs best, MRI-CGCM3_p2 second best and MRI-CGCM3_p1 third best. Again the two MRI-CGCM3 are ranked under the top three performers. Also the MMM does not perform best in a single category while placing itself on the fourth place in the mean and being among the better performing models for the single pressure levels.

3 Results

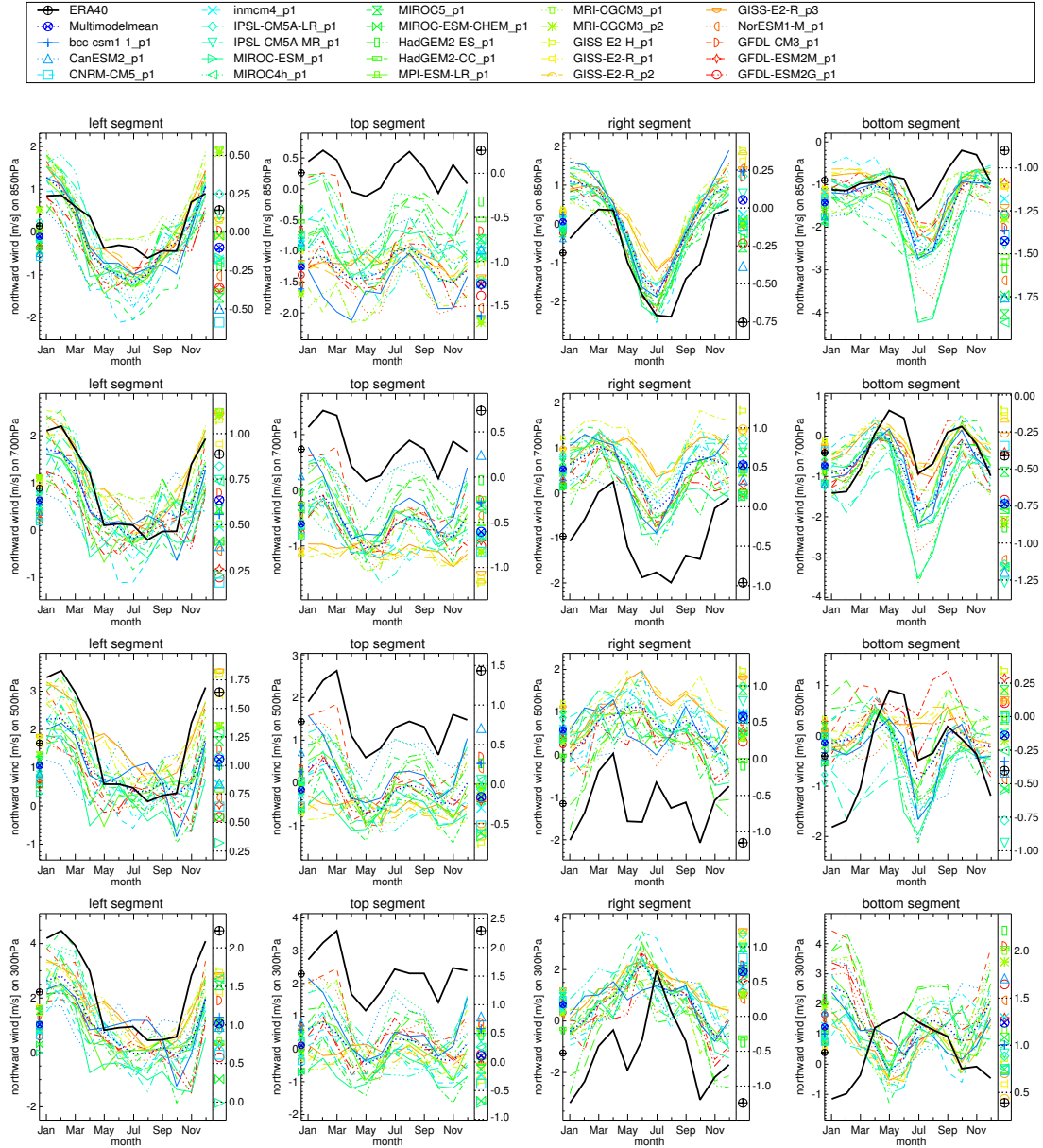


Figure 3.32: Seasonal cycle of v_a of the CMIP5-ensemble for the EURO-CORDEX lateral boundary between 1961 and 2000. The lines account for the different pressure levels, 850 hPa, 700 hPa, 500 hPa, and 300 hPa from top to bottom. The rows denote for the four segments left, top, bottom, and right from left to right.

3.2 Evaluation of Parameters over the Lateral Boundary

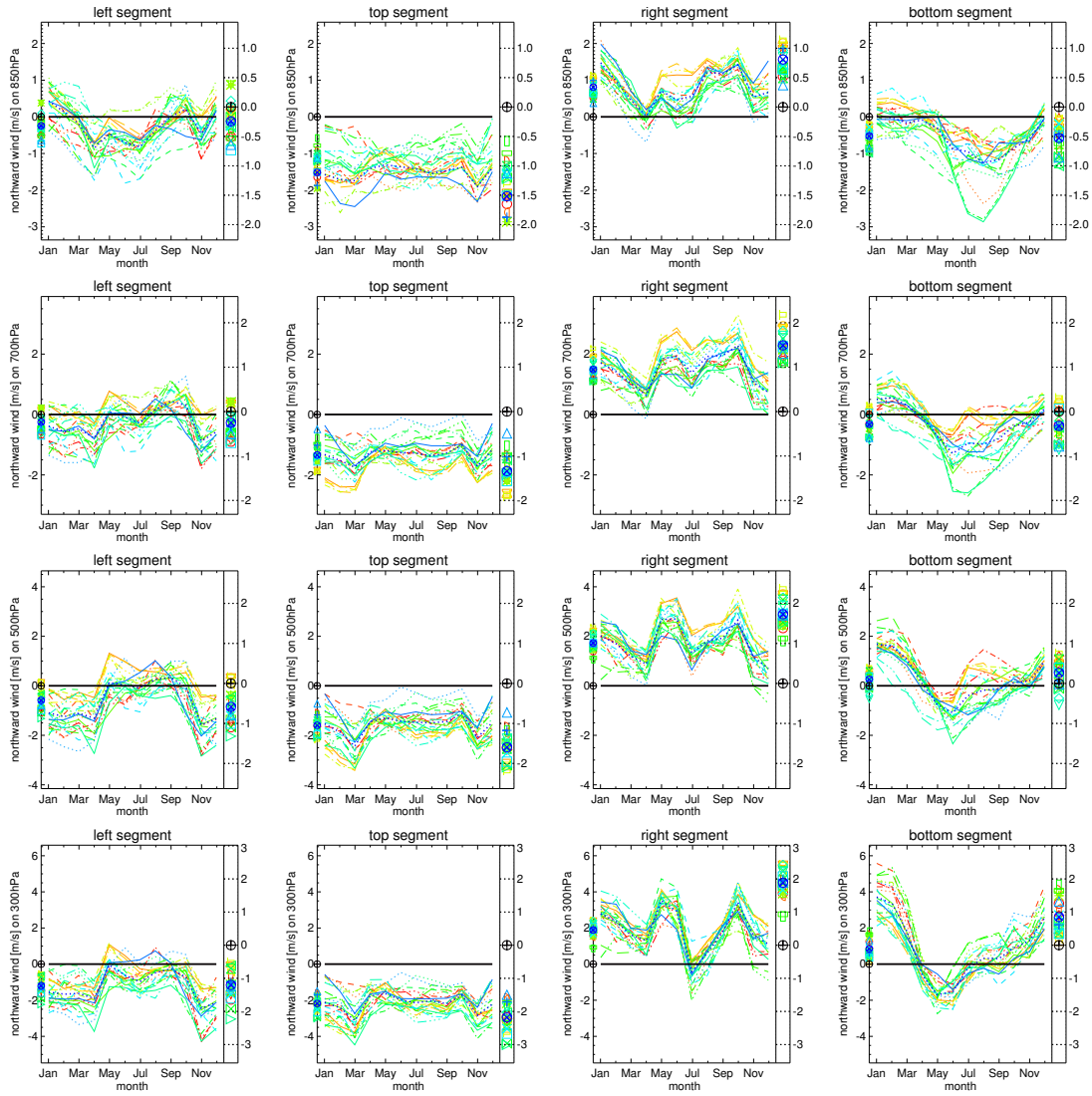


Figure 3.33: Bias in the seasonal cycle of v_a of the CMIP5-ensemble for the EURO-CORDEX lateral boundary between 1961 and 2000. The lines account for the different pressure levels, 850 hPa, 700 hPa, 500 hPa, and 300 hPa from top to bottom. The rows denote for the four segments left, top, bottom, and right from left to right. The legend is the same as in Figure 3.32.

3 Results

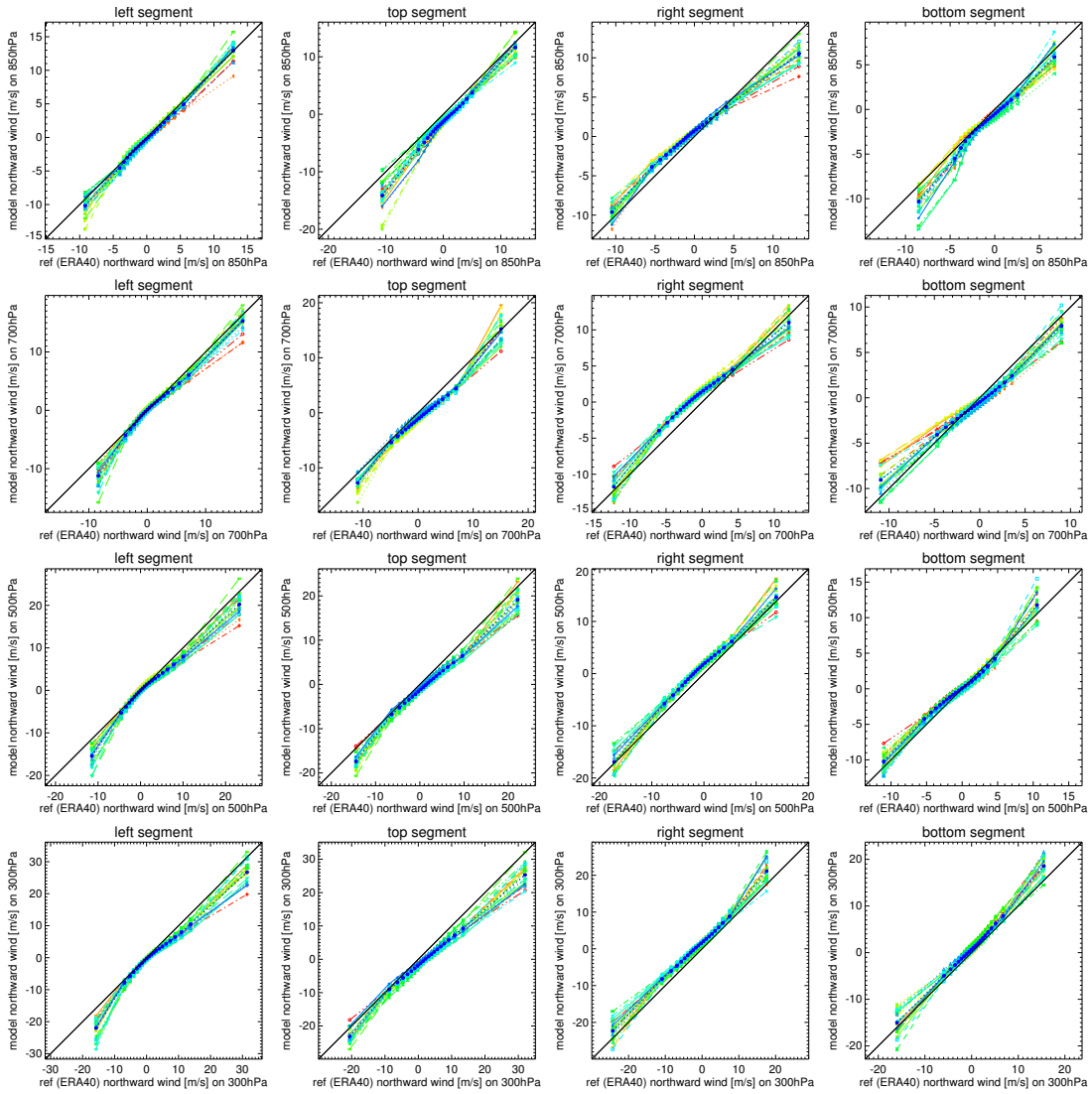


Figure 3.34: QQ plot of v_a of the CMIP5-ensemble for the EURO-CORDEX lateral boundary between 1961 and 2000 in reference to ERA-40 showing the 5 % quantiles. The lines account for the different pressure levels, 850 hPa, 700 hPa, 500 hPa, and 300 hPa from top to bottom. The rows denote for the four segments left, top, bottom, and right from left to right. The legend is the same as in Figure 3.32.

3.2 Evaluation of Parameters over the Lateral Boundary

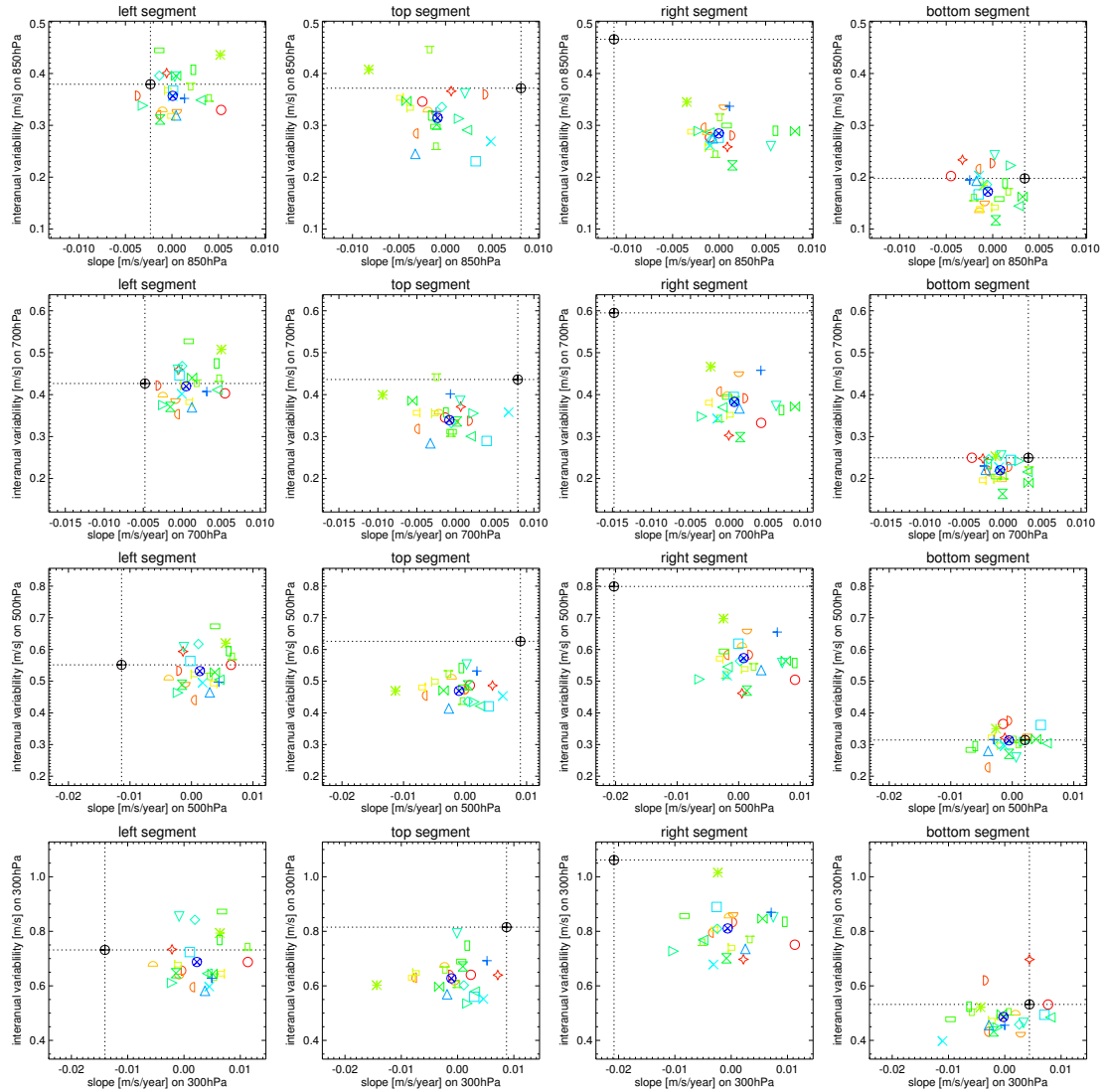


Figure 3.35: Scatter plot of slope and interannual variability based on linear regression for v_a of the CMIP5-ensemble for the EURO-CORDEX lateral boundary between 1961 and 2000. The lines account for the different pressure levels, 850 hPa, 700 hPa, 500 hPa, and 300 hPa from top to bottom. The rows denote for the four segments left, top, bottom, and right from left to right. The legend is the same as in Figure 3.32.

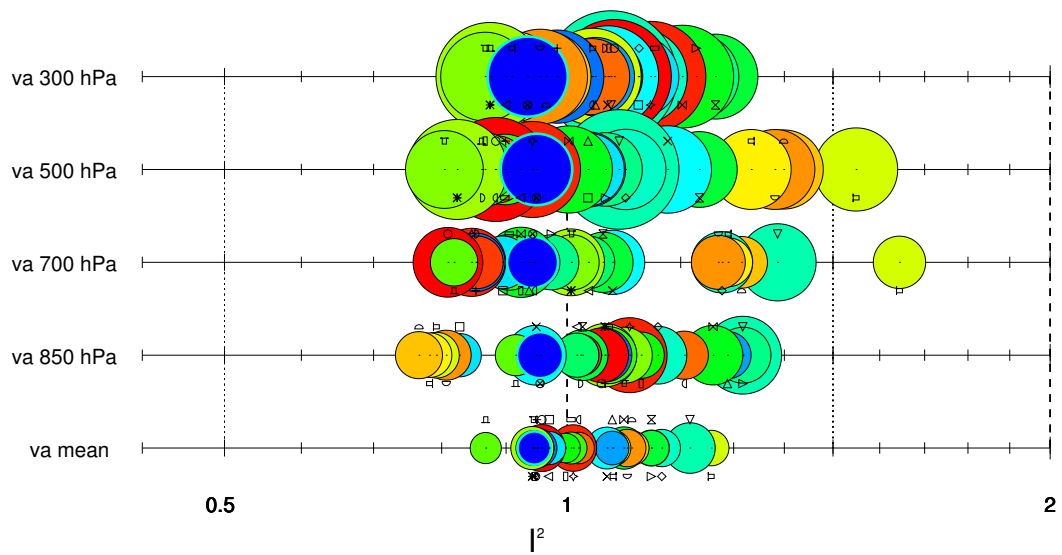


Figure 3.36: MPI of and the mean over all pressure levels of va of the CMIP5-ensemble for the EURO-CORDEX lateral boundary between 1961 and 2000. The circles account for the 90 % confidence interval. The legend is the same as in Figure 3.21.

3.2.5 Combined Assessment

Although figures combining the single parameters on the different pressure levels over the four segments of the lateral boundary were produced in the course of the thesis, the author refrains from presenting them in this section. The reason is that in the spatially distant segments single parameters feature relatively big differences in their magnitude and moreover averaging over them would possibly average out interesting aspects of the models ability to model the climate state between 1961 and 2000. Therefore, only results of a combination of the single parameter mean MPIs are presented in Figure 3.37. This MPI was calculated by averaging over the parameter MPIs on pressure levels. Not very surprisingly, considering their good performance for the single parameters¹, the two different perturbed physics ensembles of the Japanese MRI-CGCM3 model, namely MRI-CGCM3_p2 and MRI-CGCM3_p1 are performing best in the mean. In quite a distance the third best model in terms of the MPI is the French CNRM-CM5 model, the fourth best the Chinese bcc-csm1-1 model and the fifth best is the German MPI-ESM-LR model.

¹performing best for ta, hus and va and fifth and eighth best for ua, respectively.

3 Results

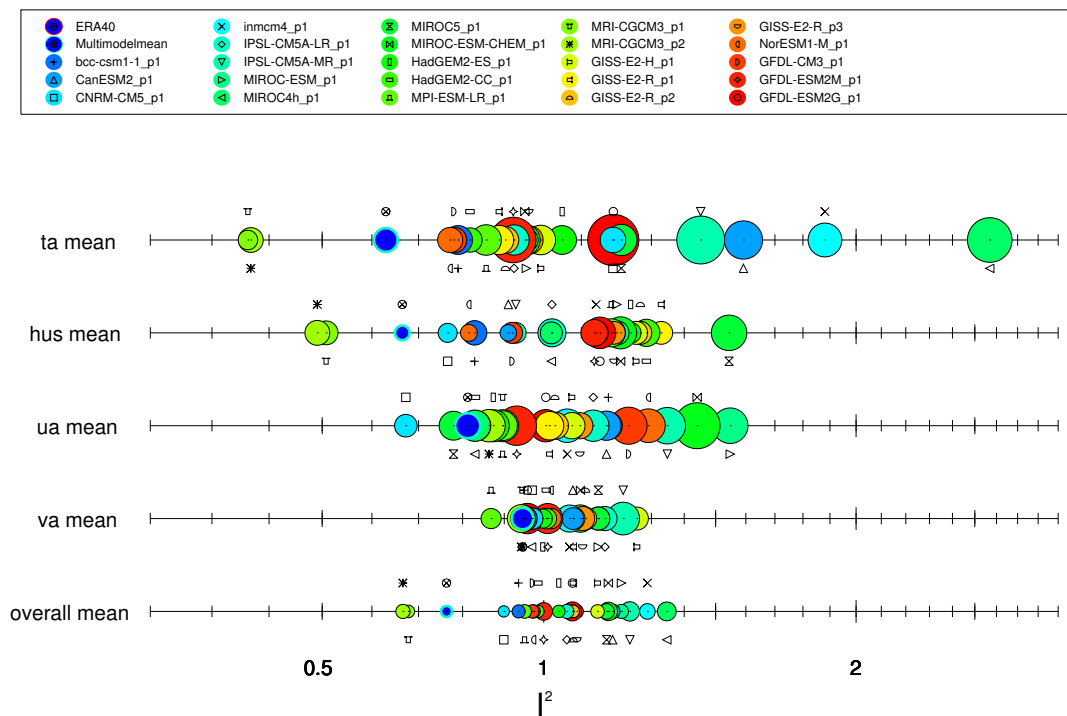


Figure 3.37: MPI of the single parameters ta, hus, ua and va mean and the mean over all parameters of the CMIP5-ensemble for the EURO-CORDEX lateral boundary between 1961 and 2000. The circles account for the 90 % confidence interval. The legend is the same as in Figure 3.21.

4 Discussion

Considering the presented seasonal cycles, Quantile-Quantile (QQ) plots, trend's slopes and interannual variabilities for the evaluated parameters the following can be noted.

The shape of the seasonal cycle reproduced by the Global Climate Model (GCM)s deviates less near the ground than on the different pressure levels over the lateral boundary zone. For surface air temperature (tas) the seasonal cycle is reproduced in terms of shape and magnitude really well in the mean over the different models and over the whole European domain, but shows a positive bias over Southern Europe (SEU) and a negative over Northern Europe (NEU). The models show a tendency of being much too wet in the case of precipitation rate (pr), and indicate a too low sea-level pressure (psl) during winter month over NEU. An assessment of the modelled seasonal cycle over the lateral boundary zone shows more deviations from the reference. These deviations are manifold over all variables and range from very small mean biases throughout the year to a minor misplacements of the seasonal cycle in terms of magnitude, width and shape for the single segments of the lateral boundary zone and on the single pressure levels. Strongest deviations and highest model spread are found over the bottom segment mainly located over the Sahara (bottom segment) likely being connected to model shortcomings when modelling within the tropical zone. There are strong differences in the models ability to remodel the references' distributions over the various parameters. Strong similarities in the form of distributions and location of quantiles are observed for tas, pr (with exception of minima for tas and maxima for pr) while they deviate more for psl (especially over SEU, where a strong skewing of the distribution to the right is present). The QQ plots accounting for similarity of distributions of the lateral boundary parameters do as well show strong similarities with the reference but only for single segments of the lateral boundary zone on single pressure levels. Nevertheless, in the case of the upper air parameters over the lateral boundary a stronger mismatch of quantiles of the monthly mean values is found.

Trend and interannual variability of tas are in very good agreement with the observed parameters. Also the two variables pr and psl show a good agreement for the whole EURO-Coordinated Regional Climate Downscaling Experiment (CORDEX) domain, while there do exist stronger deviations for the two sub regions of SEU and NEU. For pr the models show deficiencies in remodelling the severity of a decline over SEU and a rise over NEU. And for psl European high-resolution gridded data set (E-OBS) shows a rise while the Multimodel

Mean (MMM) indicates no trend over SEU. Trend differences are strongest for the set of parameters on pressure levels in terms of direction and magnitude, and are often accompanied by a too low interannual variability (especially in the case of air temperature (t_a), specific humidity (h_{us}) and northward wind (v_a)). It is unclear whether these differences arise as a result of bad model performances or are to be blamed on erroneous European re-analysis data set (ERA-40) data as argued in the next section.

4.1 The Quality of ERA-40 Reference Data

ERA-40 reanalysis data has been used as reference for the evaluations of the EURO-CORDEX lateral boundary. A major part of studies focusing on model validation by use of reanalysis data sets also selected ERA-40 as their reference (e.g. Errasti et al. 2011; Gleckler, Taylor and Doutriaux 2008; Ulden and Oldenborgh 2006). As mentioned earlier (see Subsection 1.3.4) one has to be careful when using this kind of data.

In the course of the thesis the author's aim was to diversely evaluate the Coupled Model Intercomparison Project (CMIP)5 Global Climate Models (GCMs). Trend differences as well as differences in interannual variability were planned to be made comparable by producing a single normalized index. But t_a , h_{us} and v_a trends of the evaluated GCMs and ERA-40 show a level of dissimilarity in magnitude as well as direction, that the quality of the reanalysis data itself is in doubt. E.g., t_a trends calculated from ERA-40 show a negative trend especially in the lower to mid troposphere (see Figure 4.1), while all models indicate a warming. The assumption of inappropriateness of reanalyses data for trend calculations is supported by the literature (e.g. Bengtsson, Hagemann and Hodges 2004; Dessler and Davis 2010; Santer et al. 2000). Therefore, if these differences are explainable by bad models or by deficient reference data cannot be answered in the course of this thesis. The production of a single feasible index would therefore lack consistency and present an improper approach.

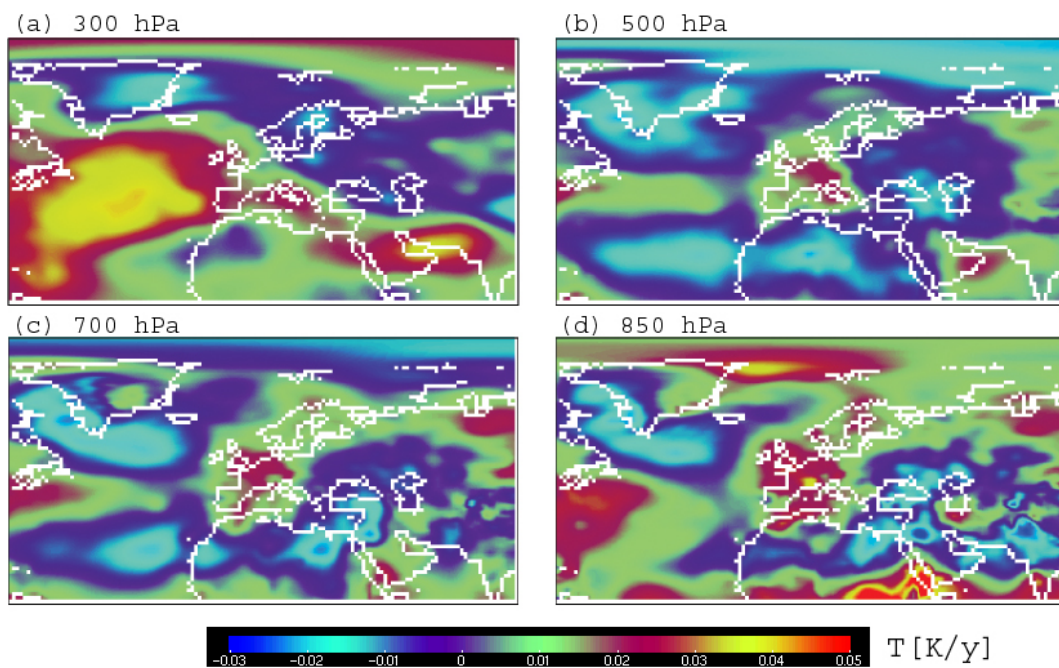


Figure 4.1: Map plots of the ERA-40 trend's slope for the period 1961-2000 on different pressure levels. A negative trend can be found over the lateral boundary segments of the EURO-CORDEX domain especially on 500 hPa, 700 hPa and 850 hPa.

4.2 Integrated Considerations

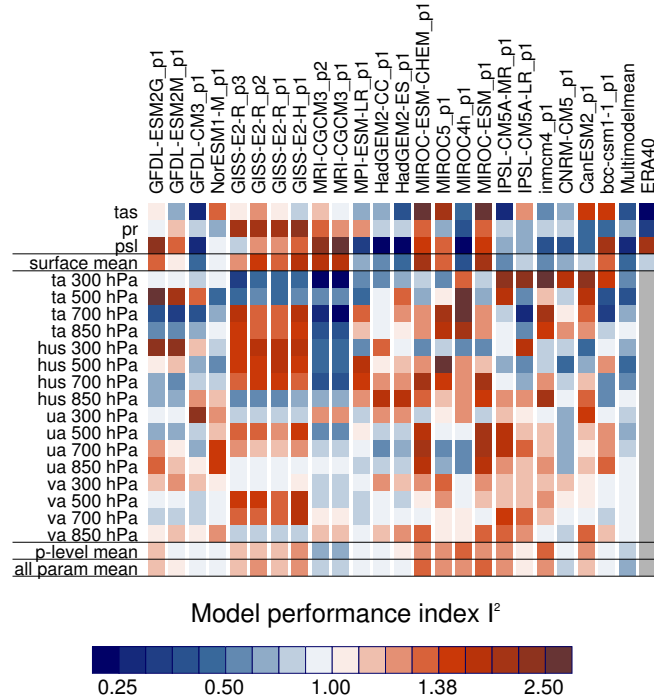


Figure 4.2: MPI of all evaluated parameters on pressure levels as well as the mean MPI over the surface parameters (surface mean), the parameters on pressure levels (p-level mean) and all parameters (all param mean) per model of the CMIP5-ensemble for the EURO-CORDEX domain and its lateral boundary between 1961 and 2000. The legend ranges from blue for the best performing models to red for the worst performing model in terms of the MPI.

The approach via the MPI allows for a comparison over the different CMIP5 models and the assessed variables. Figure 4.2 incorporates all MPIs presented in the previous sections in a portrait plot, and further adds the overall mean¹ to the list. No single model was able to perform above average (MPI $I^2 < 1$) for every single parameter. While for a single parameter strong differences can be observed between the models, differences are less strong for the mean MPIs. The top performing model over the ground parameters MIROC4h is performing below average for hus and especially for ta and worst of all models over the lateral boundary zone in the mean. Also the second best performing model for the ground parameters HadGEM2-ES is underperforming for the mean MPI of the

¹The overall mean was calculated by weighting equally over the 19 single parameter based MPIs.

parameters of the lateral boundary zone. Only the third best performing model for the ground parameters GFDL-CM3 shows a performance slightly better than the average for the lateral boundary zone. This allows to give an answer to the research question:

Do GCMs that show good results in remodeled ground parameters
also provide good driving data for a Regional Climate Model
(RCM) over the lateral boundary?

If a model does show good results in the MPI assessment of the ground parameters, this does not automatically mean, that it does show good results in the MPI assessment of the lateral boundary. This missing relationship is clearly visible in Figure 4.3. Hence a model's ability to remodel the past climate state on the ground level over a certain region, does not allow for any interpretation of its ability to reproduce the climate state of evaluated upper air parameters around that region. And further leads to the assumption that a model selection for RCM studies solely based on a GCM's ability to remodel ground parameters over the analysed region correctly may be too little and may not notice present shortcomings in the provided driving data.

Since these two different sets of MPIs seem if at all to correlate only weakly the question arises of how they may be combined to a single MPI. In the following paragraphs three different approaches addressing this issue will be presented. The first one will list models in terms of their performance in the mean over all ground parameters and in the mean over all parameters on pressure levels qualitatively. The second will present a combined single MPI by weighting all single MPIs equally. The last approach shows a ranking of the different models ranking them by fraction of times they performed best over different quantities of randomly drawn MPIs.

A performance better than the average over the EURO-CORDEX domain and its associated lateral boundary MPIs is shown by 5 models (always beginning with the best): CNRM-CM5, the already mentioned GFDL-CM3 model, MPI-ESM-LR, HadGEM2-CC and NorESM1-M. In contrast underperforming for both categories are GISS-E2-R_p3, GFDL-ESM2G, GISS-E2-R_p1, GISS-E2-R_p2, MIROC5, GISS-E2-H, MIROC-ESM-CHEM and MIROC-ESM. HadGEM2-ES, IPSL-CM5A-LR, CamESM2, IPSL-CM5A-MR, Inmcm4 and MIROC4h perform better than the average in terms of the mean MPI over ground parameters and worse than the average for the mean MPI over upper air parameters over the lateral boundary. The opposite is the case for the two perturbed physics realisations of MRI-CGCM3 (which performed best of all for the overall mean MPI), bcc-csm1-1 and GFDL-ESM2M.

When weighting single parametric MPIs equally to derive one combined MPI the two perturbed physics runs of the MRI-CGCM3 model p2 and p1 are the best performers. The third to ninth best models which all perform better than

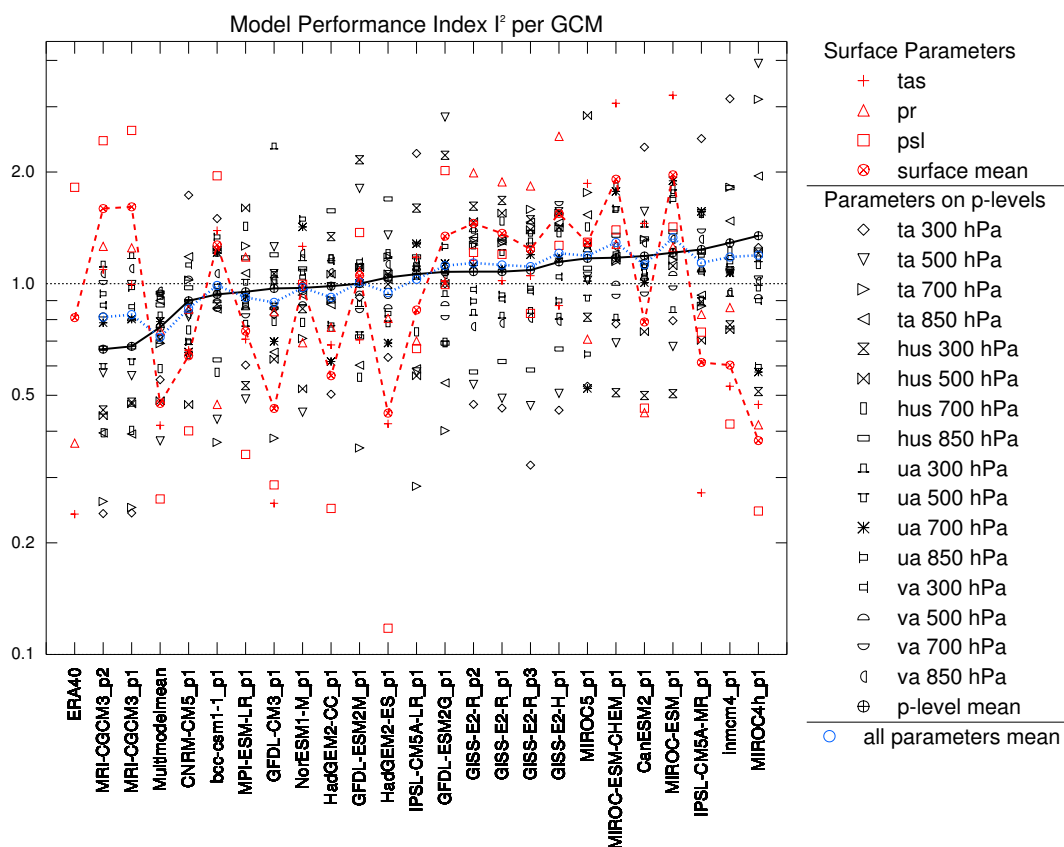


Figure 4.3: MPI of CMIP5 GCMs in the order of their performance for the mean MPI for parameters on pressure levels of the EURO-CORDEX lateral boundary between 1961 and 2000 from left to right. The lines correspond to the different mean MPIs for ground parameters (dashed), parameters on pressure levels over the lateral boundary (solid) and over all parameters when weighting them equally (dotted).

average in terms of the combined MPI are CNRM-CM5, GFDL-CM3, MPI-ESM-LR, HadGEM2-CC, HadGEM2-ES, NorESM1-M and bcc-csm1-1 respectively.

Pierce et al. [2009] tried to address the issue of a large set of different metrics² by controlling for fraction of time a model was performing best. A similar approach was performed within this thesis and is presented in Figure 4.4. Interestingly, results obtained from the MPI of equally weighted parameters are not reproduced entirely. The perturbed physics run p2 of the MRI-CGCM3 model shows the highest fraction of being ranked best no matter how many MPIs are included. Its p1 counterpart is performing much worse, since it also was performing slightly worse than p2 for a lot of parametric MPIs. When more than one MPI is included in the analysis the model CNRM-CM5 is fractionally ranked best the second most and when more than three MPIs are included in the analysis the model GFDL-CM3 is fractionally ranked best the third most.

Concerning the MMM the following issues can be noted. While the MPI of

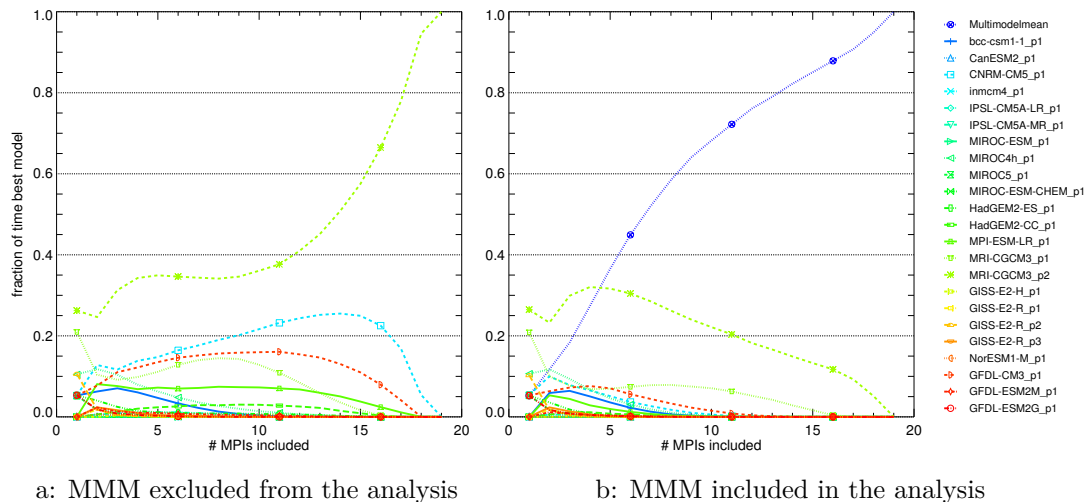


Figure 4.4: Fraction of time a model performs best in terms of the MPI when the number of included parametric MPIs ranges from 2 to 19. The single fraction of times best model values accrue from randomly picking, averaging and ranking the parametric MPIs 100.000 times.

the MMM did not perform best for a single parameter nor for mean MPIs of surface parameters or parameters on pressure levels, it is performing best for the overall mean MPI. As argued by Pierce et al. [2009] this phenomenon emerges because offsetting errors are cancelled out. This is also the case for the single

²In their study they obtained 42 single indicators of model performance assessing temperature and precipitation of 21 GCMs (see Subsection 1.3.4).

parameters in this analysis and can be noticed by the relatively good performance of the ensemble mean for the parametric MPIs, for which the MMM always scored a MPI value less than one. Bad results of the MMM for single parameters may evolve because of badly performing models (outliers) as argued by Gleckler, Taylor and Doutriaux [2008]. To cope for this outliers they introduced aside from the multi model mean the median model ensemble, which did perform best over a set of 26 parameters when testing for relative errors, but only performed slightly better than the MMM and was also outperformed by single model runs for single parameters. Figure 4.4 b also shows the superior performance of the MMM and how this superiority is connected to the number of MPIs included in the analysis.

5 Conclusion

The evaluated Coupled Model Intercomparison Project (CMIP)5 models show in the mean smaller deviations in their realisations of ground parameters over the EURO-CORDEX domain, while they show bigger deviation for parameters on pressure levels over the evaluated lateral boundary zone, although being in good agreement with the reference for single segments and on the single pressure levels. The Global Climate Model (GCM)s are too wet in terms of precipitation rate (pr) and model a too low sea-level pressure (psl) over Northern Europe (NEU) during winter. Deviations and model spread is found to be highest within the lateral boundary zone located over the Sahara. An evaluation of distributions shows, that the GCMs have shortcomings in modelling extreme months.

Although, trend intercomparisons over the EURO-Coordinated Regional Climate Downscaling Experiment (CORDEX) domain do look promising and the Global Climate Models (GCMs) show only small deviations from European high-resolution gridded data set (E-OBS) (especially for surface air temperature (tas)), they exhibit strong deviations over the lateral boundary from European re-analysis data set (ERA-40). But it is unclear whether this differences arise because of bad model performance or an imperfection of the used reanalysis data xset.

In an overall view a GCM's ability to model the current climate state near the ground does not correlate with its ability to provide correct driving data to one-way nested Regional Climate Model (RCM)s. Revealingly, the model that performs best in the terms of the Model Performance Index (MPI) for the parameters near the surface is the same model that performs worst for the upper air parameters over the lateral boundary in terms of the applied MPI.

References

- Amengual, A. et al. (2007).
‘Impact of the lateral boundary conditions resolution on dynamical downscaling of precipitation in Mediterranean Spain’.
In: *Climate Dynamics* 29, pp. 487–499 (cit. on p. 10).
- Baede, A. P. M. (ed.) (2007). ‘Glossary’. In: *Climate Change 2007: The Physical Science Basis. Contribution of Working Group I to the Fourth Assessment Report of the Intergovernmental Panel on Climate Change*. Ed. by S. Solomon et al.
Cambridge and New York: Cambridge University Press.
Chap. Annex I: pp. 941–954 (cit. on p. 2).
- Bengtsson, L., S. Hagemann and K. I. Hodges (2004).
‘Can climate trends be calculated from reanalysis data?’
In: *Journal of Geophysical Research* 109 (D11), pp. 1–8 (cit. on pp. 9, 82).
- Besselaar, E. J. M. van den et al. (2011). ‘A European daily high-resolution observational gridded data set of sea level pressure’.
In: *Journal of Geophysical Research* 116, p. 11 (cit. on pp. 26, 27).
- CMIP5 website (10th Feb. 2012). URL: <http://cmip-pcmdi.llnl.gov/>
(cit. on pp. 22, 25).
- Christensen, J. and O. Christensen (2007).
‘A summary of the PRUDENCE model projections of changes in European climate by the end of this century’. In: *Climatic Change* 81, pp. 7–30
(cit. on p. 12).
- Davies, H. C. (1975).
‘A lateral boundary formulation for multi-level prediction models’.
In: *Q. J. Roy. Meteorol. Soc.* 102, pp. 405–418 (cit. on p. 7).
- De Ridder, K. (2008). ‘Soil temperature spin-up in land surface schemes’.
In: *Theoretical and Applied Climatology* 95 (3), pp. 341–347 (cit. on p. 7).
- Dessler, A. and S. Davis (2010).
‘Trends in tropospheric humidity from reanalysis systems’.
In: *Journal of Geophysical Research* 115, p. 5 (cit. on pp. 9, 11, 82).

- Diaconescu, E. P., R. Laprise and L. Sushama (2007).
‘The impact of lateral boundary data errors on the simulated climate of a nested regional climate model’. In: *Climate Dynamics* 28, pp. 333–350 (cit. on pp. 10–12).
- Déqué, M. et al. (2007). ‘An intercomparison of regional climate simulations for Europe: assessing uncertainties in model projections’.
In: *Climatic Change* 81, pp. 53–70 (cit. on p. 12).
- EURO-CORDEX (6th Mar. 2012).
URL: <http://www.euro-cordex.net/About-Euro-Cordex.1864.0.html>
(cit. on p. 18).
- Efron, B. and R. J. Tibshirani (1993). *An Introduction to the Bootstrap*.
New York: Chapman & Hall, 436 (cit. on p. 34).
- Errasti, I. et al. (2011).
‘Validation of IPCC AR4 models over the Iberian Peninsula’.
In: *Theoretical Applied Climatology* 103, pp. 61–79 (cit. on pp. 14, 82).
- Etling, D. (2008). *Theoretische Meteorologie: Eine Einführung*.
Berlin Heidelberg New York: Springer Verlag, 376. ISBN: 978-3-540-75978-2
(cit. on p. 20).
- Finger, R., W. Hediger and S. Schmid (2011).
‘Irrigation as adaptation strategy to climate change—a biophysical and economic appraisal for Swiss maize production’.
In: *Climatic Change* 105, pp. 509–528 (cit. on p. 6).
- Giorgi, F., C. Jones and G. R. Asrar (2009). ‘Addressing climate information needs at the regional level: the CORDEX framework’.
In: *WMO Bulletin* 58 (3), pp. 175–183 (cit. on pp. 13, 18).
- Giorgi, F. and L. O. Mearns (1991).
‘Approaches to the simulation of regional climate change: A review’.
In: *Reviews of Geophysics* 29 (2), pp. 191–216 (cit. on pp. 4, 8, 18).
- (1999).
‘Introduction to special section: Regional climate modeling revisited’.
In: *Journal of Geophysical Research* 104, pp. 6335–6352 (cit. on pp. 7, 8).
- (2002). ‘Calculation of Average, Uncertainty Range, and Reliability of Regional Climate Change from AOGCM Simulations via the “Reliability Ensemble Averaging” (REA) Method’.
In: *Journal of Climate* 15, pp. 1141–1158 (cit. on p. 13).
- Gleckler, P. J., K. E. Taylor and C. Doutriaux (2008).
‘Performance metrics for climate models’.
In: *Journal of Geophysical Research* 113, pp. 1–20
(cit. on pp. 15, 33, 82, 88).

- Gobiet, A., D. Jacob and E.-C. Community (2012). ‘A new generation of regional climate simulations for Europe: The EURO-CORDEX Initiative’. In: *Geophysical Research Abstracts* 14 (EGU2012-8211), pp. 1–20 (cit. on p. 18).
- Hantel, M. (2001). ‘Klimatologie’. In: *Bergmann - Schaefer: Lehrbuch der Experimentalphysik: Erde und Planeten*. Ed. by W. Raith. Berlin, Germany, New York: Walter de Gruyter (cit. on p. 2).
- Haylock, M. R. et al. (2008). ‘A European daily high-resolution gridded data set of surface temperature and precipitation for 1950–2006’. In: *Journal of Geophysical Research* 113, p. 12 (cit. on p. 26).
- Hegerl, G. C. et al. (2007). ‘Understanding and Attributing Climate Change’. In: *Climate Change 2007: The Physical Science Basis. Contribution of Working Group I to the Fourth Assessment Report of the Intergovernmental Panel on Climate Change*. Ed. by S. Solomon et al. Cambridge and New York: Cambridge University Press. Chap. Supplementary Material: Chapter 9, pp. 1–14 (cit. on p. 18).
- Jacob, D. et al. (2007). ‘An inter-comparison of regional climate models for Europe: model performance in present-day climate’. In: *Climate Change* 81, pp. 31–52 (cit. on p. 12).
- Klok, E. J. and A. M. Klein Tank (2009). ‘Updated and extended European dataset of daily climate observations’. In: *International Journal of Climatology* 29 (8), pp. 1182–1191 (cit. on pp. 26, 27).
- Knutti, R. et al. (2010). ‘Challenges in Combining Projections from Multiple Climate Models’. In: *Journal of Climate* 23, pp. 2739–2758 (cit. on p. 13).
- Kraus, H. (2004). *Die Atmosphäre der Erde: Eine Einführung in die Meteorologie*. Berlin Heidelberg New York: Springer Verlag, 422. ISBN: 3-540-20656-6 (cit. on pp. 20–22).
- Laprise, R. (2006). ‘Regional climate modeling’. In: *Journal of Computational Physics* 227, pp. 3641–3666 (cit. on pp. 6, 12).
- Liljequist, G. and K. Cihak (1994). *Allgemeine Meteorologie*. 3rd ed. Braunschweig/Wiesbaden: Friedr. Vieweg & Sohn Verlagsgesellschaft mbH, 396. ISBN: 3-528-23555-1 (cit. on pp. 20, 21).
- Linden, P. van der and J. Mitchell, eds. (2009). *ENSEMBLES: Climate Change and its Impacts: Summary of research and results from the ENSEMBLES project*. Exeter, UK: Met Office Hadley Centre, 160 (cit. on p. 13).

- Lorenz, P. and D. Jacob (2005). 'Influence of regional scale information on the global circulation: A two-way nesting climate simulation'.
In: *Geophysical research letter* 32, pp. 1–4 (cit. on p. 7).
- MERCURE (2002). - *Final project report*. Ed. by R. Jones and Co-Workers.
EU, Brussels, Belgium (cit. on p. 12).
- Marbaix, P. et al. (2003). 'Lateral Boundary Conditions in Regional Climate Models: A Detailed Study of the Relaxation Procedure'.
In: *Monthly Weather Review* 131, pp. 461–479 (cit. on p. 10).
- Maxino, C. C. et al. (2008).
'Ranking the AR4 climate models over the Murray-Darling Basin using simulated maximum temperature, minimum temperature and precipitation'.
In: *International Journal of Climatology* 28, pp. 1097–1112 (cit. on p. 14).
- McGuffie, K. and A. Henderson-Sellers (2005). *A Climate Modelling Primer*.
3rd ed. John Wiley & Sons, Ltd, p. 296. ISBN: 9780470857618.
DOI: 10.1002/0470857617.ch1 (cit. on p. 3).
- Pierce, D. W. et al. (2009).
'Selecting global climate models for regional climate change studies'. In:
PNAS Proceedings of the National Academy of Science 106, pp. 8441–8446
(cit. on pp. 14, 33, 87).
- Prein, A. (2009). *Uncertainties in the Driving Data of Regional Climate Models in the Alpine Region*. Wegener Center Verlag Graz, p. 148.
ISBN: 978-3-9502615-7-8 (cit. on p. 1).
- Reichler, T. and J. Kim (2008a).
'How Well do Coupled Models Simulate Today's Climate?'.
In: *Bulletin of the American Meteorological Society* 89, pp. 303–311
(cit. on pp. 13, 14, 33).
- (2008b). 'Uncertainties in the climate mean state of global observations, reanalyses, and the GFDL climate model'.
In: *Journal of Geophysical Research* 113, p. 13 (cit. on pp. 9, 10).
- Roeckner, E. et al. (2006). 'Sensitivity of Simulated Climate to Horizontal and Vertical Resolution in the ECHAM5 Atmosphere Model'.
In: *Journal of Climate* 19, pp. 3771–3791. DOI: 10.1175/JCLI3824.1
(cit. on p. 25).
- Rotstayn, L. et al. (2010).
'Improved simulation of Australian climate and ENSO-related climate variability in a GCM with an interactive aerosol treatment'.
In: *International Journal of Climatology* 30 (7), pp. 1067–1088.
DOI: 10.1002/joc.1952 (cit. on p. 25).

- Rummukainen, M. (2010). ‘State-of-the-art with regional climate models’.
In: *Wiley Interdisciplinary Reviews: Climate Change* 1, pp. 82–96
(cit. on pp. 5–8, 18).
- Räisänen, J. (2007). ‘How reliable are climate models?’
In: *Tellus* 59A, pp. 2–29 (cit. on p. 13).
- Sakamoto, T. T. et al. (2012). ‘MIROC4h - A New High-resolution
Atmosphere-ocean Coupled General Circulation Model’.
In: *Journal Meteorological Society Japan* 90.3 (cit. on p. 25).
- Santer, B. D. et al. (2000). ‘Statistical significance of trends and trend
differences in layer-average atmospheric temperature time series’.
In: *Journal of Geophysical Research* 105, pp. 7337–7356 (cit. on pp. 9, 82).
- Skamarock, W. et al. (2011).
Beyond WRF: Nonhydrostatic Global Modeling with MPAS.
Presented at the 12th WRF Users’ Workshop, National Center for
Atmospheric Research June 21 (cit. on p. 6).
- Somerville, R. et al. (2007). ‘Historical Overview of Climate Change’.
In: *Climate Change 2007: The Physical Science Basis. Contribution of
Working Group I to the Fourth Assessment Report of the Intergovernmental
Panel on Climate Change*. Ed. by S. Solomon et al.
Cambridge and New York: Cambridge University Press.
Chap. 1, pp. 941–954 (cit. on pp. 2, 4, 5).
- Stouffer, R. J., K. Taylor and G. A. Meehl (2011).
‘CMIP5 Long-term experimental Design’.
In: *CLIVAR Exchanges* 16 (2), pp. 5–7. DOI: 10.1175/BAMS-D-11-00094.1
(cit. on p. 23).
- Taylor, K., R. J. Stouffer and G. A. Meehl (2012).
‘An Overview of CMIP5 and the Experiment Design’.
In: *Bulletin of the American Meteorological Society* 93, pp. 485–498.
DOI: 10.1175/BAMS-D-11-00094.1 (cit. on p. 24).
- Toynbee, J. (1949).
A Study of History. Abridgement of volumes I-VI by D.C. Somervell.
London, New York, Toronto: Oxford University Press, 617.
ISBN: 978-0-12-751966-1 (cit. on p. 1).
- Ulden, A. P. van and G. J. van Oldenborgh (2006). ‘Large-scale atmospheric
circulation biases and changes in global climate model simulations and their
importance for climate change in Central Europe’.
In: *Atmospheric Chemistry and Physics* 6, pp. 863–881 (cit. on pp. 14, 82).
- Uppala, S. M. et al. (2005). ‘The ERA-40 re-analysis’.
In: *Quarterly Journal of the Royal Meteorological Society* 131, pp. 2961–3012
(cit. on pp. 27, 28).

- Volodin, E. M., N. A. Dianskii and A. V. Gusev (2010).
‘Simulating Present Day Climate with the INMCM4.0 Coupled Model of the Atmospheric and Oceanic General Circulations’.
In: *Izvestiya, Atmospheric and Oceanic Physics* 46 (4), pp. 414–431
(cit. on p. 25).
- Wang, Y. et al. (2004).
‘Regional Climate Modeling: Progress, Challenges, and Prospects’.
In: *Journal of the Meteorological Society of Japan* 82.6, pp. 1599–1628
(cit. on pp. 6–9).
- Watanabe, S. et al. (2011). ‘MIROC-ESM: model description and basic results of CMIP5-20c3m experiments’.
In: *Geoscientific Model Development Discussions* 4.2, pp. 1063–1128.
DOI: 10.5194/gmdd-4-1063-2011.
URL: <http://www.geosci-model-dev-discuss.net/4/1063/2011/>
(cit. on p. 25).
- Wilks, D. S. (2006). *Statistical Methods in the Atmospheric Sciences*. 2nd ed.
Amsterdam/Boston/Heidelberg/London/New York/Oxford/Paris/San Diego/San Francisco/Singapore/Sydney/Tokyo: Academic Press, 627.
ISBN: 978-0-12-751966-1 (cit. on pp. 30–33).
- Wu, W., A. H. Lynch and A. Rivers (2005).
‘Estimating the Uncertainty in a Regional Climate Model Related to Initial and Lateral Boundary Conditions’. In: *Journal of Climate* 18, pp. 917–933.
DOI: 10.1175/JCLI-3293.1 (cit. on pp. 10, 11).
- Yukimoto, S. et al. (2011). ‘Meteorological Research Institute-Earth System Model v1 (MRI-ESM1) - Model Description’.
In: *Technical Report of MRI* 64, p. 83 (cit. on p. 25).
- Zhong, Z. et al. (2009).
‘Further study on the effect of buffer zone size in regional climate modeling’.
In: *Climate Dynamics* 36 (6), pp. 1027–1038 (cit. on pp. 10, 11).
- Zwiers, F. W. and V. V. Kharin (1998). ‘Intercomparison of interannual variability and potential predictability: an AMIP diagnostic subproject’.
In: *Climate Dynamics* 14, pp. 517–528 (cit. on p. 14).
- ipsl (6th Mar. 2012). URL:
http://wcrp.ipsl.jussieu.fr/RCD_Projects/CORDEX/cordex_domains_250610.pdf (cit. on p. 18).
- von Storch, H., S. Güss and M. Heimann (1999).
Das Klimasystem und seine Modellierung: Eine Einführung.
Berlin Heidelberg New York: Springer Verlag, 255. ISBN: 3-540-65830-0
(cit. on pp. 3, 20).

- von Storch, H., H. Langenberg and F. Feser (2000).
‘A spectral nudging technique for dynamical downscaling purposes’.
In: *Monthly Weather Review* 128, pp. 3664–3673 (cit. on p. 8).

List of Figures

1.1	Schematic illustration of a GCM's operating principle [McGuffie and Henderson-Sellers 2005].	3
1.2	Climate models and the increase of included processes with time. (Intergovernmental Panel on Climate Change (IPCC)'s First Assessment Report (FAR) 1990, Second Assessment Report (SAR) 1996, Third Assessment Report (TAR) 2001, and Fourth Assessment Report (AR4) 2007) [Somerville et al. 2007].	4
1.3	GCMs and the increase of spatial resolution with time. ((IPCC's First Assessment Report (FAR) 1990, Second Assessment Report (SAR) 1996, Third Assessment Report (TAR) 2001, and Fourth Assessment Report (AR4) 2007) [Somerville et al. 2007].	5
1.5	Specific humidity (hus) trends of different reanalyses over 1979 to 2010 (1989 for ERA-interim) for the tropics (20°S to 20°N), northern (20°N to 50°N) and southern (20°S to 50°N) hemisphere.	11
2.1	Flow diagram of the approach used in the evaluation.	17
2.2	The EURO-CORDEX domain (rotated north pole at 162°W 39.25°N, top left corner at 331.79°W 21.67°N).	19
2.3	Schematic summary of the CMIP5 long-term experiments.	23
2.4	E-OBS station network. To the left: tas and pr as far as 2007 [Klok and Klein Tank 2009]. To the right: psl as far as 2011 [Besselaar et al. 2011].	27
2.5	Chronology of observation types assimilated in ERA-40 from 1957 to 2002 [Uppala et al. 2005].	27
2.6	Evaluated variables on gridpoint basis over the EURO-CORDEX domain and its corresponding lateral boundary.	29
2.7	A Quantile-Quantile plot.	31
2.8	Schematic illustration of simple linear regression [Wilks 2006].	33
3.1	Mapplots of absolute and bias values of CMIP5 ensemble Multimodel Mean (MMM) of the tas over Europe between 1961 and 2000. As reference data serves E-OBS v5.	39
3.2	Seasonal cycle of tas of the CMIP5-ensemble for (a) the EURO-CORDEX domain (b) Southern Europe (SEU) and (c) NEU between 1961 and 2000.	40

3.3	Bias in the seasonal cycle of tas of the CMIP5 ensemble for (a) the EURO-CORDEX domain (b) SEU and (c) NEU between 1961 and 2000 in reference to E-OBS.	40
3.4	Quantile-Quantile (QQ) plot of tas of the CMIP5-ensemble for (a) the EURO-CORDEX domain (b) SEU and (c) NEU between 1961 and 2000 in reference to E-OBS showing the 5 % quantiles.	41
3.5	Scatter plot of slope and interannual variability based on linear regression for tas of the CMIP5-ensemble for (a) the EURO-CORDEX domain (b) SEU and (c) NEU between 1961 and 2000 in reference to E-OBS.	41
3.6	Mapplots of absolute and bias values of CMIP5 ensemble MMM of the pr over Europe between 1961 and 2000. As reference data serves E-OBS v5.	42
3.7	Seasonal cycle of pr of the CMIP5-ensemble for (a) the EURO-CORDEX domain (b) SEU and (c) NEU between 1961 and 2000.	43
3.8	Bias in the seasonal cycle of pr of the CMIP5-ensemble for (a) the EURO-CORDEX domain (b) SEU and (c) NEU between 1961 and 2000 in reference to E-OBS.	43
3.9	QQ plot of pr of the CMIP5-ensemble for (a) the EURO-CORDEX domain (b) SEU and (c) NEU between 1961 and 2000 in reference to E-OBS showing the 5 % quantiles.	44
3.10	Scatter plot of slope and interannual variability based on linear regression for pr of the CMIP5-ensemble for (a) the EURO-CORDEX domain (b) SEU and (c) NEU between 1961 and 2000 in reference to E-OBS.	45
3.11	Mapplots of absolute and bias values of CMIP5 ensemble MMM of the psl over Europe between 1961 and 2000. As reference data serves E-OBS v5.	46
3.12	Seasonal cycle of psl of the CMIP5-ensemble for (a) the EURO-CORDEX domain (b) SEU and (c) NEU between 1961 and 2000.	47
3.13	Bias in the seasonal cycle of psl of the CMIP5-ensemble for (a) the EURO-CORDEX domain (b) SEU and (c) NEU between 1961 and 2000 in reference to E-OBS.	47
3.14	QQ plot of psl of the CMIP5-ensemble for (a) the EURO-CORDEX domain (b) SEU and (c) NEU between 1961 and 2000 in reference to E-OBS showing the 5 % quantiles.	48
3.15	Scatter plot of slope and interannual variability based on linear regression for psl of the CMIP5-ensemble for (a) the EURO-CORDEX domain (b) SEU and (c) NEU between 1961 and 2000 in reference to E-OBS.	48

3.16	MPI of and the mean over all ground parameters of the CMIP5-ensemble for the EURO-CORDEX domain between 1961 and 2000. The circles account for the 80 % confidence interval.	49
3.17	Seasonal cycle of air temperature (t_a) of the CMIP5-ensemble for the EURO-CORDEX lateral boundary between 1961 and 2000.	51
3.18	Bias in the seasonal cycle of t_a of the CMIP5-ensemble for the EURO-CORDEX lateral boundary between 1961 and 2000.	52
3.19	QQ plot of t_a of the CMIP5-ensemble for the EURO-CORDEX lateral boundary between 1961 and 2000 in reference to ERA-40 showing the 5 % quantiles.	54
3.20	Scatter plot of slope and interannual variability based on linear regression for t_a of the CMIP5-ensemble for the EURO-CORDEX lateral boundary between 1961 and 2000.	55
3.21	MPI of and the mean over all pressure levels of t_a of the CMIP5-ensemble for the EURO-CORDEX lateral boundary between 1961 and 2000.	57
3.22	Seasonal cycle of specific humidity (h_{us}) of the CMIP5-ensemble for the EURO-CORDEX lateral boundary between 1961 and 2000.	59
3.23	Bias in the seasonal cycle of h_{us} of the CMIP5-ensemble for the EURO-CORDEX lateral boundary between 1961 and 2000.	60
3.24	QQ plot of h_{us} of the CMIP5-ensemble for the EURO-CORDEX lateral boundary between 1961 and 2000 in reference to ERA-40 showing the 5 % quantiles.	62
3.25	Scatter plot of slope and interannual variability based on linear regression for h_{us} of the CMIP5-ensemble for the EURO-CORDEX lateral boundary between 1961 and 2000.	63
3.26	MPI of and the mean over all pressure levels of h_{us} of the CMIP5-ensemble for the EURO-CORDEX lateral boundary between 1961 and 2000.	64
3.27	Seasonal cycle of eastward wind (u_a) of the CMIP5-ensemble for the EURO-CORDEX lateral boundary between 1961 and 2000.	67
3.28	Bias in the seasonal cycle of u_a of the CMIP5-ensemble for the EURO-CORDEX lateral boundary between 1961 and 2000.	68
3.29	QQ plot of u_a of the CMIP5-ensemble for the EURO-CORDEX lateral boundary between 1961 and 2000 in reference to ERA-40 showing the 5 % quantiles.	69
3.30	Scatter plot of slope and interannual variability based on linear regression for u_a of the CMIP5-ensemble for the EURO-CORDEX lateral boundary between 1961 and 2000.	70
3.31	MPI of and the mean over all pressure levels of u_a of the CMIP5-ensemble for the EURO-CORDEX lateral boundary between 1961 and 2000.	71

3.32	Seasonal cycle of northward wind (v_a) of the CMIP5-ensemble for the EURO-CORDEX lateral boundary between 1961 and 2000. The lines account for the different pressure levels, 850 hPa, 700 hPa, 500 hPa, and 300 hPa from top to bottom. The rows denote for the four segments left, top, bottom, and right from left to right.	74
3.33	Bias in the seasonal cycle of v_a of the CMIP5-ensemble for the EURO-CORDEX lateral boundary between 1961 and 2000.	75
3.34	QQ plot of v_a of the CMIP5-ensemble for the EURO-CORDEX lateral boundary between 1961 and 2000 in reference to ERA-40 showing the 5 % quantiles.	76
3.35	Scatter plot of slope and interannual variability based on linear regression for v_a of the CMIP5-ensemble for the EURO-CORDEX lateral boundary between 1961 and 2000.	77
3.36	MPI of and the mean over all pressure levels of v_a of the CMIP5-ensemble for the EURO-CORDEX lateral boundary between 1961 and 2000.	78
3.37	MPI of the single parameters t_a , h_{us} , u_a and v_a mean and the mean over all parameters of the CMIP5-ensemble for the EURO-CORDEX lateral boundary between 1961 and 2000.	80
4.1	Map plots of the ERA-40 trend's slope for the period 1961-2000 on different pressure levels.	83
4.2	MPI of all evaluated parameters on pressure levels as well as the mean MPI over the surface parameters (surface mean), the parameters on pressure levels (p-level mean) and all parameters (all param mean) per model of the CMIP5-ensemble for the EURO-CORDEX domain and its lateral boundary between 1961 and 2000.	84
4.3	MPI of CMIP5 GCMs in the order of their performance for the mean MPI for parameters on pressure levels of the EURO-CORDEX lateral boundary between 1961 and 2000 from left to right.	86
4.4	Fraction of time a model performs best in terms of the MPI when the number of included parametric MPIs ranges from 2 to 19.	87

List of Tables

2.1	Overview of the climate variables and corresponding units, pressure level and reference data set used in the evaluation.	20
2.2	Model overview of CMIP5 GCMs [CMIP5 website 2012].	25
2.3	E-OBS number of stations	26
2.4	Average daily counts of various types of observation supplied to the ERA-40 data assimilation, for five selected periods [Uppala et al. 2005].	28

Abstract:

In 2013 the Fifth assessment report of the Intergovernmental Panel on Climate Change (IPCC) will be published. Therein contained data from global climate models (GCMs) is collected by the fifth Coupled Model Intercomparison Project (CMIP5) since February 2011. To obtain regional information from the GCMs with their rather coarse resolution, the Coordinated Regional Climate Downscaling Experiment – in the case of Europe EURO-CORDEX – regionalises data of several GCMs via regional climate models (RCMs).

The study at hand evaluates the different CMIP5 GCMs in terms of their ability to reproduce the climate between 1961 and 2000 and to provide correct data necessary to drive RCMs. For this purpose near surface (2m) air temperature, precipitation and sea-level pressure over the land area of Europe, as well as the upper air parameters air temperature, specific humidity and horizontal wind components in the form of how they are taken over from a RCM – on different pressure levels over an area enveloping Europe – have been analysed. In doing so, applied evaluation methods include spatial distributions, seasonal cycles and respective deviations of it, quantile-quantile plots, trends and interannual variability, and also a model performance index. As a reference for the near surface parameters serves the European high-resolution gridded data set (E-OBS) and for parameters on pressure levels European re-analysis data set (ERA-40).

The analysis shows a good agreement between modeled ground fields and the reference, while parameters over the lateral boundary zone deviate stronger. Results moreover suggest, that a model's ability to correctly reproduce parameters near the surface, does not implicate that the model provides correct data necessary for driving an RCM. This leads to the conclusion that GCMs as drivers for regional climate models should not only be selected based of the quality near the surface, but also based on the quality of upper air parameters, particularly over the lateral boundary.

Zum Inhalt:

Im Jahr 2013 wird der fünfte Sachstandsbericht des Intergovernmental Panel on Climate Change (IPCC) erscheinen. Die darin enthaltenen Daten globaler Klimamodelle (GCMs) werden seit Februar 2011 im fünften Coupled Model Intercomparison Project (CMIP5) zusammengetragen. Um von der großräumigen Auflösung der GCMs zu regionalen Prognosen des Klimawandels zu gelangen, werden unter dem Coordinated Regional Climate Downscaling Experiment (CORDEX) – im Fall von Europa EURO-CORDEX – Daten aus mehreren GCMs mittels regionaler Klimamodelle (RCMs) regionalisiert.

Die vorliegende Studie evaluiert die unterschiedlichen CMIP5 Modelle hinsichtlich ihrer Fähigkeit, den Zustand des Klimas zwischen 1961 und 2000 zu reproduzieren und korrekte Daten bereitzustellen, die für das Betreiben eines RCMs nötig sind. Zu diesem Zweck wurden die modellierte bodennahe Lufttemperatur, der Niederschlag und der Luftdruck auf Meereshöhe über der Landfläche Europas, sowie die Lufttemperatur, spezifische Luftfeuchtigkeit und horizontale Windkomponenten auf verschiedenen Druckebenen in einem Europa umschließenden Gebiet analysiert. Hierfür verwendete Methoden umfassten räumliche Verteilungen, Jahresgänge und jeweilige Abweichungen, Quantile-Quantile-Plots, Trends und interannuale Variabilität sowie einen Model Performance Index. Als Referenzen dienten die bodennahen Parameter aus European high-resolution gridded data set (E-OBS) und die Parameter aus European reanalysis data set (ERA-40) auf Druckebenen.

Die Analyse zeigt eine gute Übereinstimmung modellierter Bodenfelder mit den verwendeten Beobachtungsdaten, während die Parameter der lateralen Grenzregion stärker abweichen. Die Fähigkeit eines Modells, bodennahe Parameter korrekt zu modellieren, bedeutet nicht automatisch, dass es korrekte Parameter für ein RCMs bereitstellt. Dies führt zum Schluss, dass GCMs als Antrieb für regionale Modelle nicht nur nach der Qualität ihrer bodennahen Parameter, sondern auch nach Parametern welche die freie Atmosphäre beschreiben, insbesondere in der lateralen Grenzzone, für Regionalisierungen ausgewählt werden sollten.